UNIVERSITY OF CANTERBURY
Te Whare Wānanga o Waitaha
CHRISTCHURCH NEW ZEALAND

DEPARTMENT OF MECHANICAL ENGINEERING

SPIN COATING ON A CURVED SURFACES

Supervisor

Dr Mathieu Sellier

Submitted By

Bibin Jose (58517657)

University of Canterbury

2020

ACKNOWLEDGEMENT

First and foremost, I thank the Lord for His never-ending grace and blessings in helping me through this journey of completing my research successfully.

I express my gratitude to my supervisor, Dr Mathieu Sellier, for continuously supporting my study, for his patience, immense knowledge and useful critiques.

My sincere thanks to Dr Volker Nock, for his patent guidance and encouragement towards my research. I would also like to thank the experts who were involved in my study: Researcher Ms Sevgi Onal, for her help in doing the optical profilometer measurement analysis. I would like to extend my gratitude to the technician's, Ms Helen Devereur and Mr Gary Turner of the Nano laboratory (Nano lab), Electrical and Computer Engineering. Without their passionate participation and input, the optical profilometer measurement could not have been successfully conducted. Special thanks and appreciation to KiwiNet, who supported me financially during this research.

My sincere thanks to my friends Mr Michael Coe, his wife Alison Tang, Juhy Paily, Felmi Thomas and Derrick Hetutu, for always motivating and inspiring me while completing my course. I want to thank all my church and family members for supporting me spiritually and for their constant source of inspiration. Last but not least, my deepest gratitude to my loving and supporting wife, Ms Priya Thomas, for always encouraging and comforting me while I completed my studies.

ABSTRACT

Spin coating is an important method used to form a thin film in the microelectronics industry where the thin-film coating is needed. It is a process in which the solution is spread evenly over a surface using centrifugal force when the substrate is rotating. The spin coating process includes typically four steps: a deposition stage, substrate spin up or acceleration stage, a stage of substrate rotating at a constant rate where the fluid viscosity control fluid thinning and a stage at which substrate rotating at a continuous rate and the evaporation of the solvent continue to dominate the thinning behaviour of the spin coating fluid. There are many industrial applications based on curved surfaces such as protective coating against corrosion, metal shielding grid on the window of a fairing, UV light protection optical elements including curved grating, diffractive optical elements and the thin-film amorphous silicon solar cells.

The main objective of this research was to examine the spin coating on curved surfaces. An experiment was conducted on a hemispherical substrate on single-axis spin coater. The thickness of the film was compared using an Atomic Force Microscope (AFM) and Profilm3D optical profilometer. The thickness of the flat substrate (silicon wafer), and curved hemisphere (glass) were compared.

A 2D axi-symmetric COMSOL model has been designed around the z-axis of rotation. It was created by the Boolean operation of difference from two concentric spheres of constant thickness. The difference between these two layers of spheres represents the fluid thickness. The fluid material used in this model was engine oil since it has similar fluid properties to the polymer solution used for coating in the actual test. The laminar two-phase flow, coupled with moving meshes (ALE) was used for analysis. The boundary conditions included in this model acting on the inner surface wall of the fluid layer is a no-slip condition, whereas, for the outer surface, we applied zero radial displacement and free deformation.

CONTENTS

1. INTRODUCTION

Spin coating is a technique that deposits a thin layer of photo-resist polymer solution on a substrate using centrifugal force. It is created by spinning a substrate that helps deposit a thin film in a uniform manner. In this method, a small quantity of liquid resin is spread over a substrate. A centrifugal force is employed to get a uniform layer of film thickness by rotating the material at high angular velocities. Spin coating can be used for many industrial applications where a thin layer of photo resistive substance cover relatively flat or curved surfaces. The coating process is an eminent practice in microelectronic industries where a thin-film coating is demanded. In this research, the characteristic behaviour of uniformity and distribution of the thin film on curved surfaces was analysed using a single-axis spin coater along with numerical and experimental analysis. The photo-resistive polymer material was diluted or dissolved into some solvent and then applied onto the substrate and spun to create a uniform thickness of film coating for the future processing stages.

1.1 SPIN COATING PROCESS

The spin coating process (***Fig.1.1***) involves four stages: deposition, spin-up (centrifugal force dominated), a spin-off (viscous flow dominated) and evaporation (Sahu, Parija, & Panigrahi, 2009).

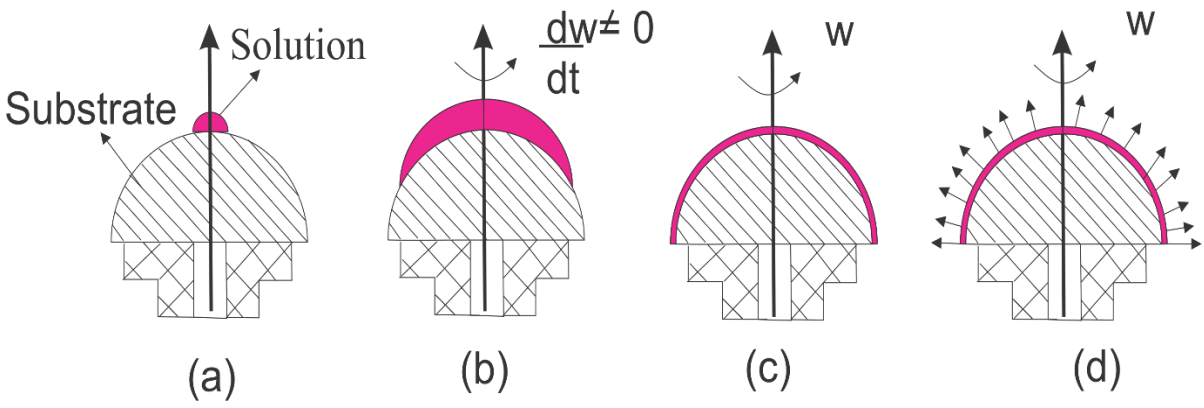

Fig. 1.1 Spin coating stages (a) Deposition (b) Spin-up (c) Spin-off (d) Evaporation

1.1.1 Deposition

In the first stage of spin coating, a photo resistive coating liquid is deposited on the substrate or wafer. The coating fluid is set to fall on a substrate, and the substrate is spun to the required angular speed. The centrifugal force spreads the photo resistive polymer over the substrate.

This stage customarily delivers a considerable excess of the polymer liquid compared to the quantity that would ultimately be necessary for the coating film thickness. A sub-micron filter can be used for dispensation to remove elements that could cause defects discussed in section **1.2.1**. A significant problem is whether the liquid can thoroughly wet the substrate surface during this dispensation point. If not, that may result in an incomplete coating of surface and can create some significant defects (Sahu et al., 2009).

1.1.2 Spin-up

In the second stage, the substrate is gradually accelerated to the required angular speed of rotation such that the desired coating thickness of the fluid can be achieved. This process is classified by the expelling of the liquid from the substrate surface. In this process, spiral vortices can form because of the significant liquid depth on the substrate. These vortices are a consequence of the twisting motion caused by the inertial force applied by the upper side of the liquid layer, while the substrate below rotates rapidly. The coating solution is thin enough to co-rotate fully with the substrate, and any indication of differences in liquid thickness is gone. Mostly, the substrate reaches its required angular speed, and the coating fluid is adequately thin to equalize the centrifugal accelerations with the viscous shear drag precisely (Sahu et al., 2009).

1.1.3 Spin-off

In the third stage, the substrate material spins at a uniform speed, and the viscous effects of the fluid govern the uniformity of the liquid. Liquid thinning is relatively consistent, although, with fluids consisting of volatile solvents, interference colours are perceived during this process discussed in section **1.2.2**. Edge effects are observed because the liquid moves radially outward consistently, nevertheless the edge droplets must be present during spin-off else the solution cannot coat the entire surface (Sahu et al., 2009).

1.1.4 Evaporation

In this stage, the coating thinning activity dominates over the centrifugal outflow, when the wafer material spins at a uniform rate and the coated liquid evaporates uniformly over the substrate surface area. Centrifugal outflow stops during this stage, and additional thinning occurs due to the loss of solvent in the coating solution. A micro-thin fluid film is created on the substrate surface. The dissolved or diluted solvent can develop viscosity change at the fluid

surface. Two main factors that control the rate of evaporation are the partial pressures of each solid species between the free surface of the fluid layers and the natural convection (ambient air) in the surrounding fluid (Sahu et al., 2009).

1.2 COMMON DEFECTS RELATED WITH SPIN COATING PROCESS

1.2.1 Comets

Comet defects (***Fig.1.2.1***) happen when a particle, more significant than the ones in the coating, interferes with the typical progression of the covering of the solution on the spinning substrate. These particles may come from dirt or dust on the substrate or from within the coating solution. The centrifugal outflow in the spin coating process usually is smooth and radial, so this defect commonly occurs in the deposition process. The use of sub-micron particle filtration during the liquid dispensing stage is beneficial to stop dirt and dust particles during the coating process. The common comet-shaped abnormalities of the film thickness often originate either from insufficient cleaning of the substrate or from an expired photo resistive solution. This defect can be eliminated by dispensing through a filter that removes unwanted particles from the solution and conducting experiments in dust-free yellow room environments can further minimize or remove the presence of comets (Tyona, 2013).

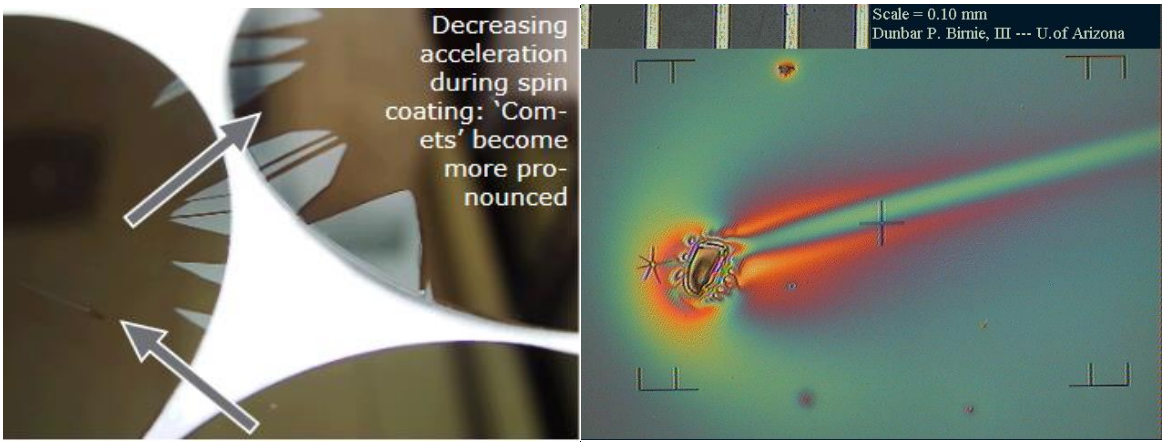

Fig 1.2.1 Spin coating Comet defect (Birnie, Zelinski, Marvel, Melpolder, & Roncone, 1992; chematscientific, 2020)

Figure (***Fig. 1.2.1)*** shows spin coating comet defect on a silicon wafer, decreasing angular speed during coating process will enhance the comet defect. A decreasing acceleration in the arrow direction on the final spin speed increases the risk of comet defects.

1.2.2 Striations

Spin coating striations defects occur because of the evaporation of one solvent rather than the other. As the name implies, striations look like stripes or waves on the surface due to the variable thickness of the spin coating. Striations are lines of varying thickness with a 50-200 micrometres range spacing or pattern, which are radially oriented in the coated film. The occurrence of this defect is due to the effects of surface tension driven by evaporation in the direction of significant fluid flow. The early evaporation of highly diluted solvents in the top surface layer may cause an accumulation of less volatile species at the bottom of the polymer coating during the spin-up stage. If this layer's surface tension is larger than the solution, then there is instability where the higher value surface tension attracts photo-resist material at intermittent intervals. This defect is due to the principle of the Marangoni effect of drainage patterns that regulate the structural expansion of film. These striation defects are now known to be the result of capillary forces that become unbalanced as a consequence of the solvent evaporation during the spin-up process. The evaporation process causes a different composition of surface tension of liquid on the top layer. The surface top layer can become unstable due to disturbances of long-wavelength, which develop striation defects. Preventing evaporation during the spin-up process is the easiest way to avoid striation formation (Tyona, 2013)

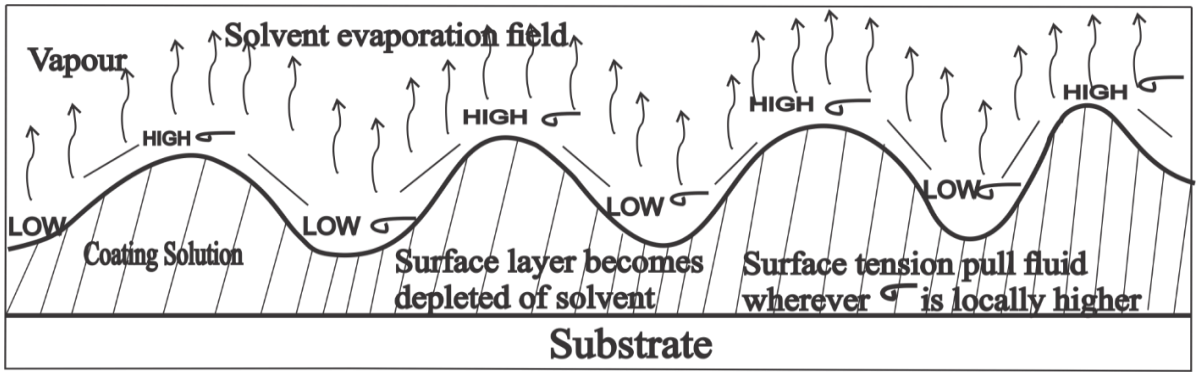

Fig1.2.2 Schematic diagram shows spin coating striation defect due to the effects of surface tension driven by evaporation

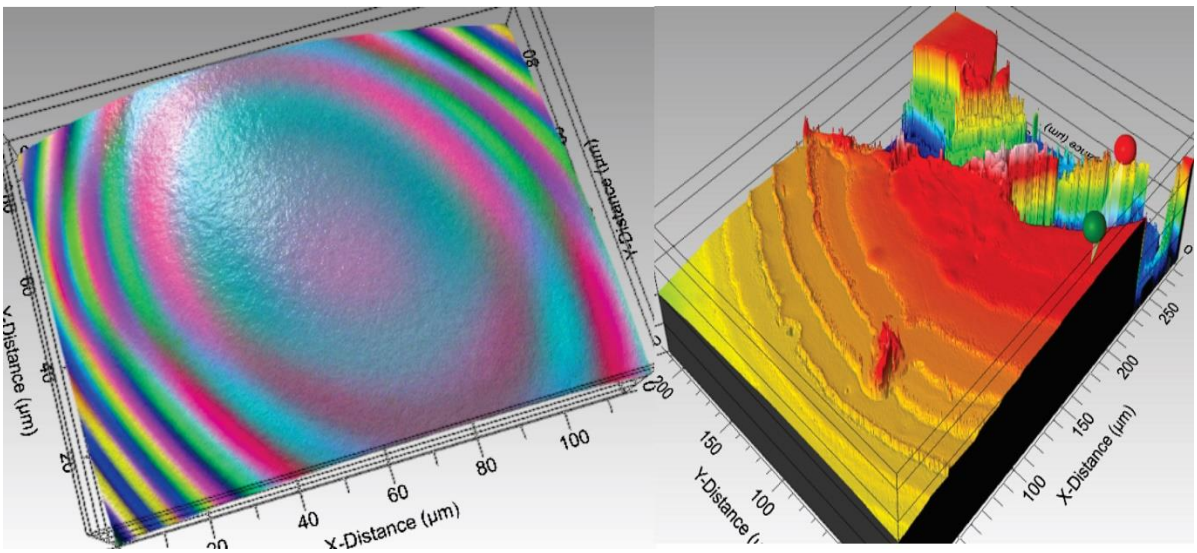

(a) ***(b)***

Fig1.2.2 Spin coating striation defects (JimE, 2019; Jose, 2020)

Figure (***Fig. 1.2.2)*** shows the schematic of the film contour evolution of the final film thickness distribution by the spin coating process. It shows the striation defects evolution of spin-coated film contour from the optical profilometer of the surface thickness on a flat plate silicon wafer and a curved glass substrate. (a) The interference colours were produced by the varying thickness of polymer film on a Si wafer. (b) The film contour was measured using optical profilometer of the surface thickness on a hemispherical glass substrate. When a positive photo-resist polymer AZ1518 was spun at a uniform angular speed of 3500 rpm.

Chuck marking defects can be formed by the heat transfer between the spin coating solution on the substrate top and the metallic vacuum chuck attached on the substrate backside. This defect occurs when the temperature of the chuck is different from that of the substrate, making the material thermal conductivity extremely relevant. Chuck marks defects mainly occur during the evaporation process. Even though chuck marks faults are entirely caused by solvent evaporation, lowering solvent volatility or spinning in solvent-rich environments can help to alleviate that problem. It is recommended that suction chucks are modified so that they have uniform physical contact on the rear of the substrate (Birnie et al., 1992).

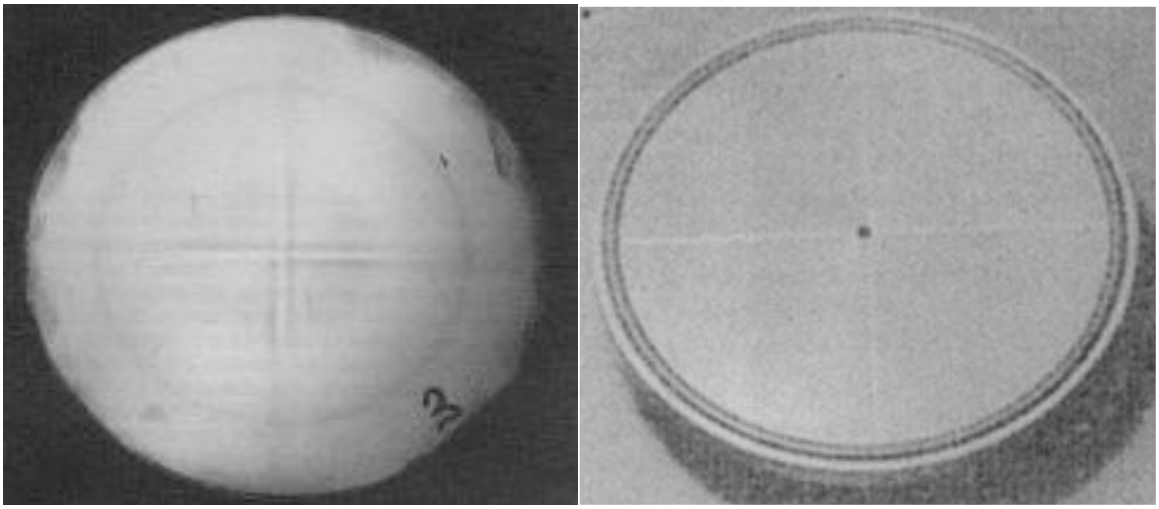

Fig 1.2. Chuck mark defects on the spin coated flat substrate (Birnie et al., 1992)

1.2.4 Wafer Edge Effects

Surface tension may cause a bead to form at the edge of the substrate creating a thicker layer on the outermost edge as the bead spins. Edges are also problematic on square-edged substrates, as the corners produce a different airflow compared to the round shapes. In the process of thick coating photo-resistant films, an edge bead defect can impede the photolithographic mask to stick together and create an unwanted proximity gap during exposure. The solution to avoiding wafer edge effects is to retain the uniformity during spin coating. The photo resistive film should be solvent-less enough to avoid further evaporation, while the edge bead requires a viscosity small enough to spin-off properly.

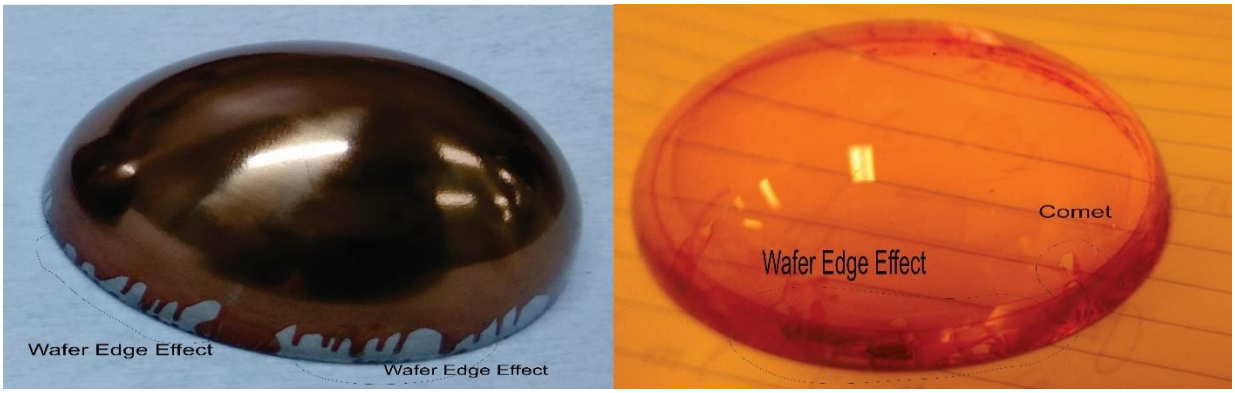

Fig 1.2.4 Wafer edge effect defects in metal and glass spin-coated hemispherical substrate when a positive photo-resist polymer AZ1518 was spun at a uniform angular speed of 3500rpm.

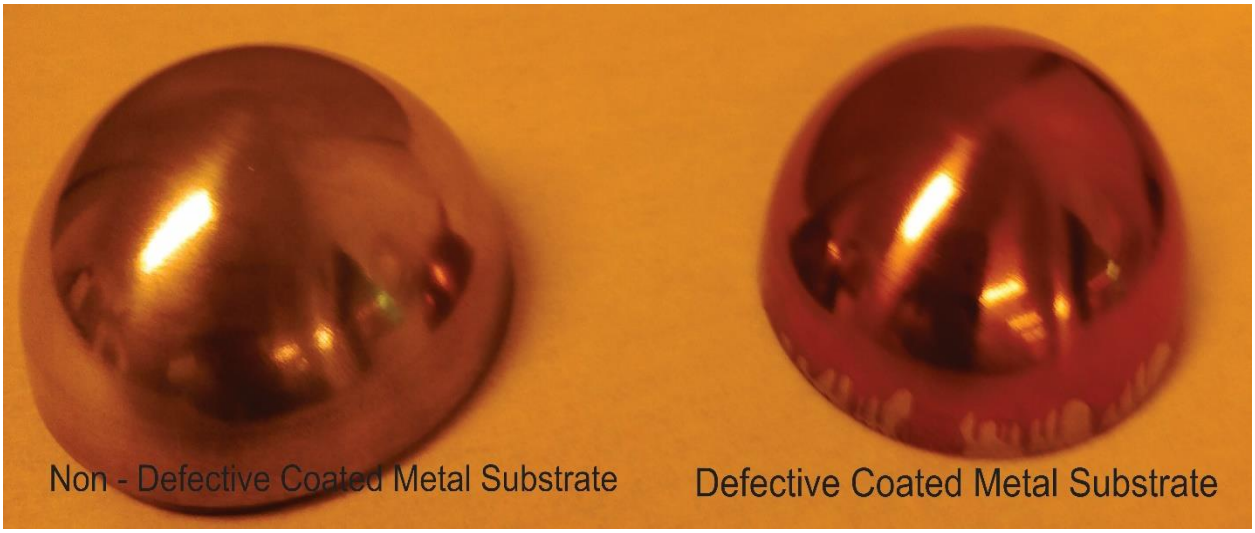

Fig 1.2.5 Wafer edge effect defect on the spin-coated hemispherical metal substrate with and without defect, when a positive photo-resist polymer AZ1518 was spun at a uniform angular speed of 3500rpm

Figures (***Fig. 1.2.4 and Fig.1.2.5*)** show the wafer edge effect defect on a spin-coated hemispherical metal substrate of 50 mm diameter and glass substrate of 60 mm diameter when a positive photo-resist polymer AZ1518 was spun at a uniform angular speed of 3500rpm.

1.2.5 Environmental Sensitivity

During the process of spin coating in an experimental environment, the surrounding region may affect the consistency of the coating. The environmental property of the ambient air is relevant to the uniformity of the film, especially in the evaporation stage. Varying quantities of moisture in the nearby region may result in the quality of the coated film. This defect can result in the roughness of the coating, micro cracking on the film after further dehydration, and excessive striation defect. Closer monitoring of the surrounding during the spin coating process is essential to mitigate the chance of environmental sensitivity defects.

1.2.6 Particles or Bubbles in Etching patterns

Particles and bubbles can serve as a channel for wet etching or masking processes on the resist film. The best method to avoid this defect is the double coating on the substrate because two particles or bubbles are difficult to pile one on top of the other (Tyona, 2013). The double spin coating can only be ensured with a high-viscous photo-resistivity solution since a high solvent concentration in the second coating would allow the current resist film to dissolve. In the case

of a low viscous photo-resistive solution, this defect can be avoided by a soft bake between the two coating phases (***Fig. 1.2.6***). Spin coating directly after the second photo-resist solution dispersion in alliance with an increase of velocity suppresses the dissolution of the first resist film.

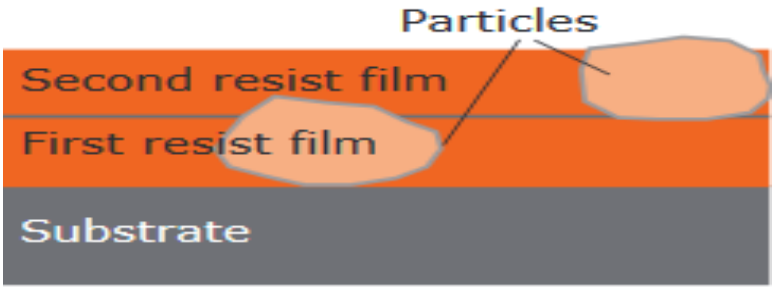

Fig 1.2.6 Spin coating particle and bubble defect (microchemicals, 2020)

The main reason for a defective coating on the substrate surface can be an insufficient resist solution volume. It was recommended that 1-5 ml volume per substrate surface subject to the viscosity of photo resistant solution, the required substrate dimensions and coated film thickness (microchemicals, 2020). The coating can be improved by dispensing the photo resistive solution as centrally as possible. In the case of flat substrates, a high acceleration (> 1000 rpm) towards the final spin speed eradicates the presence of uncoated or defected parts on the substrates. Alternatively, the textured substrates might require a two-step spin profile. In the first step, a comparable quantity of high-resistant liquid has been distributed for a few seconds at a lower spinning rate (<1000 rpm). In the second stage, the ramping up to the required spin speed adjusts the final photo-resist film thickness.

1.3 APPLICATIONS

Spin-coating techniques are used widely for microelectronic industry applications. Silicon wafers are photo-lithographically masked with a circuit design by coating wafers of semiconductors with a polymeric photo resistant film which is eventually exposed by masks to the circuit design. Microelectronic application of polymers should have low dielectric coefficients, strong adhesive capacity and excellent mechanical and thermal characteristics (Sahu et al., 2009). Due to the hygroscopic properties of many polymers, they have proved relevant in the domain of psychometric property measurements, which was used to manufacture the products related to medicine, metrology, process control, and agriculture.

There are many applications of spin coating from the past few years in the area of sensors. A spin-coated thin layer of protective coatings was extensively used in industrial applications, such as UV light protection, protective coating against corrosion and diffractive optical elements (***Fig 1.3.1***). Recently, the spin coating has been used for optical data mass storage in media. Spin coating is currently limited to flat surfaces, but there is an increasing need for this process on curved surfaces. The recent application of the spin coating in thin-film amorphous silicon solar cells is beneficial since amorphous silicon could be made thinner, which might result in reduced costs of production.

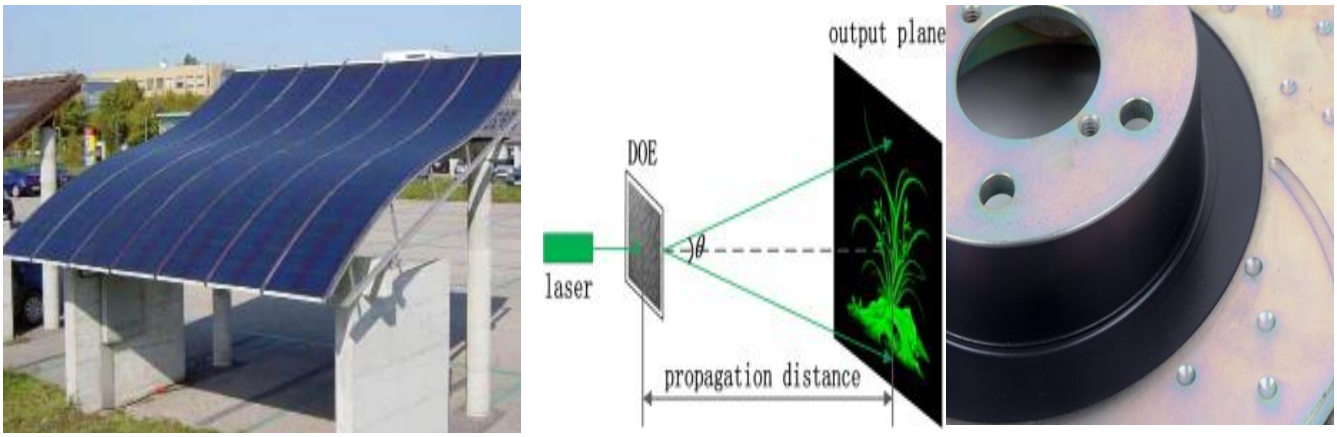

(a) **(b)** **(c)**

Fig 1.3.1 (a) Amorphous silicon solar cells (b) Diffractive optical element (c) Protective coating against corrosion(cells, 2020; Pang, Yin, Deng, Qiu, & Du, 2015)

1.4 OBJECTIVES

This research seeks to analyse the characteristic behaviour of spin coated thin film on a curved surface with the help of single-axis spin coater and how the film thickness differs from a flat surface. A study on the uniformity and distribution of film thickness were conducted with the help of numerical and experimental analysis based on the radial distribution of film thickness.

1.5 METHODOLOGY

1.5.1 Numerical Analysis

The numerical model describes the evolution of the coating layer thickness on a curved surface subject to complex motion kinematics. Design and numerical analysis of spin coating on curved surfaces were carried out using CFD analysis software COMSOL 5.3a Multiphysics, with the microfluidic module.

1.5.2 Experimental analysis

The characteristics behaviour of the spin coated hemispherical glass, and metal substrate thin film was examined in the Nanofabrication laboratory (Nano Lab) in Electrical and Computer Engineering (ECE) Department, University of Canterbury. These facilities allow for the analysis of radial and circumferential distribution of film thickness. The experiment analysis was conducted in the following three steps:

Step 1: An experiment was conducted on a silicon wafer flat substrate using a single axis spin coater (Spin coater -Laurell WS-650 and Headway PWM32-PSR790). The coating thickness of the spin-coated flat substrate was analysed using an optical profilometer (Filmetrics, Profilm3D). A comparative study was conducted on a spin coated glass substrate and a hemispherical glass substrate **(Step 2).**

Step 2: An experiment was conducted on a hemispherical glass substrate with a diameter of 60mm using a single axis spin coater (Spin coater -Laurell WS-650). The coating thickness of the spin-coated hemispherical substrate was analysed using an optical profilometer (Filmetrics, Profilm3D), and the measurement was compared with an Atomic Force Microscope (AFM).

Step 3: An experiment was conducted on a hemispherical metal substrate with a diameter of 50 mm using the single-axis spin coater. The same analysis outlined in step 1 conducted.
The types of equipment that employed for estimating film thickness are LEO FEG-SEM, Atomic Force Microscope (AFM) Digital Instruments Dimension 3100, Surface Profilometer DEKTAK 150, Filmetrics Profilm3D optical profilometer, optical microscopy, and an ellipsometer.

2 LITERATURE REVIEW

For several years, a variety of approaches and considerable effort has been devoted to the study of spin coating on flat surfaces. M. D. Tyona and Sahu et al., examined the theory of the spin coating process, clearly outlining the basic concepts, and parameters governing the procedure (Sahu et al., 2009; Tyona, 2013). These parameters include spin time, angular acceleration, spin speed, and solution evaporation. The spin coating process involves four stages: a dispensing stage (dispensation), substrate acceleration stage (spin-up), a stage of substrate spinning at a constant rate where fluid viscous forces dominate fluid thinning performance (spin-off), and a stage of substrate spinning at a constant rate where solvent evaporation dominates the thinning performance of the coating (evaporation) (Sahu et al., 2009; Tyona, 2013). Their study explored some typical thin-film defects related to the spin coating process: comet, edge effect marks, striation, environmental sensitivity, and chuck marks. A mathematical model for comprehending the powerful mechanism governing the formation of films was derived. It led to a relationship between film thickness and radial position on the film.

2.1 SPIN COATING ON FLAT SUBSTRATES: THEORETICAL MODEL

The spin coating technique has been employed for many decades for the application of thin films. A mathematical model was suggested by Meyerhofer which examined the linear shear force, centrifugal force, and uniform evaporation of the solvent (Meyerhofer, 1978) and compared the model with experimental results acquired from positive photoresists solvent. During the process of spinning, the liquid forms a uniform level surface which is independent of the size of the substrate. Meyerhofer found that the rate of evaporation is proportional to the rate of airflow over the substrate. The author further established a spin coating model for a Newtonian fluid using the continuity equation but allowed for the evaporation of the solvent during the spinning process. He estimated that fluid height h could be segregated into solid-phase S height and liquid phase height$L$.

Emslie et al., created a mathematical model describing the flow of a Newtonian liquid on a rotating disk which helped in constructing characteristic curves and surface contours at successive intervals for any arbitrary initial fluid distribution (Emslie, Bonner, & Peck, 1958). It was proven that the uniformity of the initial fluid layer remains constant after centrifugation

even when the height of the fluid layer was reduced. For any initial successive plot, a new contour could be created after any given time of centrifugation. The successive surface contours were created to obtain corresponding families of initial distributions using Gaussian, slowly falling, Gaussian plus uniform and sinusoidal distribution. The authors incorporated the edge effects on rotating planes with rising rim and fluid flow on nonplanar surfaces. Their assumptions on the fluid exhibiting Newtonian flow behaviour was violated in various situations that involved suspensions and highly viscous fluids.

A one- dimensional model of spin coating with film thinning was presented by Bornside et al., using convective outflow and solvent evaporation. This model depends on solution viscosity, variations of concentration, and diffusivity across the thickness of the spin-coated film. In this model, a balance between centrifugal force and viscous drag force are the main factors influencing the flow (Bornside, Macosko, & Scriven, 1989). However, the authors did not consider radial variations in film thickness and concentration. To solve the model, they employed the Galerkin / finite element method (FEM), a modern solver technique. Initially, the rate of film thinning reduces as the film thickness decreased; however, the increasing viscosity of the coating liquid due to solvent evaporation enhanced the rate of film thinning. Two methods were suggested to enhance the film thinning, one of which was to saturate the overlay gas with liquid and the other was to use a coating liquid which had various volatile solvents. The temperature of the coated film remained almost constant with the surrounding temperature.

According to Acrivos et al., a general theoretical model of flow using a power-law on a rotating disk was formulated. They studied the possibility of calculating the variation of the shape of an initial contour with time (Acrivos, Shah, & Petersen, 1960). Their motivation was that non-Newtonian fluids have more potential industrial application than Newtonian fluids. The possibility of getting the desired film thickness was low because even an initial uniform thickness was distorted during spinning, in contrast to Newtonian fluids, where the initial uniform thickness after spinning remained the same. They formulated a mathematical expression for the possibility of the surface contour of non – Newtonian fluid with spinning time and concluded that the spin coating process for obtaining uniform film thickness has a much better possibility if the fluid is Newtonian than non- Newtonian.

Flack et al., noted that polymer resists film thickness and profile uniformity are the two critical factors for creating better lithography in micro process manufacturing (Flack, Soong, Bell, &

Hess, 1984). An empirical correlation was generated to elucidate the numerous process variables such as concentration, spinner acceleration, and final spin speed, which independently dominate the mechanism of film formation. The non-Newtonian behaviour of the resist solution, as well as, the solution viscosity and diffusivity with varying polymer concentration, was considered. The authors found that solvent evaporation and convective radial flow of the resist solution are the two critical factors which affect polymer film thickness. During the early stages of film thinning, convective radial flow dominates, whereas, in the end, solvent evaporation has a significant role in film formation.

B.D. Washo developed a mathematical model and a quantitative relationship between both the thickness of the spin coating and polymer material (Washo, 1977). The model predicts that the most straightforward and most reproducible outcome of the spin coating process occurs when the process is operating with the area defined by the low, steady-state, radial flow. The author experimented on Newtonian-like polyamide in iso-amyl alcohol solutions on large rotating substrates, and the model showed excellent correlation with the measurement.

L.H. Tanner studied the spreading of silicon oil drops on a horizontal surface with emphasis on the surface tension and the dominant effects of the condition near the edge (Tanner, 1979). The author predicted the edge profile and showed that the slope at the inflexion is proportional to the cube root of edge velocity at the inflexion. The profile deviates from the circular arc with a combination of surface tension and gravitational force, causing the displacement. The observations were correlated with silicon oil experiments conducted on a horizontal surface and obtained good agreement.

Lin Wu performed a numerical study of spin coating on an axis-symmetrically heated disk under zero dimensionless, Biot number and lubrication (Wu, 2006). The author included many process parameters in the simulation such as thermoviscosity (temperature-dependent viscosity), thermocapillarity (temperature-dependent surface tension), radial acceleration, surface tension, viscosity, external air shearing, and disjoining pressure. The effects of thermocapillarity and thermoviscosity considerably enhanced the film thinning rate when the temperature of the outer disk edge was lower than the disk centre. The thermocapillarity effect on the film coating was insignificant at the initial stage of the spin coating when the film thickness was large. However, it became dominant when the film thickness was reduced.

A theoretical and numerical analysis was proposed by Sadao Shimoji based on both Newtonian

and non-Newtonian fluid for the changes of the film thickness of a polymer solution on a flat rotating disk (Shimoji, 1989). Regarding the non-Newtonian characteristics, the power-law and Carreau models were used. The influence of the dry-film thickness on the initial solute concentration anticipated by the Newtonian fluids was well in line with experimental data. This evaporation model successfully demonstrated the dependence of dry film thickness.

According to Stanley Middleman, airflow induced by disk rotation in the spin-coating process for the production of thin films provided shear stress at the liquid-air interface which improved the thinning rate of the liquid film on the disk (Middleman, 1987). The author provided a comparative analysis using the classical Cochran solution (Cochran, 1934) for the induced airflow. The impact of induced airflow enhanced the rate at which thin film was obtained. As film thickness became quite small, the centrifugal effect was dominated by external airflow, and the final thinning rate was controlled.

In the theoretical and semi-empirical model proposed by Mouhamad et al., the initial phase of film formation was usually not presented by standard models explaining the spin coating of polymer solutions when hydrodynamic forces regulate the behaviour of the solution (Mouhamad, Mokarian-Tabari, Clarke, Jones, & Geoghegan, 2014). It was found that the inertial forces played an essential role in the amount of thinning of the solution. A semi-empirical method was formulated, which allowed an estimate of the rate of solvent evaporation and temporal evolution of the fraction of the solute volume and the corresponding viscosity of the solution.

The flow of non-Newtonian liquids on a flat rotating disc surface was studied by Jenekhe et al., using the power-law and Carreau equations (Jenekhe & Schuldt, 1984). Numerical solutions obtained by numerical integration of the diagnostic method for the film thickness profile were expressed as a function of spinning time, displaying the dynamics of the spin coating process for the formation of polymer films for microelectronic devices. Even irregular (sinusoidal, Gaussian) initial film thickness profiles of Carreau fluids were found to smooth out into uniform films after an adequate spinning time. Power-law fluids had shown steep gradients in their film thickness profiles and a significant rise at the origin.

The progressive formation of a thin fluid film on a rotating disk was analytically studied by Dandapat et al., under the action of thermocapillary force (Dandapat & Ray, 1994). The thermocapillary parameter is an indicator of the surface tension component with temperature.

The thermocapillary force on the free surface was employed to stimulate the thinning rate for cooling the disk. The film thickness for heating increases with increments of thermocapillary variable whereas when the disk is cooled, this variable improves the thinning of film. As the disc was axi-symmetrically cooled, the surface tension at the disk centre was weak, and thus, a thermocapillary flow was induced at the free surface in the radial direction of flow.

2.2 SPIN COATING ON FLAT SUBSTRATES: EXPERIMENTAL MODEL

Hall et al., examined the film coating of thin (>200 nm) and ultra-thin (<200 nm) films by varying the volatile concentration of polymer and spinning speed (Hall, Underhill, & Torkelson, 1998). They compared their experimental analysis with the previous mathematical model proposed by (Bornside et al., 1989). They successfully predicted the film thickness using the initial properties of the solution, solvent and spin speed and were able to predict the experimental and theoretical variation by 10 %. The Bornside's mathematical model was under-predicted when the solution had high initial polymer concentration, whereas it was over predicted when the solution had a very dilute polymer concentration. The over-prediction may have been due to the negligence of solvent evaporation in the model.

A methodology by Manske et al., was proposed for real-time, in situ calculation of film thickness evolution over confined topography during spin coating (Manske, Graves, & Oldham, 1990). To illuminate a microscope based on a confined feature being coated on the wafer, a laser was pulsed synchronously with a spinning wafer switch. Interference fringes were photographically captured to allow the observation of film thickness contours from the initial spin-up to the final dried film. Using this approach, the team observed the effect of flow direction and the microscopic shape and orientation of film profiles during spinning and drying processes.

2.3 SPIN COATING ON CURVED SUBSTRATES: THEORETICAL MODEL

Feng et al., examined the final film thickness of spin-coated photoresist on a spherical substrate (Feng & Sun, 2005). The authors found that the final photoresist thickness is independent of initial film thickness and initial material amount. They derived a mathematical expression governing the final film thickness, shown in equation (4).

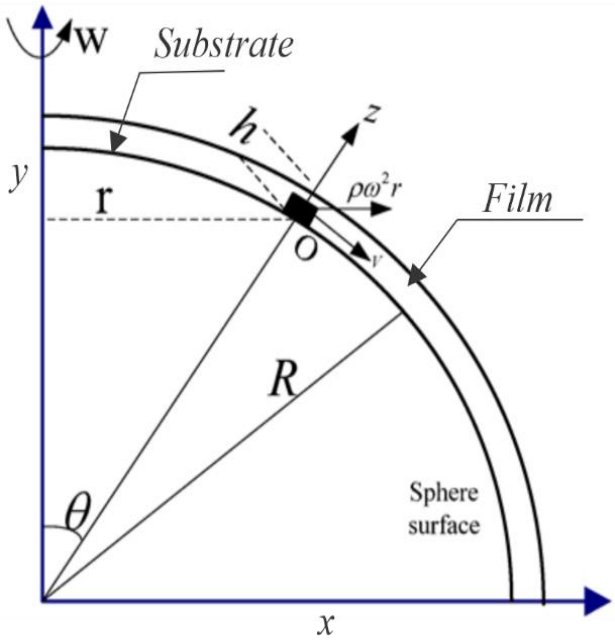

Fig.2.1 The schematic diagram of Infinitesimal fluid rotating on a spherical substrate (Feng & Sun, 2005)

$$h = h_0\left(1 - \frac{4gh_0^2t}{3\mu R}\right)^{-\frac{1}{2}} \quad (1)$$

$$r \leq \sqrt{R^2 - \frac{g^2}{\rho^2\omega^4}}, \quad (2)$$

$$\frac{r}{R} \approx 0.816 \quad (3)$$

$$h_f = S_f = c_0 h_{\frac{1}{3}} = c_0\left[\frac{3\mu R.C\sqrt{\omega}}{(1-c_0)(2\rho\omega^2\sqrt{R^2-r^2} - \frac{\rho\omega^2 r^2}{\sqrt{R^2-r^2}} - 2g)}\right]^{\frac{1}{3}} \quad (4)$$

where, r is the radial position, ω is the angular velocity, R is the sphere radius, ρ is the fluid density, C is the laboratory coefficient of device, S_f is the final solute thickness, g is the gravity force, e is the rate at which solvent evaporation takes place and h_f is the final film thickness. The mathematical expression with experimental results on a spherical concave substrate of radius 20mm, the angular speed of 2000rpm, c_0=0.015, g=0, $\mu/\rho \cdot C\sqrt{\omega}$ =0.03 $\frac{m^2}{s^2}$ Moreover, tested and validated the final film thickness by Atomic Force Microscope

Schwartz et al., formulated the effect of substrate curvature on the temporal evaluation of a thin film coating (Schwartz & Weidner, 1995). The authors derived a mathematical model for a Newtonian viscous liquid that included various substrate shapes, possessing both inside and outside corners. They derived from a model that the viscosity of the liquid is not constant and can vary with time of evaporation. They studied how surface-active material and liquid composition affect surface tension and found that the main reason for corner defects is due to continuous changes caused by the surface tension gradient of the liquid film. A technique was proposed to achieve uniform film coating for the corners, either by introducing surface tension force parameters in the liquid when the liquid is pulled back into the corner before drying or by suitably arranging the time of evaporation.

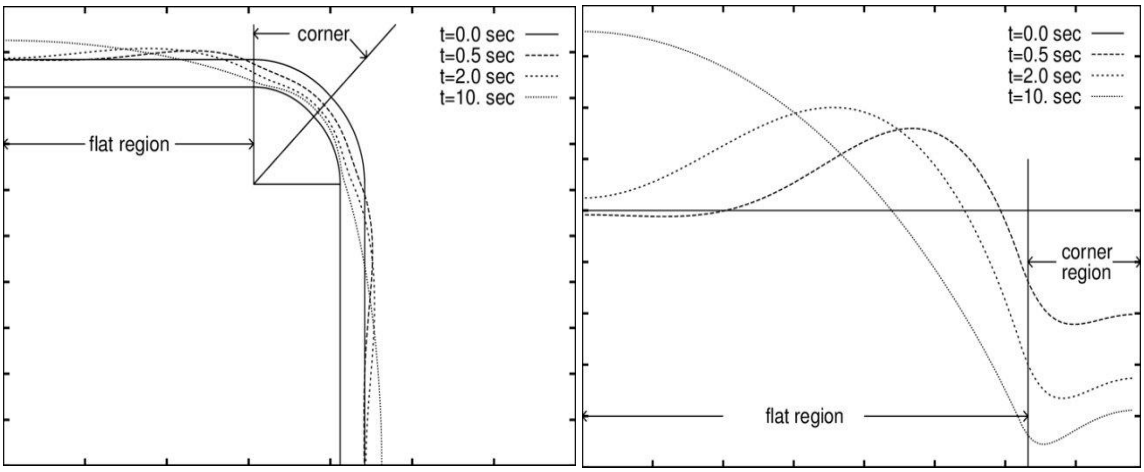

Fig.2.2 The flow away from an outside corner for a non-evaporating Newtonian liquid of constant surface tension. Here the corner radius is 0.1 cm. The coating profiles were shown at various times. (Schwartz & Weidner, 1995)

Roy et al. introduced a lubrication model of dynamics to express film thickness (Roy, Roberts, & Simpson, 2002). In this model, the Navier-stokes equation for a Newtonian fluid was expressed in a co-ordinate system fitted to the curved substrate. The effect of the curvature of the substrate was effectively and accurately demonstrated using the physical multiple-scale approach. They successfully simulated the flow around a torus and the evaporation of a film down a cylinder.

The lubrication Theory was used by Howell to solve the mathematical model governing thin viscous film over a moving curved substrate. The author formulated an asymptotic expression to solve the leading order equation (Howell, 2003). It was found that for a small substrate curvature, film flow is a fourth-order non-linear parabolic equation, whereas for an extensive

substrate curvature film profile follows a hyperbolic partial differential equation. The author applied this theory to two exceptional cases: flow over a torus and flow on the inside of a flexible axisymmetric tube.

Weidner derived the lubrication form of an equation with the use of a scaling argument and perturbation method to formulate the fluid motion of thin liquid film on a curved, rotating axisymmetric substrate (Weidner, 2018). The author successfully developed a numerical model to simulate the interior of food and beverage cans using an implicit finite difference approach.

Kang et al., studied the dynamics of a thin viscous liquid film on the external surface of a sphere, which rotates around its vertical axis in the presence of gravity (Kang, Nadim, & Chugunova, 2016). In a rotating co-ordinate scheme based on the lubricant approximation, a non-linear model of film thickness distribution was obtained. The model identifies the influences of centrifugal and gravity forces, and the surface tension stabilizing effect. In their analysis, the sphere surface is entirely stationary and entirely stable. Due to rotation, the centrifugal force guides the fluid towards the equator.

Hansen et al., investigated steady, free-surface, viscous flow on a rotating cylinder using an iterative, integral-equation formulation applied to the Stokes approximation of the Navier-Stokes equations (Hansen & Kelmanson, 1994). A range of flow parameters, free-surface profiles and free-surface velocity distributions were provided. Results exhibited a high degree of symmetry on a horizontal axis for all film thicknesses and surface tension while the field of gravity was vertical.

Evans et al. presented a theoretical and numerical model for steady and unsteady solution for coating flow on a rotating horizontal cylinder (Evans, Schwartz, & Roy, 2004). This cylinder rotated about its z-axis carrying liquid around its contour. The authors included parameters such as rotational effect, surface tension, and gravity. For the model, which was implemented using an implicit method of finite difference, a numerical methodology was designed to extract solutions to the two-dimensional form. The surface tension had limited influence over most of the cylinder at a slow rate of rotation resulting in hanging pendant drops beneath the cylinder. When the rotation rate increased, the distribution of liquid over the cylinder increased.

M.I. Khodabocus et al., introduced a mathematical model for the film thickness in the fourth-

order non-linear h-evolution equation subject to volatile liquid source and wind blow effect (Khodabocus, Sellier, & Nock, 2019). They found that under the volatile solvent source and air-blow effect characteristics of thin-film would enhance the surface tension, which led to the flow induced by the Marangoni effect. They analyzed the surface tension gradient on the surface layer and the continuous pressure gradient flow in parabolic transformation. The surface tension gradient affected the equilibrium of fluid film thickness, which was ignored by various authors.

R.G. Shepherd et al., investigated an extended model based on lubrication approximation of spin coating on a rotating sphere by introducing an arbitrary body force (R.G. Shepherd, 2020). The authors found the centrifugal force to be the principal cause of accumulation of liquid near the rotating sphere equator. In this model, they managed non-dimensionalized parameters, including surface tension effect, gravity, polymer evaporation, and centrifugal force. They analyzed that the smoothness and uniformity of spin-coated spherical substrates deteriorated with an increase of centrifugal force and either the non-dimensional parameters Bond or Galilei numbers.

2.4 SPIN COATING ON CURVED SUBSTRATES: EXPERIMENTAL MODEL

A study by Chen et al., introduced the photoresist thickness distribution on a convex surface substrate (Chen, Liang, Luo, Zhang, & Yang, 2009). They conducted an experiment using the same rotational speed with different radii of curvature, and the same substrate at different rotational speeds. The group introduced a theoretical thickness distribution model which guided convex surface coating. They measured the film thickness using spectroscopy, ellipsometry, and a profilometer.

Mahmoodi et al., studied a new technique for spin coating called two- dimensional (2D) spin coating (Mahmoodi, Guoqing, & Khajavi, 2016) (Mahmoodi et al., 2020). The authors considered vertical centrifugal force (VCF) on a rotating machine perpendicular to the substrate. They found that high gravity acceleration due to VCF adjusts and normalizes the high and low surface tension stresses. An experimental and theoretical analysis of 2D spin coating was conducted using AFM and scanning electron microscopy (SEM) to analyze surface roughness. They found that 2D spin coating could minimize some common coating defects such as edge beading, cloudiness, inner layer bubbling, and unsmooth surface levelling.

Additional research by Liu et al., formulated a mathematical model for solving spin coating on the spherical surface with large central angles (Liu, Fang, Meng, & Wang, 2017). The values of a film thickness of the spherical surface by spin coating were validated with experimental results. They introduced new dimensionless parameters which control film thickness and uniformity. Their model successfully predicted the film thickness profile on a spherical surface with large central angles but did not incorporate the evaporation effect and non-Newtonian fluid property.

Lee et al., studied the rapid production of hemispheric elastic shells by coating a polymer solution on a curved surface (A. Lee et al., 2016). The authors found that the coating thickness of the elastic shells was a function of the geometry of the substrate and material properties of the polymer. They noted that the final thickness of the coating depended on the pouring direction and orientation of the surface. The variation of film thickness from the equator to the pole in hemispherical shells was found and compared to the theoretical model.

Yoon et. al., explained the spin coating process for creating microstructures with curved surfaces. A liquid photoresist was used to fill an engraved microchannel profile on a silicon wafer (Yoon, Yoo, & Choi, 2012). Dependence on the surface tension of the liquid, curved surfaces, or rectangular channel shapes of microstructures could be achieved by photoresist spin coating. The outcome could vary depending on coating conditions, microstructure geometry and properties of photoresist. The final profiles of curved surfaces were analyzed using a replica of polymer that was added to the photoresist surface. The size, direction of the structures, viscosity, capillary force, and surface tension also influenced the result. The dimensionless parameter bond number was used to describe these parameters.

Spin coating applications are not only restricted to flat substrates (Acrivos, Shah, & Petersen, 1960; Bornside et al., 1989; Emslie et al., 1958) but also include curved substrates (Chen et al., 2009; A. Lee et al., 2016; Liu et al., 2017). Few authors have considered film coating on concave (Feng & Sun, 2005) and convex surfaces (Liu et al., 2017). This research seeks to analyse the characteristic behaviour of spin coated thin film on a curved surface with the help of single-axis spin coater and how it differs from a flat surface. This study also emphasizes mainly on the uniformity and distribution of film thickness on spin coated hemispherical substrates conducted with the help of numerical and experimental analysis.

3. EXPERIMENTAL METHODOLOGY

A single-axis spin coater (Laurell WS-650) experimental set up was used to coat a photoresist polymer of a thin film on a silicon wafer flat plate and hemispherical glass substrate of 60mm diameter as well as a hemispherical metal substrate of 50mm diameter. A positive photoresist polymer AZ1518 (MicroChemical, Germany), was used as a solution for coating. The photoresist is a light-sensitive material which, when exposed to light, changes its physical and chemical characteristics. Photoresist allows the structure of the circuit pattern to be transferred directly to a substrate

The substrate was attached to a single-axis spin coater (Laurell WS-650) (***Fig.3.1***) using a vaccum suction arrangement. It was recommended that 1-5 ml volume of photoresist per substrate surface area subject to the fluid viscosity of photo resistant solution, the required final thickness of the film and the substrate size(microchemicals, 2020). The result was improved by dispensing the photo resistive solution as centrally as possible on a substrate. To get consistent film coating thickness, the substrate should rotate first at a gradual speed (spin-up) and then a constant pace (spin-off). After, the coated photoresist was exposed to ordinary light. In this experiment, the substrate was spun at 0 -3500 rpm for 20 s at a ramped angular speed and then turned again at rpm of 3500 for 20 s at a uniform rate (***Fig.3.2*).**

Fig. 3.1 Experimental set up of single-axis spin coater (Laurell WS-650) on a hemispherical glass substrate

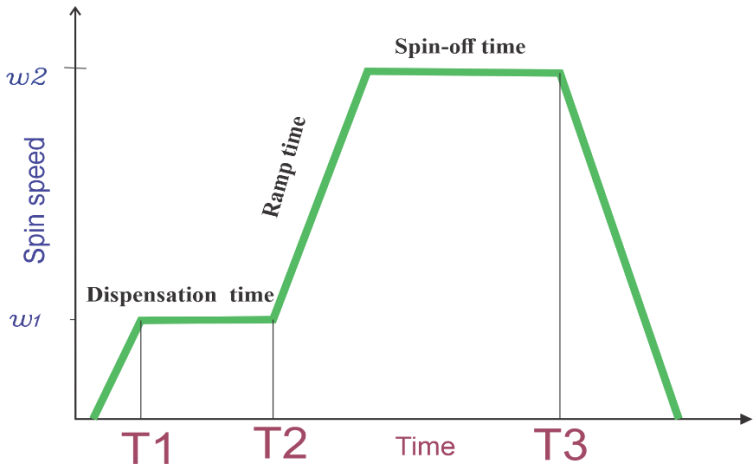

Speed variation with time

SPEED (rpm)	TIME (s)
0-500	5
500-1000	5
1000-2000	5
2000-3500	5
3500	20

Fig 3.2 schematic of single-axis spin coating experimental procedure

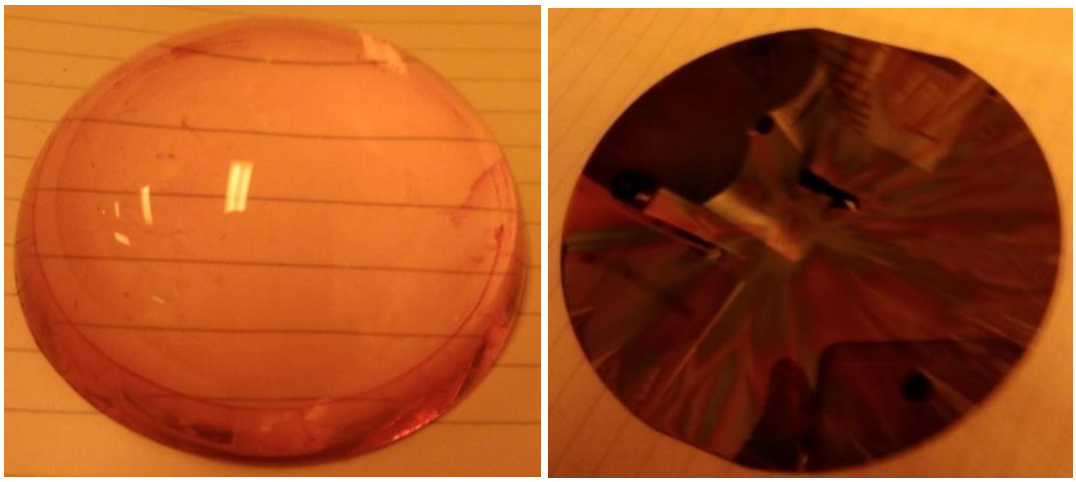

(a) (b)

Fig.3.3 Single-axis spin coated substrate with polymer AZ1518 spun at 3500 rpm

(a) Hemispherical glass (b) Flat silicon wafer plate

Figures (***Fig.3.3***) shows the positive photoresist spin coating of polymer AZ1518 on a curved hemispherical glass and a flat silicon wafer flat-plate substrate spun at 3500 rpm

A scratch was made on the coating surface, exposing the underlying substrate and enabling the measurement of the film thickness. The scratch corresponds to the height difference between the coated surface and the top of the substrate.

Figures (***Fig. 3.4*** and ***Fig.3.5*****)** show the radial distribution of film thickness measurement set up on spin coated hemispherical substrate using an optical profilometer (Profilm 3D, Filmetrics) with an angle plate attachment.

Fig 3.4 Measurement window for profilm 3D optical profilometer indicating zooming and focusing option.

The optical profilometer (***Fig.3.4***) has options: 10X, 20X and 50X, and for each focusing option, there are three zooming options: 1X, 2X and 4X. To determine the radial distribution of thickness on a curved coated hemispherical glass substrate, angle plates were used for mounting with varying angles (0 degrees for the top -90 degrees for the edges of the hemisphere).

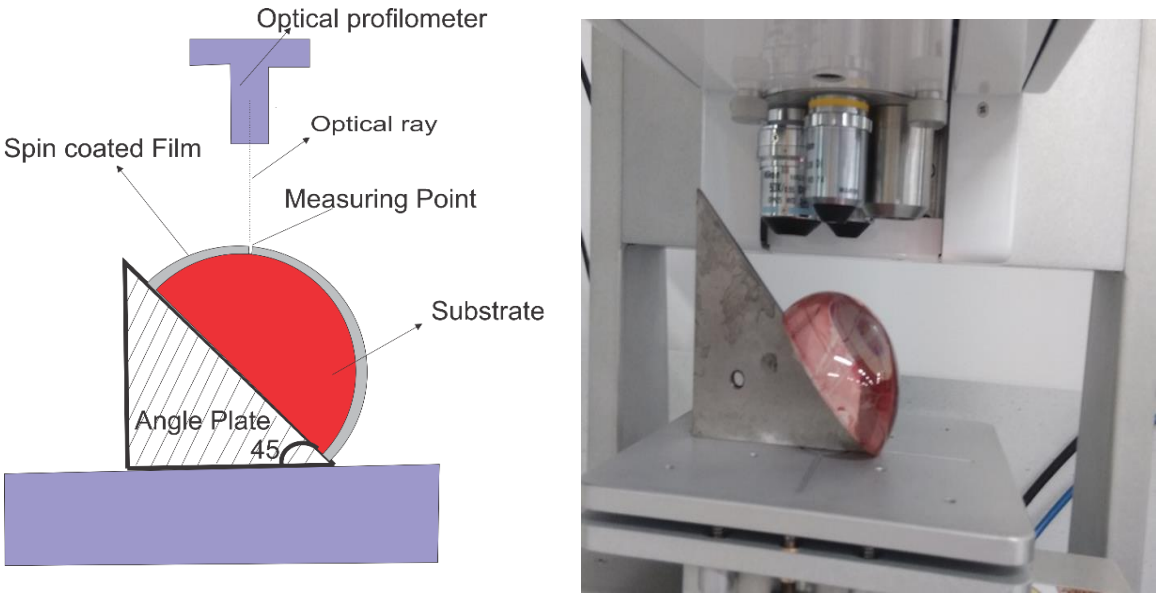

(a) **(b)**

Fig. 3.5 (a) Schematic of measurement setup for spin coated film thickness on a hemispherical substrate on an optical profilometer using an angle plate attachment (b) Spin coated film thickness measurement set up using profilm 3D optical profilometer with angle plate attachment.

The film thickness measurement ***(Fig. 3.5)*** was taken by scraping out a bit of the coated parts from the surface. The spin coated film thickness was obtained by differentiating the height between the coated surface and the uncoated surface of the substrate

3.1 MEASUREMENT OF THICKNESS USING OPTICAL PROFILOMETER

A profilometry is a tool for extracting surface topographical data with either a physical probe or even with light. Profilometry has the purpose of obtaining surface structure, phase elevations and layer thickness. Profilometry could be a specific element, a line checks or maybe even a 3D scan.

Profilometers contain two parts: a sample stage and a detector. The detector determines where the specific positions are on the, and what holds the sample is the sample stage. In some devices, the sample stage movement enables measurement while the detector kept stationary. Whereas, some profilometers the movement of the detector and the sample stage provides the measurement.

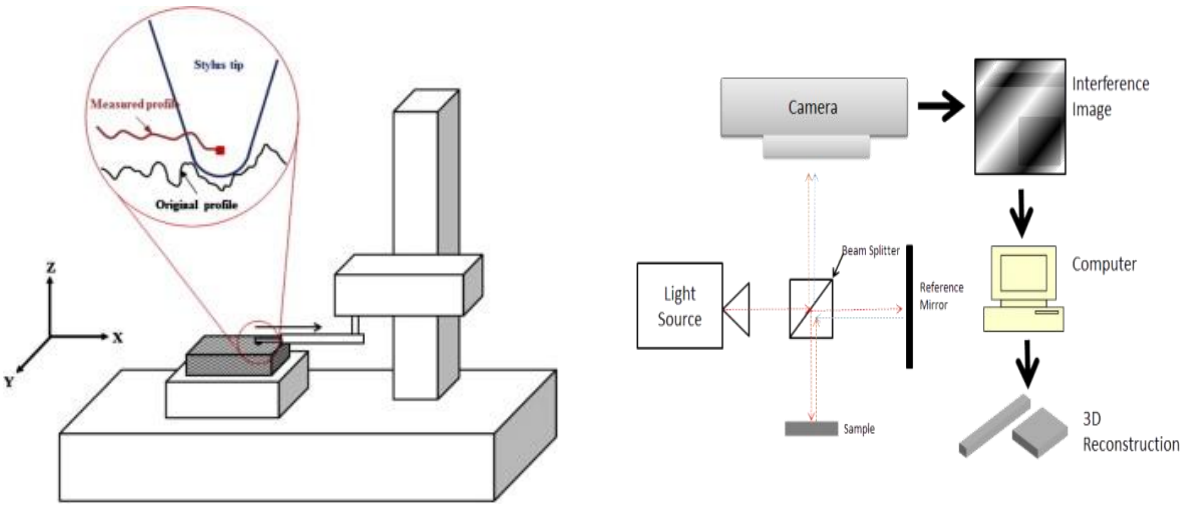

(a) (b)

Fig 3.1.1 Graphical representation of (a) Stylus Profilometry (b) Optical Profilometry (NanoscienceInst, 2020)

There are two kinds of profilometer, stylus and optical profilometers. Stylus profilometers use a probe to detect the surface measurements, physically moving a probe along the surface to measure the surface height. Mechanically, measurement is accomplished with a feedback mechanism that detects the reaction from the specimen pushing against sensor as it detects

along the surface. A response method is used to retain the arm, known as the setpoint, with a specific amount of torque (NanoscienceInst, 2020). The changes in the arm holder in z-direction could be used during the reconstruction of the surface

3.1.1 Stylus Profilometry

Stylus profilometry (***Fig 3.1.1(a)***) involves force feedback and physical contact of the substrate, so while being highly sensitive and providing high Z resolution, it is receptive to smooth surfaces and can destroy the surface of the probe. This method can also be damaging to some substrates. It is longer than contactless techniques because a stylus profilometer requires movement patterns in X, Y, and Z direction while retaining layer on the surface. The dimension and configuration of the stylus tip can impact the observations and restrict the spatial resolution.

3.1.2 Optical Profilometry

Optical profilometry (***Fig 3.1.1(b)***) takes the help of light rather than a physical probe. There are several ways to do this. The critical component of optical profilometry method was to guide the light in such a way that the surface can be detected in the 3D scan. Key components involve optical interference, the use of a confocal aperture, focus and phase detection, and the projection of a pattern on to three-dimensional image (D.-H. Lee, 2013).

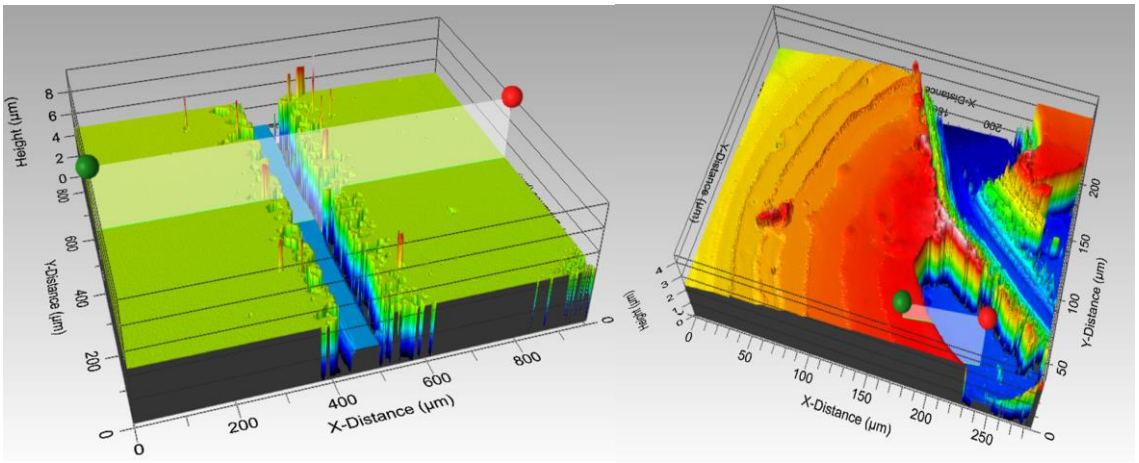

(a) (b)

Fig.3.1.2 Single-axis spin-coated substrate with polymer AZ1518 spun at 3500 rpm (a) Flat silicon wafer plate (b) Hemispherical glass

Figure (***Fig.3.1.2***) shows the graphical representation of the final film thickness distribution by a single axis spin coated substrate with polymer AZ1518 spun at 3500rpm. It shows the evolution of film contour from the optical profilometer of the surface thickness on (a) a flat plate silicon wafer and (b) a curved glass substrate.

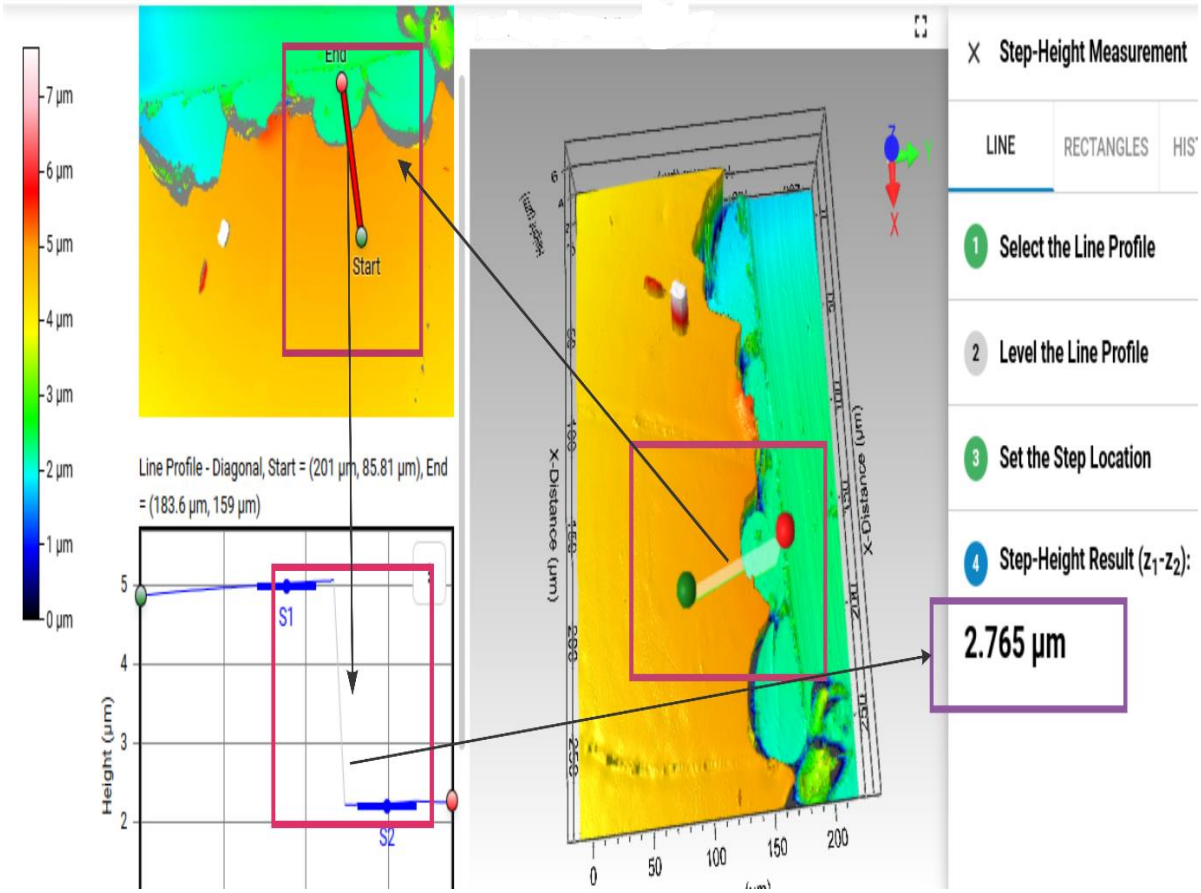

Fig. 3.1.3 Optical profilometer film contour of measurement of thickness on a coated hemispherical glass substrate

The film contours (***Fig.3.1.3***,) shows a single axis spin coated hemispherical glass substrate with polymer AZ1518 spun at 3500rpm film thickness measurement using an optical profilometer. A scrape was made on the spin coated surface, exposing the underlying hemispherical glass substrate and permitting the measurement of the film thickness. The scratch corresponds to the height difference (S1-S2) between the coated surface and the top of the substrate

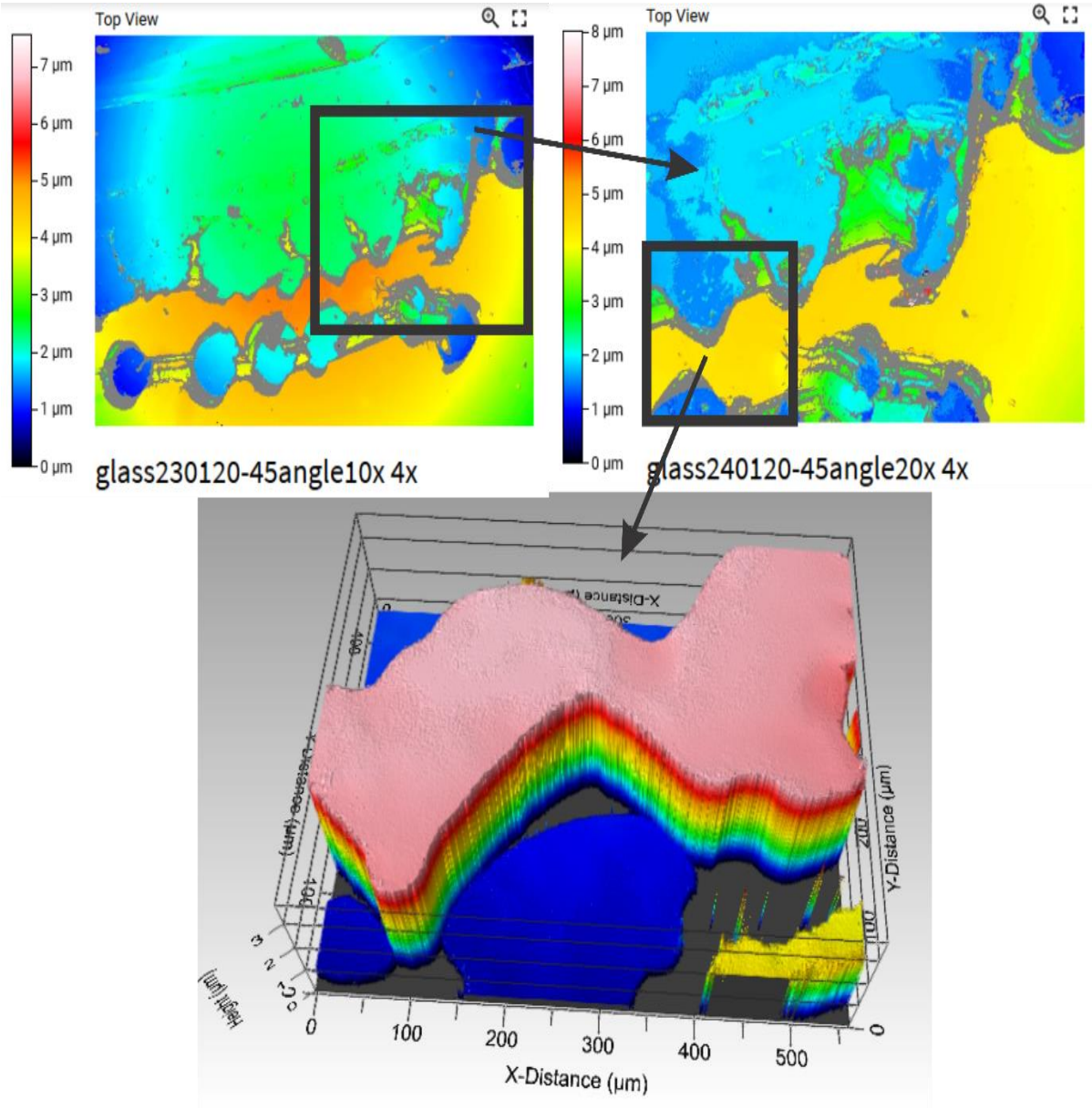

Fig 3.1.4 Surface thickness on a hemispherical glass substrate with angle plate attachment at an angle of 45 deg. with 10X, 20X and 50X focusing optical arrangements of 4X zoom (Jose, 2020)

Figures (***Fig.3.1.4***) show the graphical representation of film contour of final film thickness distribution on a single axis spin coated hemispherical glass substrate with polymer AZ1518 spun at 3500rpm. The film thickness was measured using optical profilometer of the surface thickness on a hemispherical glass substrate with angle plate attachment at an angle of 45 deg. with 10X, 20X and 50X focusing optical arrangements and 4X zoom.

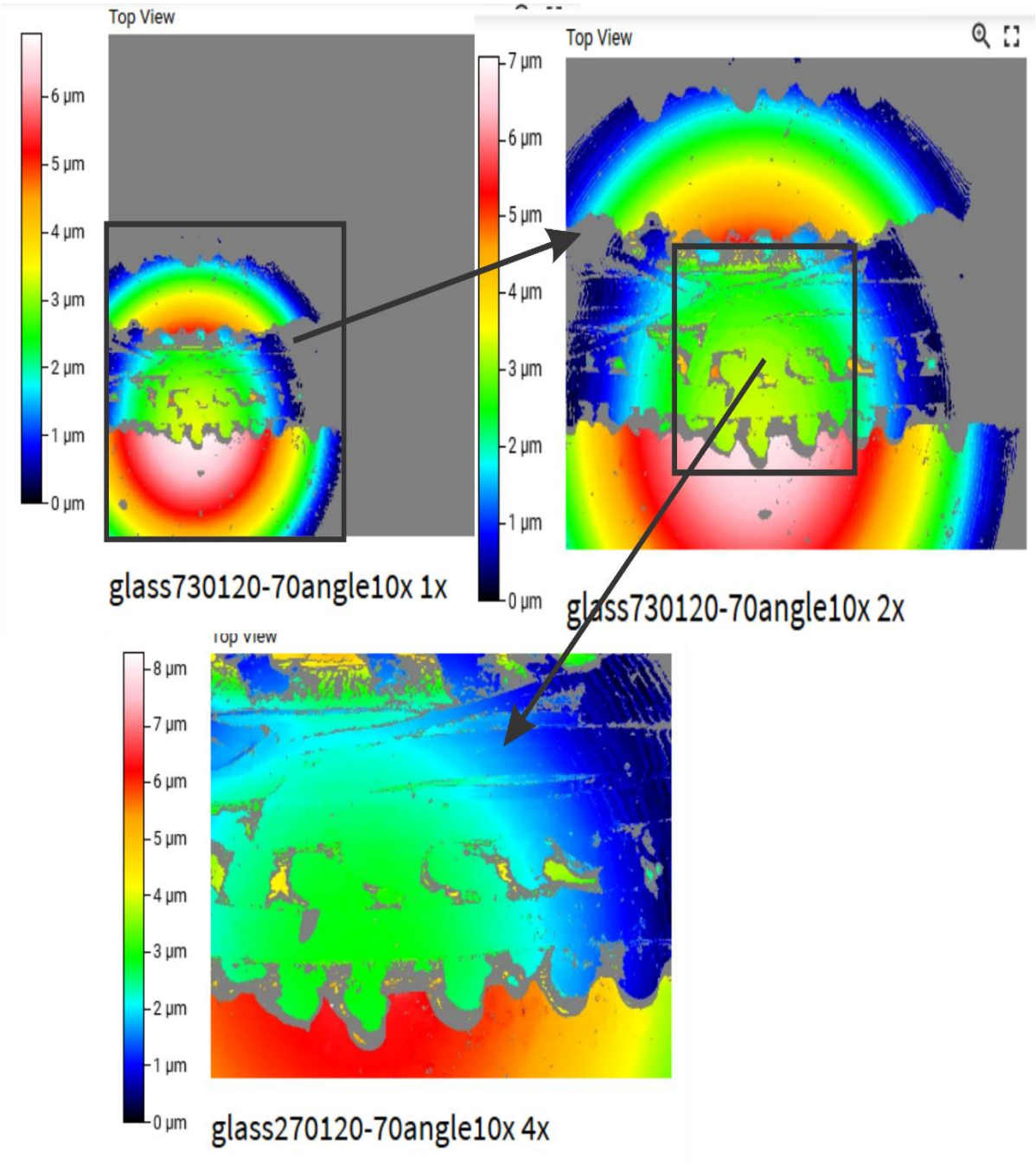

Fig. 3.1.5 Surface thickness on a hemispherical glass substrate with an angle plate attachment angle of 70 deg. with 1X, 2X and 4X zoom with 10X optical arrangement

Figure ***(Fig 3.1.5)*** shows the graphical representation of film contour of final film thickness distribution on a single axis spin coated hemispherical glass substrate with polymer AZ1518 spun at 3500rpm. The film thickness was measured using optical profilometer of the surface thickness on a hemispherical glass substrate with angle plate attachment at an angle of 70 deg. with 1X, 2X and 4X zoom with 10X focusing optical arrangement.

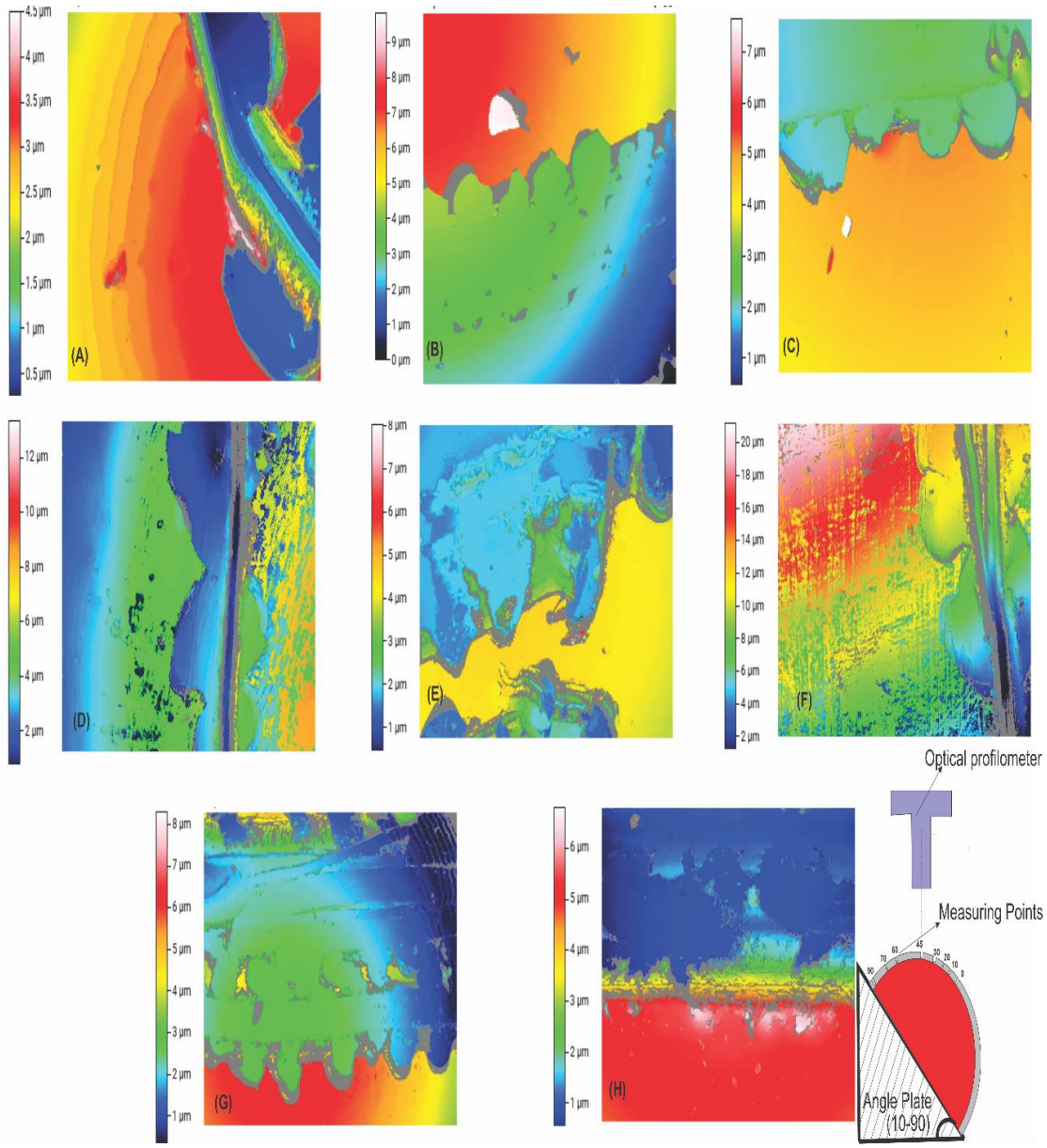

Fig 3.1.6 shows the surface thickness on a hemispherical glass substrate at an angle of (a) top surface 0 deg. (b) 10 deg. (c) 20 deg. (d) 30 deg. (e) 45 deg. (f) 60 deg. (g) 70 deg. (h) edge 90 deg. with 20X focusing optical arrangements of 4X zoom.

Figure (***Fig.3.1.6***) shows the graphical illustration of film contour of final film thickness distribution on a single axis spin coated hemispherical glass substrate with polymer AZ1518 spun at 3500rpm. The film thickness was measured at eight different points ***(Fig.3.1.6)*** on a hemispherical glass substrate using optical profilometer with angle plate attachment at a varying angle (0-90 deg.) and focusing arrangements. These values were used for obtaining the radial distribution of thickness.

3.2 RADIAL DISTRIBUTION OF THICKNESS

Figure (***Fig.3.2.1***) shows the radial distribution thickness of the photoresist polymer-coated hemispherical glass substrate. The y -axis represents the normalized distance from the axis ($\frac{r}{R}$) such that $\frac{r}{R} = 0$ is at the pole and $\frac{r}{R} = 1$ is at the equator. The y -axis shows the distribution of film thickness in meters. The measurements used in this radial distribution were taken from the above figure (***Fig.3.1.6***).

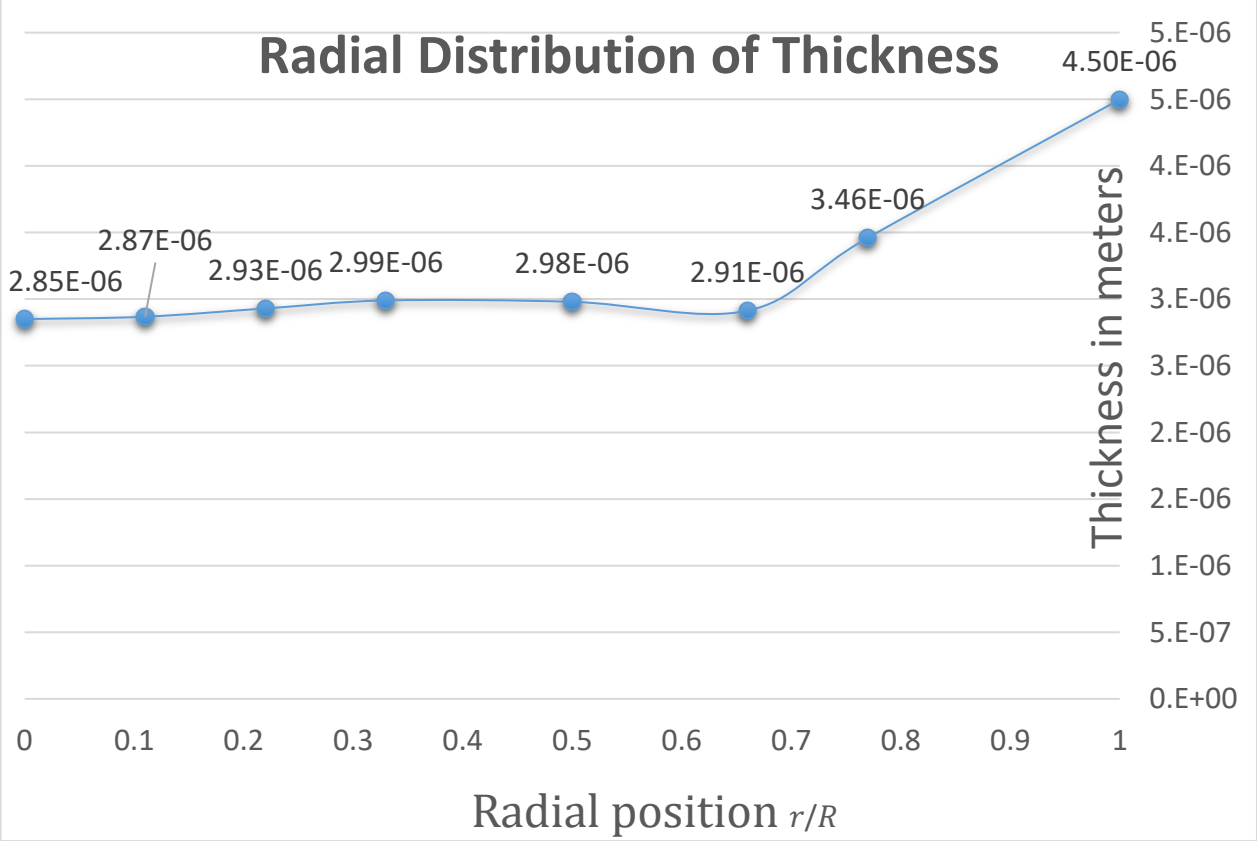

Fig. 3.2.1 Radial distribution of final film thickness on spin coated hemispherical glass substrate

There are three significant results ***(Fig. 3.2.1):***

- The film thickness gets thicker closer to the equator and thinner in the poles.
- For the radial dimension (r/R) < 0.66, the distribution of thickness is uniform.
- If the radial position is above $\frac{r}{R}$ >0.6, there is an increase in the thickness of the distribution.

3.3 COMPARISON STUDY

The film thickness distribution measurements were compared to published literature. Figures **(*Fig.3.3.1*** and ***Fig.3.3.2*)** show the radial distribution for different substrates and solutions at varying speeds ***(Table 3.3.1).***

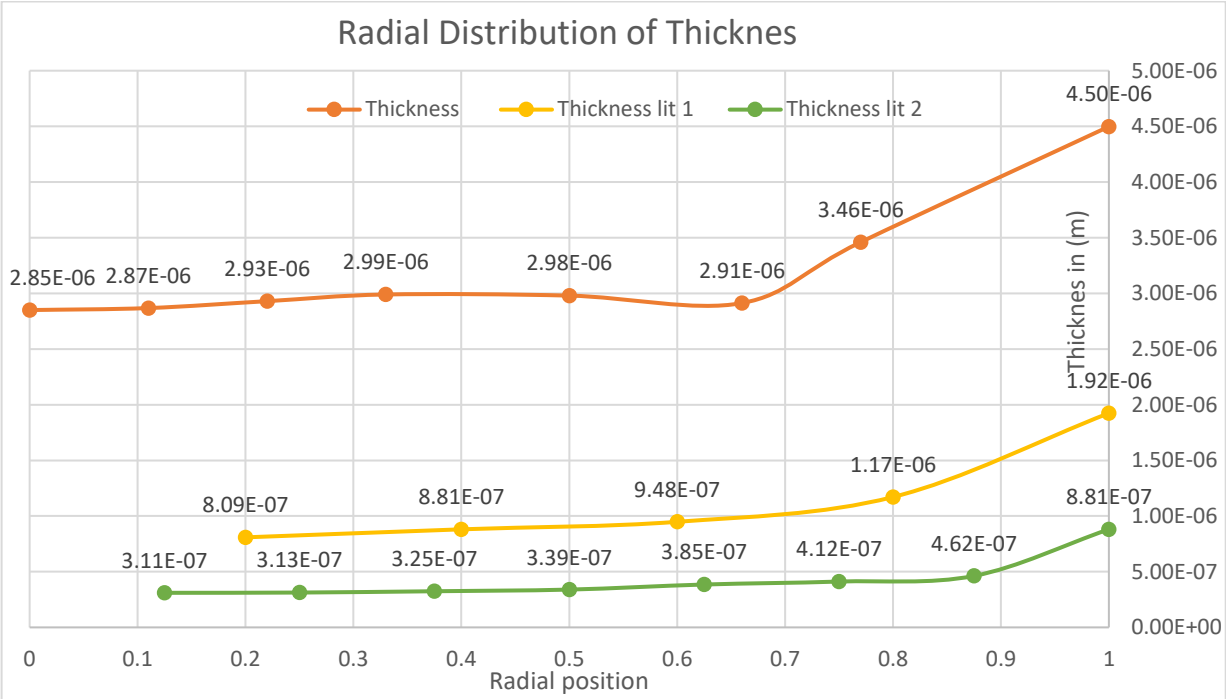

Fig. 3.3.1 Comparison study of radial distribution of thickness

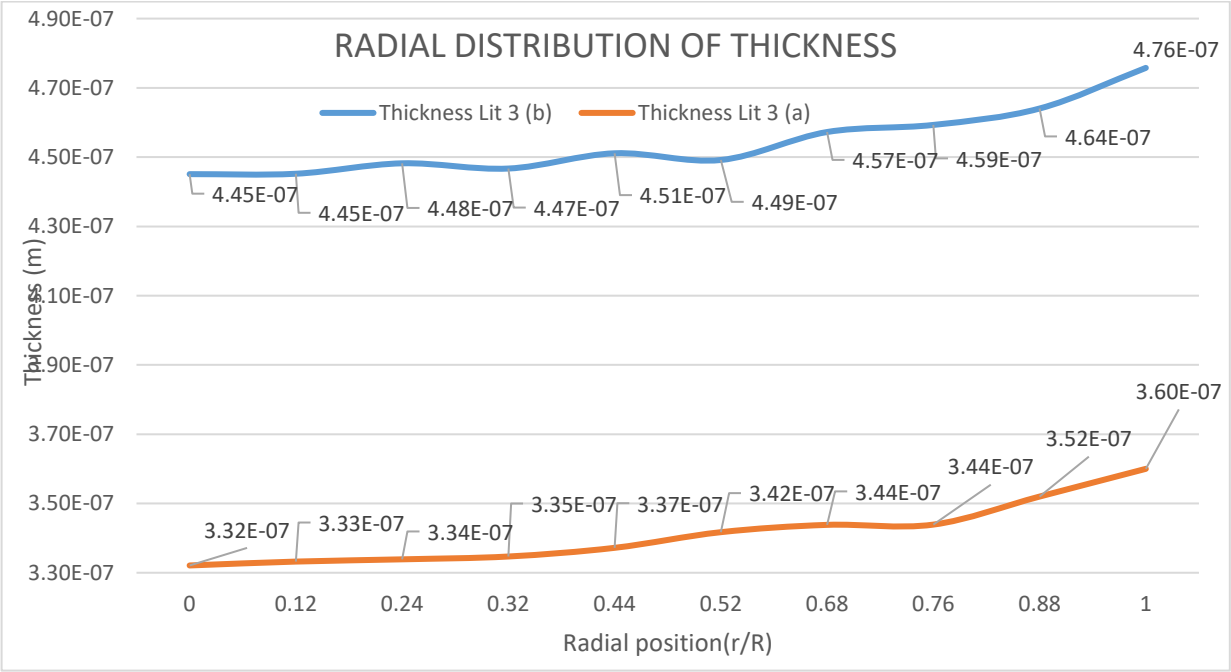

Fig. 3.3.2 Comparison study of radial distribution of thickness.

Name	Speed (rpm)	Solute	Substrate	Paper title
Thickness	3500	AZ1518	Glass Hemisphere of 60mm	
Thickness Lit 1	Unknown	Epoxy	Convex lens-K9LFocal length of 60mmCurvature radius of 31mm	(Liu et al., 2017)
Thickness Lit 2	2000	BP212-6	Concave lens spherical radius of 20mm	(Feng & Sun, 2005)
Thickness Lit 3 (a)	2000	AZ4620	Convex lens diameter 50mm Curvature radii R_0 =100mm	(Chen et al., 2009)
Thickness Lit 3 (b)	2000	AZ4620	Convex lens diameter 50mm Curvature radii R_0 =500mm	(Chen et al., 2009)

Table 3.3.1 Literature details

The following observations were made from the figures **(Fig. 3.2.1, Fig.3.3.1, and Fig.3.3.2)**

- All radial distributions follow the same trend.
- When $\frac{r}{R}$ < 0.6, the radial distribution is almost uniform.
- A similar pattern of radial distribution is compared (Fig. 3.3.1) from published literature (Feng & Sun, 2005).
- Feng & Sun shows the film thickness of the spin-coated changes for $\frac{r}{R}$ > 0.816.
- If the radial position is above $\frac{r}{R}$ >0.6, there is an increase in the thickness of the distribution.
- The radial distribution of thickness obtained from the hemispherical glass substrate shows a good correlation with published literature.
- The radial distribution of thickness data for validation was obtained from each paper uses different photoresist polymer solution and angular speed.

3.4 MEASUREMENT USING ATOMIC FORCE MICROSCOPE (AFM)

Atomic force microscopy (AFM) is a useful technique allowing the imaging of almost any sample surface type, such as glass, composites, polymers, biological, and ceramic samples. AFM is used to measure and locate several different forces such as the magnetic forces, mechanical properties, and strength of adhesion. AFM contains a sharp tip, which is about 10 to 20 nm in diameter and fixed to a cantilever. The tip continues to move in response to tip-surface contacts, and this mobility is measured by focusing a laser beam with a photodiode detector (Ray, 2013).

An AFM consists of two basic modes, contact and tapping (Non-contact). The AFM tip is in prolonged contact with the sample surface during contact mode. In contrast, the AFM cantilever in the tapping mode is vibrated above the surface of the sample, so that the tip is only in interrupted contact with the sample surface. This process helps reduce the shear forces associated with the movement of the tips. The commonly recommended mode of AFM measurement is the tapping mode whereas the contact mode is used for specific applications, like measurements of the force curve (Ray, 2013).

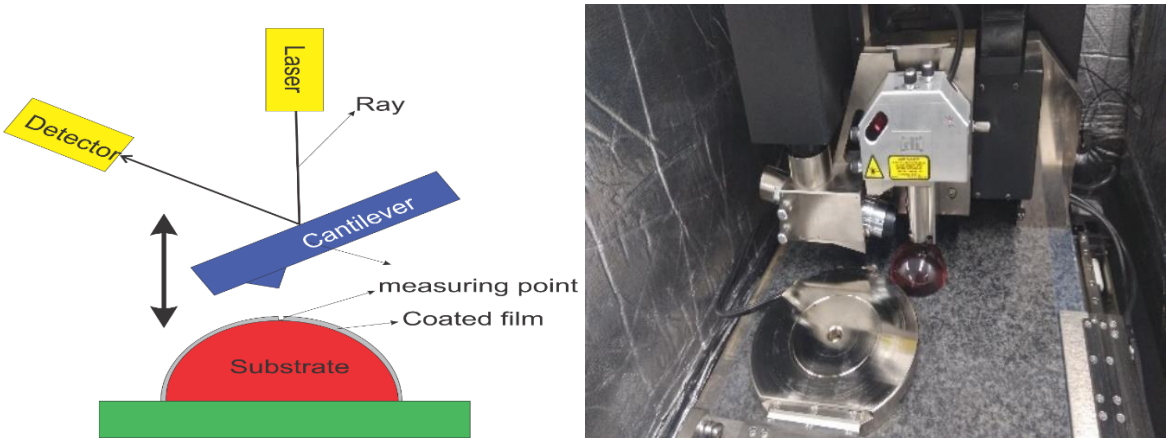

(a) (b)

Fig.3.4.1 (a) Schematic of measurement setup for a spin coated film thickness on hemispherical glass substrate using an Atomic force microscope (AFM). (b Spin coated film thickness measurement set up using AFM

Figure (***Fig.3.4.1***) shows the Atomic Force Microscope (AFM, Digital Instruments Dimension 3100) was used to measure the film thickness on the top of a coated hemispherical glass substrate of a diameter of 60mm (***Fig.3.3 (a)***).

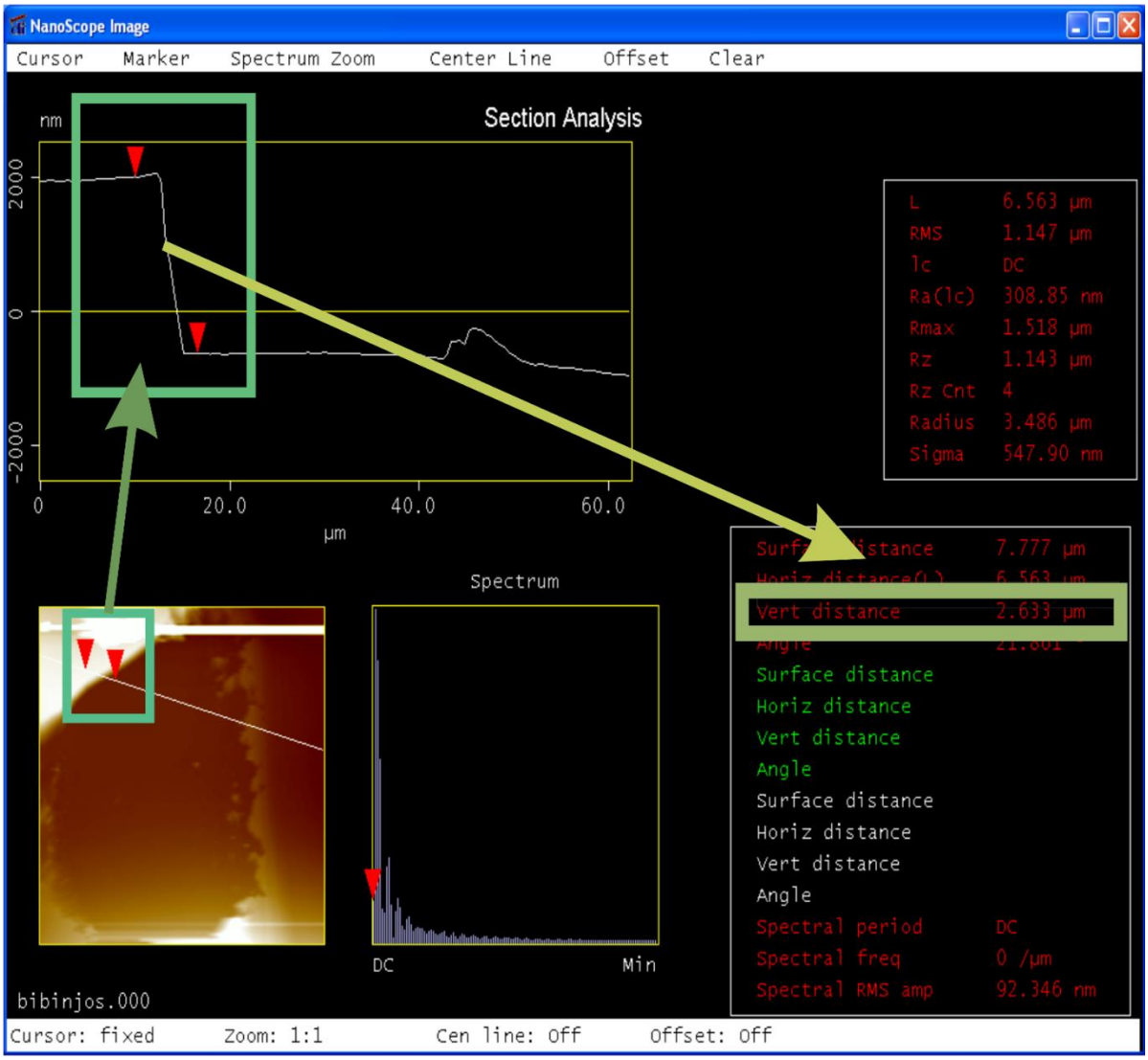

Fig 3.4.2 AFM film contour of measurement of thickness on a coated hemispherical glass substrate

The film contours (***Fig.3.4.2***,) shows a single axis spin coated hemispherical glass substrate with polymer AZ1518 spun at 3500 rpm film thickness measurement using AFM. A scrape was made on the spin coated surface, exposing the underlying hemispherical substrate and enabling the measurement of the film thickness. The scratch corresponds to the height difference between the coated surface and the top of the substrate. The film thickness measured on the north pole (top surface of the substrate) using AFM was 2.633µm. However, it was challenging to develop a complete radial distribution of thickness since the vertical range of AFM was 45mm, and a glass hemisphere diameter was 60mm. Hence, there was insufficient space for the AFM to measure complete radial distribution.

3.5 MEASUREMENT OF THICKNESS USING A METAL SUBSTRATE

A single-axis spin coater experimental set up was used to coat a photoresist polymer of a thin film on a hemispherical metal substrate of 50mm. A positive photoresist polymer AZ1518 (MicroChemical, Germany), was used as a solution for coating.

(a) **(b)**

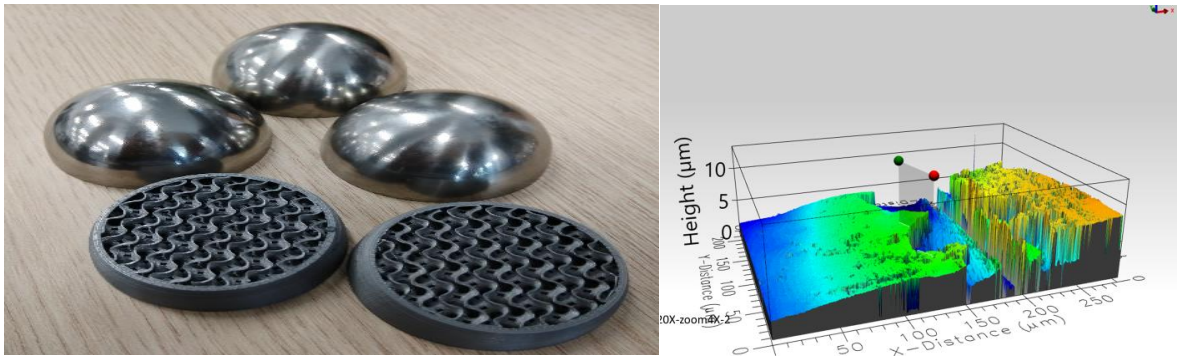

(c) **(d)**

Fig. 3..4.1 (a),(b), (c) Experiment and measurement set up for hemispherical metal substrate, (d) The film contour of the thickness of a coated hemispherical metal substrate on an optical profilometer

- Figure (Fig. 3.4.1(a)) shows the measurement set up for spin-coated metal sphere where the angle plate was used to measure the coated surface.
- Figure (Fig. 3.4.1(b)) displays the uncoated and coated metal hemispherical substrate.
- Figure (Fig. 3.4.1(c)) indicates the experimental set up for metal hemispherical substrate with a 3D printed base.
- Figure (Fig. 3.4.1(d)) illustrates the optical profilometer film contour of the thickness of a spin coated hemispherical metal substrate.

4 THEORETICAL METHODOLOGY AND VALIDATION

To determine the flow formation of the spin coating process on the hemispherical substrate, the actual process is very complicated, with combined energy transfer, momentum and mass. The parameters considered are time-dependent: the surface tension, the centrifugal force, the viscous force, the Coriolis force and solvent volatilization. This analysis follows the works of *Mathematical model of spin coated photoresist on a spherical substrate (Feng & Sun, 2005)*. The following assumptions to simplify the spin coating process were made:

- The fluid density ρ is uniform throughout the spin coating process.
- The photo-resist is a Newtonian liquid.
- The spherical substrate is an axi- symmetrical shape; therefore, the Coriolis force was neglected.
- Shear drag force due to airflow was ignored.
- Lubrication approximation was implemented.
- Evaporation of the volatile fluid was insignificant.

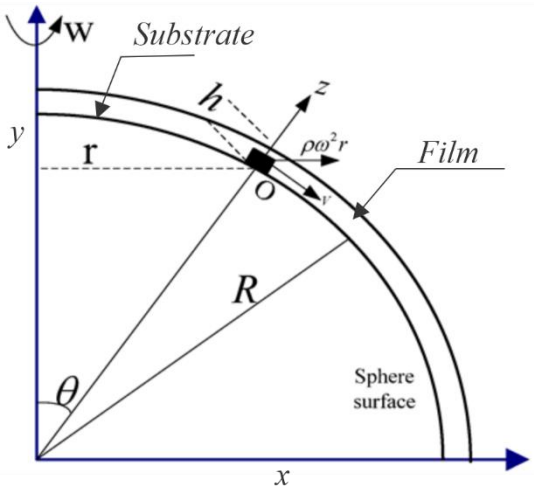

Fig 4.1 Schematic of the spherical substrate surface in vertical axis position

where, r is the horizontal distance to the y-axis, θ is the central angle between a position on the spherical substrate surface and y-axis, h is the coated final film thickness, v is the tangential velocity of the fluid of the substrate, z is the distance from the spherical surface

along normal direction, R is the radius of the hemisphere, ω is the angular speed of the hemisphere spinning along the y-axis.

The photo-resistive film thickness is a function of the balance between the shear force of the liquid resin to the edge of the substrate and the evaporation rate that affects the fluid viscosity. As the liquid evaporates, the viscosity of the coating rises until the centrifugal force of the spinning process can no longer move the solution significantly over the substrate surface.

When the viscous forces and the radial force are in balance, the Equation below is satisfied for a flat substrate (Emslie et al., 1958).

$$-\mu\frac{\partial^2 v}{\partial z^2} = \rho\omega^2 r \quad (1)$$

where, μ is the viscosity of the liquid; ρ is the density of the photo resistive fluid; $\rho\omega^2 r$ is the centrifugal force. The connection between r and R is attained from the figure (Fig.4.1)

$$sin\theta = \frac{r}{\mathrm{R}} \quad (2)$$

The addition of the gravitational effect on the coated film gives a spin-coated spherical substrate photo-resist equation of motion

$$-\mu\frac{\partial^2 v}{\partial z^2} = \rho\omega^2 r sin\theta - gcos\theta \quad (3)$$

For an initial photo-resist thickness of h_0

$$h(\theta, t)_{t=0} = h_0 \quad (4)$$

In Equation (3), g is the force of gravity of a tiny liquid element. Because the lubrication approximation of the liquid is fulfilled, convolution can be applied

A hemispherical substrate surface ($z = 0$)

$$\boldsymbol{v}(r, \theta, t) = 0 \quad (5)$$

The lubrication approximation implies the gradient on the free surface of the film is zero

$$\frac{\partial v(r,\theta,t)}{\partial z}_{(z=h)} = 0 \tag{6}$$

Taking Equations (1)-(6) collectively, the integral expression of Equation (3) can be obtained.

$$v = \frac{r}{\mu R}\left(-\frac{1}{2}z^2 + hz\right)\left(\rho\omega^2\sqrt{R^2 - r^2} - g\right) \tag{7}$$

The incompressible fluid mass continuity equation is

$$\frac{\partial h}{\partial t} + \frac{1}{r}\frac{\partial}{\partial r}\left(r\int_0^h v\, dz\right) = 0 \tag{8}$$

Substituting Equation (7) into Equation (8) gives

$$\left(2g - 2\rho\omega^2\sqrt{R^2 - r^2} + \frac{\rho\omega^2 r^2}{\sqrt{R^2 - r^2}}\right)\frac{h^3}{3\mu R} = \frac{\partial h}{\partial t} + \frac{rh^2\left(\rho\omega^2\sqrt{R^2 - r^2} - g\right)}{\mu R}\frac{\partial h}{\partial r} \tag{9}$$

The differential expression of the optimal position of film thickness $h = h\,(r, t)$, the photo-resist film thickness radial position r is a function of the coating time t, which means

$r = r(t)$. The PDE can be stated in terms of r and$t$.

$$\frac{dh}{dt} = \frac{\partial h}{\partial t} + \frac{\partial h}{\partial r}\frac{\partial r}{\partial t} \tag{10}$$

Comparing Equation (9) and (10), two evolution equations of thickness concerning the radial position of thickness are obtained.

$$\frac{dh}{dt} = \left(2g - 2\rho\omega^2\sqrt{R^2 - r^2} + \frac{\rho\omega^2 r^2}{\sqrt{R^2 - r^2}}\right)\frac{h^3}{3\mu R} \tag{11}$$

$$\frac{\partial r}{\partial t} = \frac{rh^2\left(\rho\omega^2\sqrt{R^2 - r^2} - g\right)}{\mu R} \tag{12}$$

The mathematical expression of $h = h\,(r, t)$ is determined by integrating Equation (11).

$$h = h(r, t) = h_0\left[1 + \left[2\rho\omega^2\sqrt{R^2 - r^2} - 2g - \frac{\rho\omega^2 r^2}{\sqrt{R^2 - r^2}}\right]\frac{2h_0^2 t}{3\mu R}\right]^{\frac{-1}{2}} \tag{13}$$

In Equation (14), h_0 is the initial film thickness. Equation (13) is the variation of radial position (r) to that initial film thickness (h_0)

According to Equation (3), the essential condition for liquid film outflow is

$$\rho\omega^2 r cos\theta \geq g sin\theta \tag{14}$$

The solution of Equation (14) is:

$$r \leq \sqrt{R^2 - \frac{g2}{\rho^2\omega^4}} \tag{15}$$

$$0 < r \leq \sqrt{R^2 - \frac{g2}{\rho^2\omega^4}} \tag{16}$$

According to Equation (14), r ≈ 0.816R

$$h = h_0\left(1 - \frac{4gh_0^2 t}{3\mu R}\right)^{\frac{-1}{2}} \tag{17}$$

Provided that $\sqrt{R^2 - \frac{g2}{\rho^2\omega^4}} > 0.816R$, the position r ≈ 0.816R is an essential point following Equation (14). Even though $0< r <$0.816R, the thinning of the coated film depends on the centrifugal force where $h< h_0$. However, in the interval 0.816R$< r < \sqrt{R^2 - \frac{g2}{\rho^2\omega^4}}$, the film thinning behaviour depends on gravitational force, where $h> h_0$.

In the case of the high-speed spin coating process, typically above 2000rpm, the gravitational effect can be ignored, the modified Equation for the film thickness then becomes

$$h = h_0\left(1 + \frac{4gh_0^2 t}{3\mu R}\right)^{\frac{-1}{2}} \tag{18}$$

The solvent evaporation can be included to achieve the final film thickness. The following assumptions are made:

- The initial solvent concentration is uniform, and the evaporation of the solvent charges solute concentration (C_t) uniform.

- Solute concentration does not depend on r; therefore, changes in the z-direction can be neglected.

- The density of solvent and solute is uniform, the total volume of the photo-resist polymer solution is the sum of solvent volume (L) and solute volume (S)

$$C_t = S/(S + L) \tag{19}$$

(Meyerhofer, 1978) established (20) a spin coating model for a Newtonian fluid using continuity equation but allowed the evaporation of the solvent during the spinning process. The author estimated that fluid height h could be segregated into solid-phase S height and liquid phase height L

$$h = \text{S+L} \tag{20}$$

The variation in concentration of solute and solvent arises with changes in viscosity of the fluid, and it influences the dynamic behaviour of the liquid. The following equations are the rate of change of solute (S) and solvent (L)

$$\frac{ds}{dt} = -C\left(2\rho\omega^2\sqrt{R^2 - r^2} - 2g - \frac{\rho\omega^2 r^2}{\sqrt{R^2 - r^2}}\right)\frac{h^3}{3\mu R} \tag{21}$$

$$\frac{dL}{dt} = -(1 - C)\left(2\rho\omega^2\sqrt{R^2 - r^2} - 2g - \frac{\rho\omega^2 r^2}{\sqrt{R^2 - r^2}}\right)\frac{h^3}{3\mu R} - e \tag{22}$$

where, e is the rate at which solvent evaporation takes place; C is the solute concentration. After drying, the final film thickness and final solute thickness are equal.

$$h_f = S_f \tag{23}$$

where, the final film thickness is h_f and the final solute thickness is S_f Thus, the final thickness of film on a spherical substrate may be attained by:

$$h_f = S_f = c_0 h_{\frac{1}{3}} = c_0\left[\frac{3\mu R.C\sqrt{\omega}}{(1-c_0)(2\rho\omega^2\sqrt{R^2-r^2} - \frac{\rho\omega^2 r^2}{\sqrt{R^2-r^2}} - 2g)}\right]^{\frac{1}{3}} \tag{24}$$

where, c_0 is non-volatile photo-resistive polymer material density in the photo resistive solution.

Here, r is the radial position, ω is the angular velocity, R is the sphere radius, C is the coefficient of laboratory, ρ is the fluid density, S_f is the final solute thickness, h_f is the final film thickness, and g is the gravity force ***(Fig.4.2***).

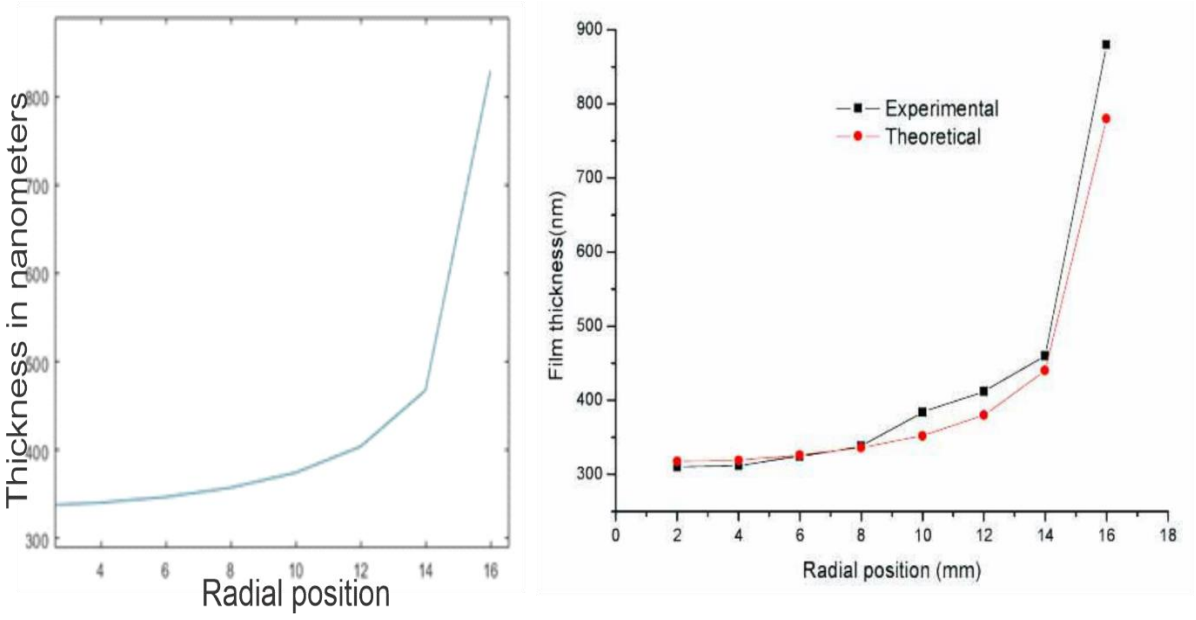

(a) (b)

Fig. 4.2 Radial distribution thickness for the mathematical model(24),(a) using MATLAB (b) from the published literature (Feng & Sun, 2005).

Figure ***(Fig.4.2***) shows radial distribution of thickness for the mathematical model the, final photo-resist film thickness of a concave spherical substrate with a 20 mm spherical radius, the 2000 rpm angular velocity, using MATLAB code discussed in section **A.1** and from the published literature (Feng & Sun, 2005).

The mathematical expression (24) with experimental results on a spherical concave substrate of radius 20mm, the angular speed of 2000rpm, c_0=0.015, g= 0, $\mu/\rho \cdot C \sqrt{\omega}$ =0.03 $\frac{m^2}{s^2}$, moreover, tested and validated the film thickness by atomic force microscope (AFM).

4.1 VALIDATION

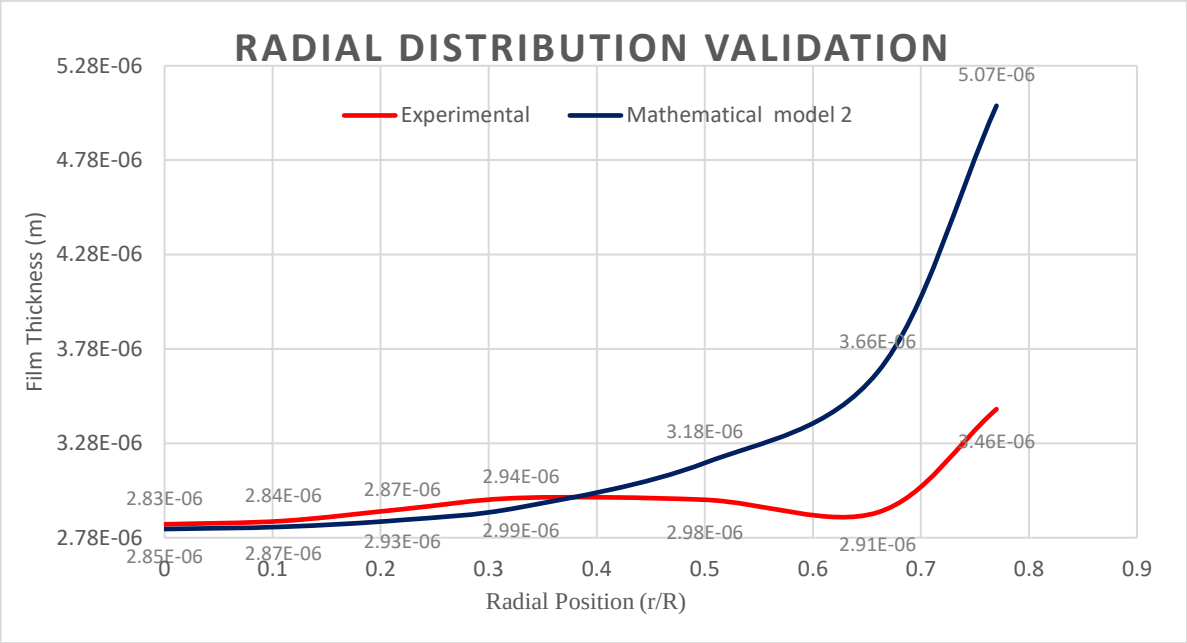

Fig. 4.1.1 Validation of radial distribution of thickness with a mathematical model from (Feng & Sun, 2005)

- The radial distributions of Feng & Sun mathematical model and experimental data from single-axis spin coated hemispherical substrate follow the same trend (Feng & Sun, 2005).
- When radial position $\frac{r}{R}$ < 0.6, the radial distribution for the experimental result is almost uniform.
- A similar pattern of radial distribution is validated discussed in section **A.2** (***Fig. 4.1.1***) with published literature (Feng & Sun, 2005).
- Feng & Sun mathematical model shows a uniform film thickness of the spin-coated substrate for $\frac{r}{R}$ < 0.4.
- If the radial position is above $\frac{r}{R}$ > 0.6, there is an increase in the thickness of the distribution.
- The radial distribution of thickness obtained discussed in section **A.2** from the hemispherical glass substrate shows good agreement with published literature.

5 NUMERICAL MODELING

Advanced numerical models have developed applied mathematics for solving PDEs. The motive for this is that analytical solutions to mathematical equations can be attained in particular cases, such as certain formulae and secure morphologies configurations. Though from a theoretical perspective, these cases are relevant, they were less exploited by the professionals. This limitation does not apply to numerical analysis so that they can manage non-linear problems and complex geometries.

In space and time, the solution was described alongside the independent variables x, y, z, and t. However, many numerical approaches were based on some discretization of the patterned field and the dependent variables. The most frequently used techniques for this discretization are the finite difference, volume, and element methods.

The objective of the Finite Element Analyse (FEA) system is for design, optimization, and monitoring of devices and processes to decrease the number of prototypes and experiments needed. When the FEA model has been developed and considered useful for forecasting the real-life properties of the system or operation, it contributes to a greater understanding and intuition. The last stage of progress can be accomplished with intuition alone in the optimization methods and automated control phase. Most modern FEA software has automatic control description methodologies, and these descriptions can be integrated with numerical and mathematical models. The presence of high-fidelity models also helped accelerate understanding. New concepts and entirely new designs and operating structures have been produced that would have been impossible without modelling. FEA is thus an essential part of companies and organizations operating in competitive industries for research and development. Over a period, the application of FEA software has spread from more prominent corporations and organizations that aid education for engineers to smaller enterprises in several sectors and institutions.

The basis of FEA software was established by the laws conveyed in physical-mathematical models. For FEA, such laws were composed of different conservation equations: momentum conservation (Navier-Stokes), energy conservation (Bernoulli's equation), mass conservation (the continuity equation). The purpose of theoretical physics was meant to explain the physics laws, which result in partial differential equations for time and space-dependent descriptions. Dependent variables, such as temperature fields, structural displacements, fluid fields and

velocity fields, depict the solution to the PDEs.

For two-phase flow, three main approaches of mesh are available: level-set, phase-field, and moving mesh. These were used to model two fluids separated by a fluid boundary and where the moving boundary interface that includes surface tension forces and surface curvature is tracked in detail. The level-set and phase-field approaches employ a fixed background mesh and solve additional equations to track the location of the interface ("Microfluidics Software - For Simulating Microfluidics Devices," 2020). In order to represent the fluid interface, the moving mesh approach solves the flow equations on a moving mesh with limit conditions. In this case, the mesh deformation was solved using the arbitrary Lagrangian-Eulerian (ALE) technique. All these approaches and their interfaces with physics helps both incompressible and compressible laminar flows where one or both fluids perhaps non-Newtonian (COMSOL, 2020b).

A numerical study was conducted exploiting COMSOL Multiphysics 5.3a to explain the incompressible, two-dimensional axial symmetric Navier-Stokes equations, made of the laminar flow module, presuming incompressible flow. An implicit time-stepping method for Backward Differentiation Formula (BDF) was used with variable order time stepping to regulate the step variables for convergence automatically. This time-stepping condition was set to "intermediate" for the time-dependent simulations so that COMSOL software has to resolve at least a one-time step within each specified period. The time-stepping condition was to prevent numerical crashing (Ramsay, Sellier, & Ho, 2020a).

The COMSOL Microfluidics Module provides dedicated methods with the level set, phase field, and moving mesh for simulating two-phase flow. The Microfluidics Module's capabilities include capillary forces, Marangoni effects and surface tension forces (COMSOL, 2020b).

5.1 GOVERNING EQUATIONS

The basic modelling of fluid flow consists of the equation from the conservation of momentum and mass. For example, fluid flow modelling was involved in computational fluid dynamics (CFD) in accepting designs and processes for different applications.

The equation for conservation of momentum becomes

$$\frac{\partial \rho \boldsymbol{v}}{\partial t} + \nabla \cdot (\rho \boldsymbol{v}\boldsymbol{v}) + \nabla p - \nabla \cdot \boldsymbol{\tau} - \boldsymbol{F} = 0 \quad (1)$$

The above equation is known as the Navier–Stokes equation. The Navier–Stokes equation consists of three dependent variables for the velocity vector component ($\boldsymbol{v} = (\boldsymbol{u}, \boldsymbol{v}, \boldsymbol{\omega})$), one for the pressure (p), and one for the material density (ρ).

The different components of the momentum equation are normally solved in combination with conservation of mass (the continuity equation):

$$\frac{\partial \rho}{\partial t} + \nabla \cdot (\rho \boldsymbol{v}) = 0 \quad (2)$$

For constant density and viscosity, the Navier–Stokes and the continuity equations can be explained to comply with the following four-equation system for the velocity and pressure:(COMSOL, 2020c)

$$\rho \frac{\partial \boldsymbol{v}}{\partial t} - \mu \nabla^2 \boldsymbol{v} + \rho \boldsymbol{v} \nabla \boldsymbol{v} + \nabla p - \boldsymbol{F} = 0 \quad (3)$$

$$\nabla \cdot \boldsymbol{v} = 0 \quad (4)$$

$$\frac{\partial \rho}{\partial t} + \nabla \cdot (\rho \boldsymbol{v}) = 0 \quad (5)$$

where ρ is the material density, $\boldsymbol{v}$ is the velocity vector component, p is the pressure component, $\boldsymbol{I}$ is the unit matrix, μ is the dynamic viscosity component, and $\boldsymbol{F}$ is the force vector.

The complexity of the Navier-Stokes equations, which regulate the fluid flow formulae, makes the simulation of CFD problems a necessary practice. An add-on to COMSOL Multiphysics, the CFD Module is a powerful tool that allows users to perform these simulations for a variety of fluid flow. The CFD Module included laminar and creeping flow, non-Newtonian flow, turbulent flow, double-phase flow, thin-film flow and rotating equipment.

5.2 ARBITRARY LAGRANGIAN-EULERIAN (ALE)

An arbitrary Lagrangian-Eulerian (ALE) formulation leads to a smooth and accurate treatment of the interfaces between the fluid-structure and allows significant fluid sloshing and swirling without producing excessive distortions of the computational mesh. Finite element models for predicting the non-linear response of fluid-structure systems exposed to transient dynamic loading were presented. The computational mesh inside the domains shifts arbitrarily to optimize element structures. In contrast, the mesh at the phase boundary and interfaces shift along with materials to accurately monitor the boundaries and interfaces of a sophisticated shaped device. An arbitrary Lagrangian-Eulerian (ALE) kinematic description of the fluid domain was adopted in which the grid points can be displaced regardless of the fluid motion.

ALE-based formulations of finite elements can be reduced either to Lagrangian-based formulations by equating mesh motion to material motion or Eulerian-based formulations by fixing mesh inside space. Finite element program could be used to conduct detailed simulations of science, namely energy transfer, fluid dynamics, Fluid-structure interaction (FSI) and metal processing.

Physical systems are typically established and computationally resolved in one of two coordinate systems: the spatial coordinate system, known as the Eulerian methodology, fixes the coordinate references in space, and the material coordinate system, known as the Lagrangian methodology, fixes the coordinates to the reference material and continues to follow the material in its deformation. The Eulerian formulation tends to be more useful for fluid methods since it is very computationally complicated following the particles. However, since the connected components were patched to a spatial system, an Eulerian method cannot follow the boundaries of moving domains that are a mainstay in free surface flow (Szott & Ruzic, 2020).

COMSOL determines a frame time derivative on the mesh time frame and spatial derivative on the fixed mesh points using the arbitrary Lagrangian-Eulerian (ALE) system. For ALE, there are two kinds of time derivatives:

The frame time derivative, which is valid for a fixed point in either the material or the spatial frame, and the mesh time derivative, which was taken for a fixed point in the mesh. This

derivative is denoted v_t in some physics interfaces. The mesh time derivative is defined as:

$$v_t(x_0, y_0) = \frac{\partial v}{\partial t}|_{(x_0,y_0)} \tag{7}$$

equation (7) gives the Eulerian formulation for the interfaces,

$$v_t(X_0, Y_0) = \frac{\partial v}{\partial t}|_{(X_0,Y_0)} \tag{8}$$

equation (8) gives the Lagrangian formulation for the interfaces,

And both velocities are related by the mesh time derivative, which was taken for a fixed point mesh

$$v_{TIME}(, X_{mesh}Y_{mesh}) = \frac{\partial v}{\partial t}|_{(X_{mesh},Y_{mesh})} \tag{9}$$

The chain rule relates the two derivatives. For example, for a spatial frame derivative:

$$v_t = v_{TIME} - \boldsymbol{v_x} x_{TIME} - \boldsymbol{v_y} y_{TIME} \tag{10}$$

where, [$\boldsymbol{v}_x$, v_y] is the spatial frame gradient and [x_{TIME}, y_{TIME}] is the spatial mesh velocity, and $v_t(X_{TIME}, Y_{TIME})$ is the velocity of mesh. The mesh time component is usually less important from a user point of view because its value depends on the mesh movement, which often has no physical significance. However, for the particular case when the mesh follows the material's deformation, the mesh time component is physically significant and is also known as the material time component (COMSOL, 2020a). A mesh displacement equation is solved within deformative domains to evaluate how the region deforms.

5.3 MOVING MESH

One way to overcome the level set and phase field issue is by using a convenient feature that was integrated with COMSOL – the moving mesh. The mesh locations generated in COMSOL have an exact mapping to locations of the material field. Therefore, if the mesh deforms and follows the free domain, an Eulerian mapping can be used to solve for a shearing Lagrangian-type system. The moving mesh is known as a Lagrangian-Eulerian arbitrary (ALE) process and was included in the moving mesh module as the solver. The mesh is stretched and compressed accompanying with the domain movement, as the domain deforms. While this

deformation can lead to deterioration of the mesh refinement that can result in an accumulation of solver inaccuracy, slight disturbances can be effectively resolved with a fine enough mesh. Implementing the moving mesh requires choosing which boundaries and domains can be deformed and how. There is only one domain for this system which is permitted free deformation. Prescribed displacements are used on the edges to restrict that deformation and keep it in its trench shape. The bottom surface is a non-slip surface in both horizontal and vertical directions with a prescribed displacement of 0 m keeping the bottom fixed continuously. At the sides of the domain, the inlet and outlet edges have a prescribed displacement of 0 m in the horizontal direction with no vertical constraint. Although still acting as a fixed inlet or outlet, this allows the edges to obey any vertical motion in the domain, such as dry out or pileup. The free surface at the top was modelled using a specified mesh size. This phase was combined with speeds solved by the laminar flow module, and the mesh deforms to match the fluid's true nature in both horizontal and vertical directions (Szott & Ruzic, 2020).

COMSOL Multiphysics Software contains four methods for modelling free liquid surfaces: level set, phase field, moving mesh, and stationery free surface. The moving mesh interface is suitable if, at every point in the domain, we want to define the material strain uniquely. If the domain deformation can be fully defined, it is most applicable for modelling a stable domain. A volume change means the material is stretched or compressed, but the total mass is always the same. For two-phase flow, three main approaches have been proposed: level-set, phase-field, and moving mesh approaches. The moving mesh was used to design two fluids isolated by a fluid interface where the moving interface, surface curvature and surface tension forces, are monitored in detail. The level-set and phase-field methods employ a fixed context mesh and solve additional equations to map the position of the interface.

Consider a 2D geometry, where the spatial frame and material frame components were called (x, y) and (X, Y), sequentially. Let (x_0, y_0) can be the spatial coordinates of a mesh frame node in the initial material contour. The spatial coordinates (X_0, Y_0) of the corresponding mesh node at some other time, t, is then given by the function (11).

$$x_0 = x(X_0, Y_0, t) \qquad y_0 = y(X_0, Y_0, t) \tag{11}$$

These functions are explicit transformations (expressions) or the solution to a mesh smoothing equation. The mesh node's material coordinates (X_0, Y_0) were seen as functions of an underlying system of geometry coordinates (X_g, Y_g) and a parameter, p..

$$X_0 = X(X_g, Y_g, p) \quad Y_0 = Y(X_g, Y_g, p) \tag{12}$$

The changes can also be chained such that (x_0, y_0) are functions of (X_g, Y_g), t, and p.

Introducing a vector notation for the coordinates:

(a) Spatial coordinates $\mathbf{x} = (x, y, z)$

(b) Material coordinates $\mathbf{X}_{mat} = (X_{mat}, Y_{mat}, Z_{mat})$

(c) Geometry coordinates $\mathbf{X}_g = (X_g, Y_g, Z_g)$

(d) Mesh coordinates $\mathbf{X}_{mesh} = (X_{mesh}, Y_{mesh}, Z_{mesh})$

The general relation between the frames can be written as

$$\boldsymbol{x} = \boldsymbol{f}(\boldsymbol{X}_{mat}, t) = \boldsymbol{f}(\boldsymbol{g}(\boldsymbol{X}_g, p), t) \tag{13}$$

$$\boldsymbol{x} = \boldsymbol{g}(\mathbf{X}_g, p) \tag{14}$$

$$\boldsymbol{f}(\boldsymbol{g}(\mathbf{X}_g, p), t) \tag{15}$$

$$\mathbf{X} = \boldsymbol{h}(\mathbf{X}_g, i) \tag{16}$$

$$\mathbf{X}_g = \boldsymbol{h}^{-1}(\mathbf{X}_{mesh}, i) \tag{17}$$

$$\boldsymbol{x} = \boldsymbol{f}(\mathbf{X}_{mat}, t) = \boldsymbol{f}(\boldsymbol{g}(\mathbf{X}_g, p), t) = \boldsymbol{f}(\boldsymbol{g}(\boldsymbol{h}^{-1}(\mathbf{X}_{mesh}, i), p), t) \tag{18}$$

where, $\boldsymbol{f}$, $\boldsymbol{g}$, and $\boldsymbol{h}$ are vector-valued functions, t is time, p is some set of parameters controlling a deformed geometry interface, and *i* is the number of times the geometry has been remeshed. $\boldsymbol{f}$ is a unit map if the spatial and material frames coincide, $\boldsymbol{g}$ is a unit map if the material and geometry frames coincide

There are four types of approaches within each domain to compute the mesh deformation: types Laplace, Winslow, Hyperelastic, and Yeoh smoothing. In this numerical analysis, a Winslow smoothing algorithm is chosen, which leads the software to solve.

$$\frac{\partial^2 X}{\partial x^2} + \frac{\partial^2 X}{\partial y^2} = 0 \text{ and } \frac{\partial^2 Y}{\partial x^2} + \frac{\partial^2 Y}{\partial y^2} = 0 \quad (19)$$

The Laplace smoothing approach tries to solve inside the domain the following partial differential equation

$$\frac{\partial^2 x}{\partial X^2} + \frac{\partial^2 x}{\partial Y^2} += 0 \quad (20)$$

$$\frac{\partial^2 y}{\partial X^2} + \frac{\partial^2 y}{\partial Y^2} += 0 \quad (21)$$

here, X and Y are the material build components, and x and y are the components of the spatial frame.

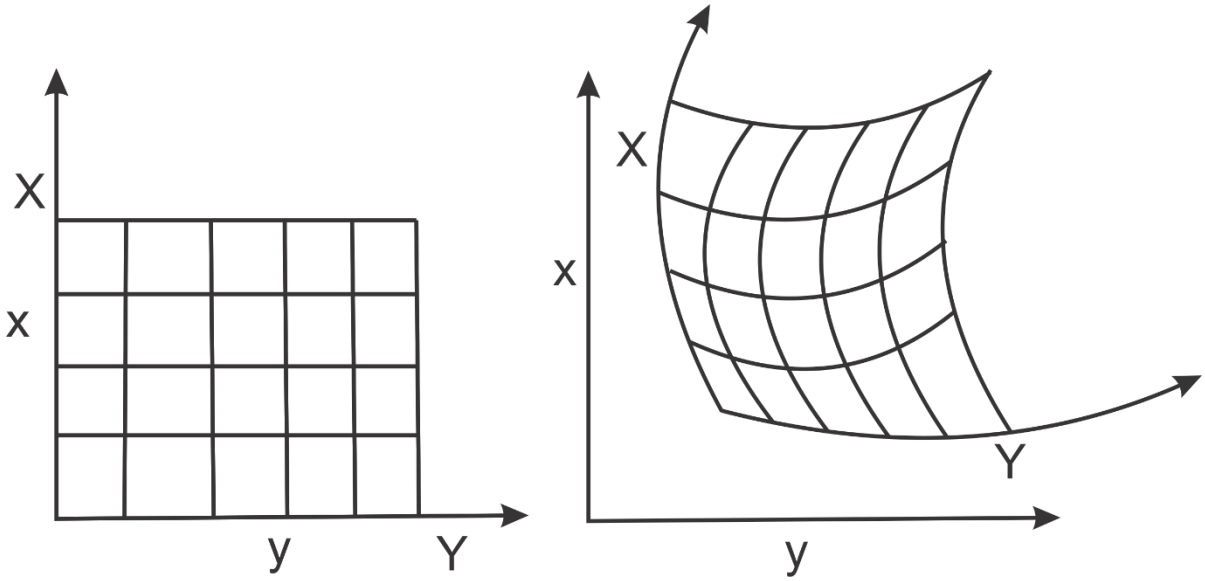

(a) (b)

Fig. 5.1.3 (a) An undeformed Mesh. (b) Deformed Mesh (Moving Mesh)(COMSOL, 2020a)

The Fig.5.1.3 shows (a) an undeformed mesh, in the reference configuration, which can be the actual configuration with a reference time or a hypothetical state, the spatial frame component (x, y) and the material frame component (X, Y) match (b) After deformation of the material frame, the spatial frame (x, y) remains constant, while the material frame coordinates system (X, Y) distorted, succeeding the material. Meanwhile, the material coordinates of each material

point remain constant, but its spatial co-ordinates have changed (COMSOL, 2020a).

5.4 DISCRETE TIME-STEPPING SCHEMES

The COMSOL Multiphysics offers three different time-stepping methods in their time-dependent solver: the implicit backward differentiation formula (BDF), generalized -alpha methods, and the explicit Runge – Kutta methods.

The BDF solver is an implicit solver with variable discretization order and automatic step-size selection using backward differentiation formulas. When the accuracy of the solution allows, the higher-order schemes were used, and the lower-order schemes were used when additional robustness is required. BDF methods are well known for their stability and were used by default for diffusion, convection, and reaction problems.

The Generalized-α method is a second-order implicit scheme that is widespread for problems with structural mechanics and is also well suited for problems with wave propagation. The Generalized Alpha Scheme users to control high-frequency damping, and typically has less damping than the BDF scheme of the second order. The Generalized Alpha scheme is more accurate than BDF in many cases but is less stable.

The Runge – Kutta family of methods are explicit method used in ordinary differential equation (ODE) systems. Usually, they are not as efficient for solving finite element method (FEM) problems. The Times list in the Time-Dependent study was employed specifying an explicit list of times from the start time through the end time. Utilizing the range operator can be a quick means of specifying a list of intermediate time points.

Time-dependent simulations were performed for 2D axisymmetric, laminar flow, two-phase, and moving mesh studies. For Backward Differentiation Formula (BDF), an implicit time-stepping method was used with variable order time stepping to adjust the step parameters for convergence automatically. For the time-dependent simulations, this time-stepping condition was set to "intermediate," so that COMSOL must solve at least one-time step within each specified interval. The time-stepping condition prevents numerical crashes and could stop instability from growing (Ramsay, Sellier, & Ho, 2020b).

For the steps taken by the solver in the time step section of the time-dependent solver, the following configurations are available that affect the actual selection of time steps:

- *Free*: An adaptive time step size is selected based on the estimates of local errors.
- *Strict*: This is similar to the *Free* setting, but the solver adjusts its time step to solve the specified output times.
- *Intermediate*: This is same as for the *Free* setting, but the solver adjusts its time step to solve each of the sub-intervals defined by the output times for at least one time.
- *Manual*: Instead of an automatic one, a user-specified time step was taken (COMSOL, 2020c).

The time-dependent partial differential equations (PDEs) were converted utilizing a finite element spatial discretization into an implicit system of ordinary differential equations (ODEs) or differential-algebraic equations (DAEs). For the new degrees of freedom, a time discretization was used to generate a set of algebraic equations. In each step of the time, the algebraic equations are solved through automatic linearization using a Newton method, Fully Coupled solver or Segregated solver with damping. The resulting linear equations are solved either by direct solvers (e.g., MUMPS or PARDISO) or by iterative solvers.

The finite element discretization of the time-dependent PDE problem is, which was often referred to as the method of lines.

$$L\left(U, \dot{U}, \ddot{U}, t\right) - N_F(U,t)\Lambda = 0 \tag{22}$$

$$\mathrm{M}(U,t) = 0 \tag{23}$$

Before solving this system, the algorithm eliminates the Lagrange multipliers Λ. If the constraints $\mathrm{M}(U,t) = 0$ are linear, time-independent, and the constraint force Jacobian N_F is constant, then the algorithm also eliminates the constraints from the system. Otherwise, it keeps the constraints, leading to a differential-algebraic system.

The linearization of the above system used in the Newton iteration is:

$$EU + DU + KU = L - N_F \wedge \tag{24}$$

$$E = -\frac{\partial L}{\partial(\ddot{U})} \quad (25)$$

$$D = -\frac{\partial L}{\partial(\dot{U})} \quad (26)$$

$$K = -\frac{\partial L}{\partial(U)} \quad (27)$$

where, E is the mass matrix, K is the stiffness matrix, and D is the damping matrix.

When E =0, D is often called the mass matrix

5.5 COMSOL MESH

The mesh selected for modelling with COMSOL Multiphysics strongly affects analysis needs. Meshing is one of the most memory-demanding steps when it comes to establishing and solving a problem with finite elements. The mesh used in a geometric model plays a crucial role in how the model was explained, as it determines factors such as: how the geometry was divided, with which the size shape or element type the geometry was divided, density and number of elements in the geometry, and the quality of the element (Meshing, 2020). These factors directly affect the problem calculation, including how long it takes a model to solve.

Two methods to mesh model geometry in COMSOL Multiphysics software: having the software do it automatically, or by choosing to build a custom mesh manually. The meshing can be done by a type of mesh sequence that is governed by physics or a user, respectively. Whichever mesh sequence type was chosen, there are plenty of meshing options, settings, tools, and generators could use to create an optimized mesh for geometry and analytics (COMSOL, 2020c).

In COMSOL Multiphysics, meshing uses four different types of elements: tetrahedra (tets), hexahedra (bricks), prisms (prisms), and pyramids. There are also nine preset sizes of elements that range from Extremely fine to Extremely coarse. Images of different types of elements are shown in the figure (***Fig. 5.5.1***)

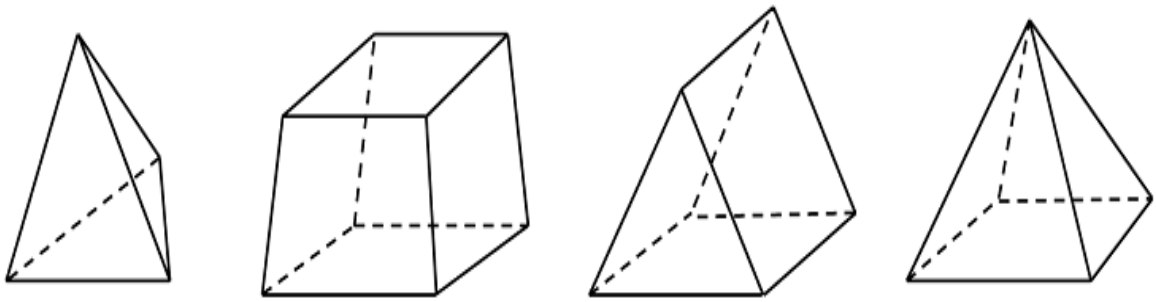

Fig 5.5.1 Images of different types of mesh elements. From the left side to right side: a tetrahedron, hexahedron, triangular prism, and pyramid ("Efficiently Mesh Your Model Geometry with Meshing Sequences," 2020).

The quality of the mesh often influences the quality of a computational fluid dynamics (CFD) model. A good mesh enables convergence, helps reduce memory needs, and delivers efficient results. There are two categories of meshing operations: unstructured and structured. The unstructured operations are Free Triangular, Free Quad, and Free Tetrahedral. Unstructured mesh, and the structured operations, are Mapped and Swept to create a structured mesh.

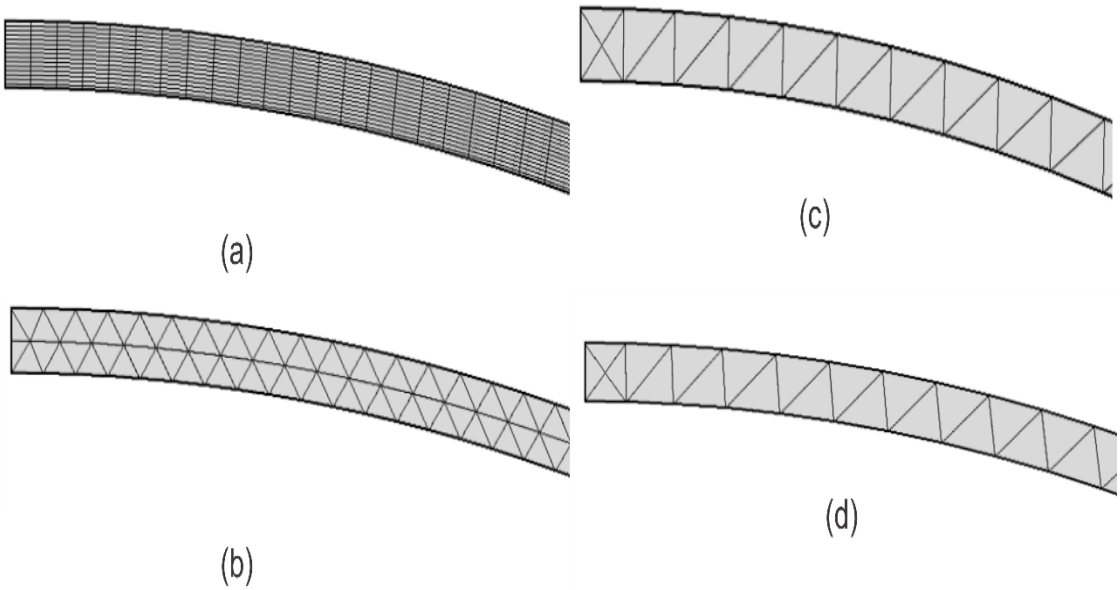

Fig .5.5.2 Different mesh quality configurations (a) Structured swept mesh and Unstructured meshes (b) Extremely Fine (c) Coarser (d) Fine (Table 5.5.1)

Description	Swept Mesh	Coarse Mesh	Normal Mesh	Finer Mesh	Ex Fine Mesh	Adaptive Mesh
Minimum element quality	**0.9966**	0.596	0.5964	0.6007	0.5483	0.4944
Average element quality	**0.9966**	0.7388	0.7407	0.7452	0.7591	0.7281
Quad	**4500**	278	278	280	966	460
Edge element	**630**	276	276	278	484	382

Table 5.5.1 Mesh statistics of different mesh configuration used for mesh refinement study (a) Swept mesh (b) Coarse mesh (c) Normal mesh (d) Finer mesh (e) Extremely fine mesh (f) Adaptive Mesh

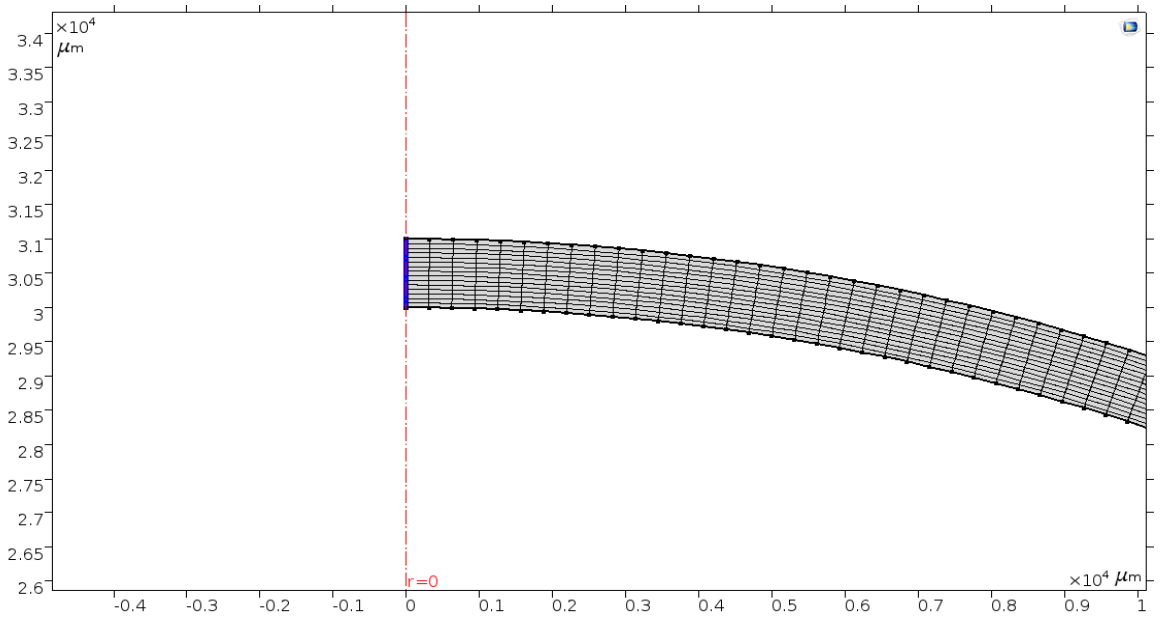

Figure 5.5.3 Illustration of the structured swept mesh near the North Pole of the 2D axi-symmetric hemispherical substrate Structured mesh with uniform distribution (15x150)

5.6 GEOMETRY: 2D AXI-SYMMETRIC COMSOL MODEL

COMSOL Multiphysics can create objects in 1D, 2D, and 3D by using solid modelling or boundary modelling. A geometry was formed during solid modelling combining solid objects, using Boolean operations such as union, intersection, and difference. Parts created by joining a collection of established solids using Boolean operations are known as solid composite objects. Boundary modelling is the method of defining a solid in terms of its boundaries, for example, using lines to create a solid hexagonal in the 2D domain ("COMSOL Multiphysics |

Manualzz," 2020). Such a solid model can be combined with geometric primitives which are common solid modelling forms such as blocks, cones, spheres, rectangles and circles that are directly available in COMSOL Multiphysics. Utilizing symmetry is one of the most efficient ways to reduce a model's size. A 2D axi-symmetric model works well for axially symmetric geometries. Using a Revolution 2D data set, the results of 3D geometry can be easily visualized. In the real world, most problems solved with COMSOL Multiphysics are three-dimensional (3D). In many cases, a two-dimensional (2D) or one-dimensional (1D) problem close to, or equivalent to, the real 3D problem is used. The 2D models are more comfortable to modify and generally solve much faster, making it easier to find modelling errors (COMSOL, 2020a).

A 2D axi-symmetric COMSOL model has been modelled, taking into consideration the axis of rotation around the z-axis. This geometry was created by a difference of two concentric circles of constant radii using Boolean operation ***(Fig. 5.6.1).*** The difference between these two layers of circles represents the fluid film thickness.

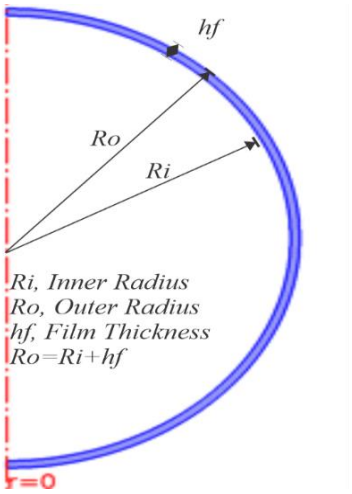

Fig. 5.6.1 COMSOL 2D axisymmetric model geometry and parameters

Name	Expression	Value
Ri	30[mm]	0.03 m
Ro	Ri + hf	0.031 m
omega0	350.0[rad/s]	350 rad/s
hf	1000[µm]	0.001 m
sigma	0.07[N/m]	0.07 N/m

Table 5.6.1 The parameters used for creating 2D axi-symmetric COMSOL model.

5.6.1 Laminar Two-Phase Flow, Moving Mesh Governing equations

For constant density and viscosity, the Navier–Stokes and continuity equations can be simplified to yield a four-equation system for the velocity and pressure ("Comprehensive Introduction to Physics, PDEs, and Numerical Modeling," 2020):

The fluid material used is engine oil since it has similar fluid properties to the polymer solution used for coating in experiments. The physics used for analysis is Laminar two-phase flow coupled with moving meshes. A no-slip condition was imposed on the inner surface wall of the fluid layer.

Name	Value	Unit
Dynamic viscosity	0.0342[Pa*s]	Pa·s
Density	rho(T[1/K])[kg/m^3]	kg/m³

Table 5.6.2 Material parameters used for the COMSOL model

5.6.2 Boundary conditions

(a) Axi-symmetry on the z-axis

A 2D axisymmetric formulation of equation (5) and (6) requires $\frac{\partial}{\partial \phi}$ to be zero. That is, there must be no gradients in the ϕ -direction. An additional common assumption is that $u_\phi = 0$.

The default 2D axisymmetric formulation,

$$\frac{\partial}{\partial \phi} = 0,\ u_\phi = 0 \tag{28}$$

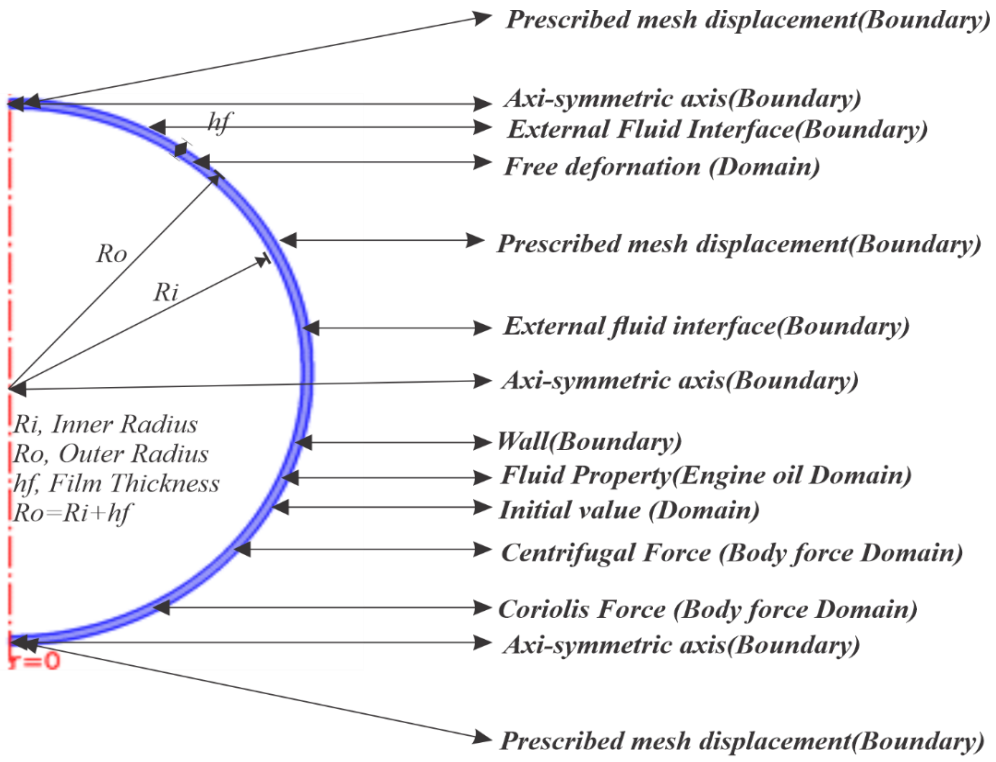

Fig.5.6.2 Schematic of Boundary condition and domain constrains for 2D Axi-symmetric, Laminar, Two-phase, moving mesh COMSOL model for a hemi-spherical substrate.

(b) No-slip on the substrate

The no-slip condition assumes that at the wall, no relative velocity between the fluid and the wall. Mathematically, the constraint can be formulated as

$$\boldsymbol{v} \cdot \boldsymbol{n} = 0 \tag{29}$$

$$\boldsymbol{v} \cdot \boldsymbol{n} = 0, \boldsymbol{K} - (\boldsymbol{K}.\boldsymbol{n})\boldsymbol{n} = 0 \tag{30}$$

where, $\boldsymbol{K} = \mu(\nabla \boldsymbol{v} + (\nabla \boldsymbol{v})^T)\boldsymbol{n}$ (31)

expressing that there is no fluid flow across the interface and no tangential viscous stress. For a moving wall with a translational velocity $\boldsymbol{v}_{\mathbf{tr}}$, u in the above equations can be replaced by the relative velocity $\boldsymbol{v}_{\boldsymbol{rel}} = \boldsymbol{v} - \boldsymbol{v}_{\mathbf{tr}}$

(c) The free surface boundary condition

Kinematic boundary condition and balance of stresses at the free surface

$$\boldsymbol{n}.\boldsymbol{T} = -p_{ext} + \sigma(\nabla - in)n - \nabla_t\sigma \quad (32)$$

(d) Body forces

The forces acting on the fluid were derived, assuming rotation around the z-axis. Allied forces were determined to be the Coriolis and centrifugal forces, the derivation assuming a single axis of rotation is shown below:

With the Coriolis and centrifugal forces, the equation for conservation of momentum becomes

$$\rho\frac{\partial \boldsymbol{v}}{\partial t} + \rho(\boldsymbol{v}\cdot\nabla)\boldsymbol{v} = \nabla\left[-p\boldsymbol{I} + \mu\left(\nabla\boldsymbol{v} + (\nabla\boldsymbol{v})\right)^T - \frac{2}{3}\mu(\nabla\cdot\boldsymbol{v})\boldsymbol{I}\right] + \boldsymbol{F} \quad (33)$$

F= Centrifugal force + Coriolis force

Name	Expression	Unit	Description
tpfmm.Fr	tpfmm.rho*omega0^2*r	N/m³	Centrifugal force, r component
tpfmm.Fphi	0	N/m³	Centrifugal force, z component
tpfmm.Fr	2*tpfmm.rho*omega0*u	N/m³	Coriolis force, r component
tpfmm.Fphi	0	N/m³	Coriolis force, z component

Table.5.6.3 Schematic of Boundary condition and domain constraints for 2D axial symmetric, Laminar, Two-Phase, Moving Mesh model for Hemi-spherical substrate

5.7 RESULT

5.7.1 Parametric Analysis

In COMSOL Multiphysics, the Parametric Sweep category used to run a parametric analysis of one instance with many parameter cases. Typically the cases of the parameters are handled one by one, and all the compute resources (processes and cores) assigned to the single COMSOL Multiphysics instance were included. The Parametric Sweep node controls the parameter ranges of the respective parameter. The solutions in the analysis were either accessible in the solution sequence as parametric values (if the Parametric Solver was used), or under a Parametric Solutions node. The parameters used for this numerical analysis were thickness (hf), surface tension (sigma), and angular velocity (omega)

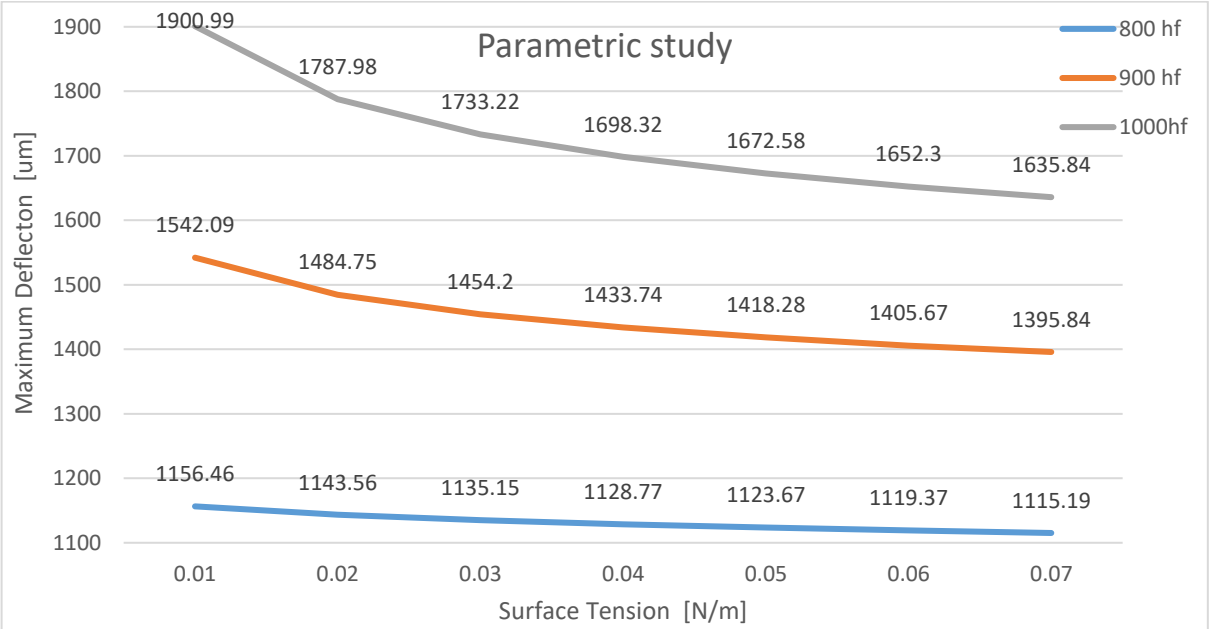

Fig.5.7.1 Parametric study of surface tension on the 2D axi-symmetric model of various film thickness (hf) 1000µm, 900µm and 800µm at an angular velocity of 100rad/s.

Fig.5.7.1 shows the parametric study of surface tension on the 2D axi-symmetric COMSOL model of various initial film thickness (hf) 1000µm, 900µm and 800µm at an angular velocity of 100rad/s. The final film thickness on the equator of the spherical substrate decreased as the surface tension increased.

5.7.2 Mesh Refinement Study

The numerical methods used within COMSOL Multiphysics discretize the modelling space through a mesh for two-purposes. First, this mesh serves to approximate the geometry of the CAD. Second, at discrete points in the space defined by this mesh, which has an approximate solution to the boundary value problem. As the mesh was refined, the solution tends to approximate more accurately the exact solution to the boundary value problem.

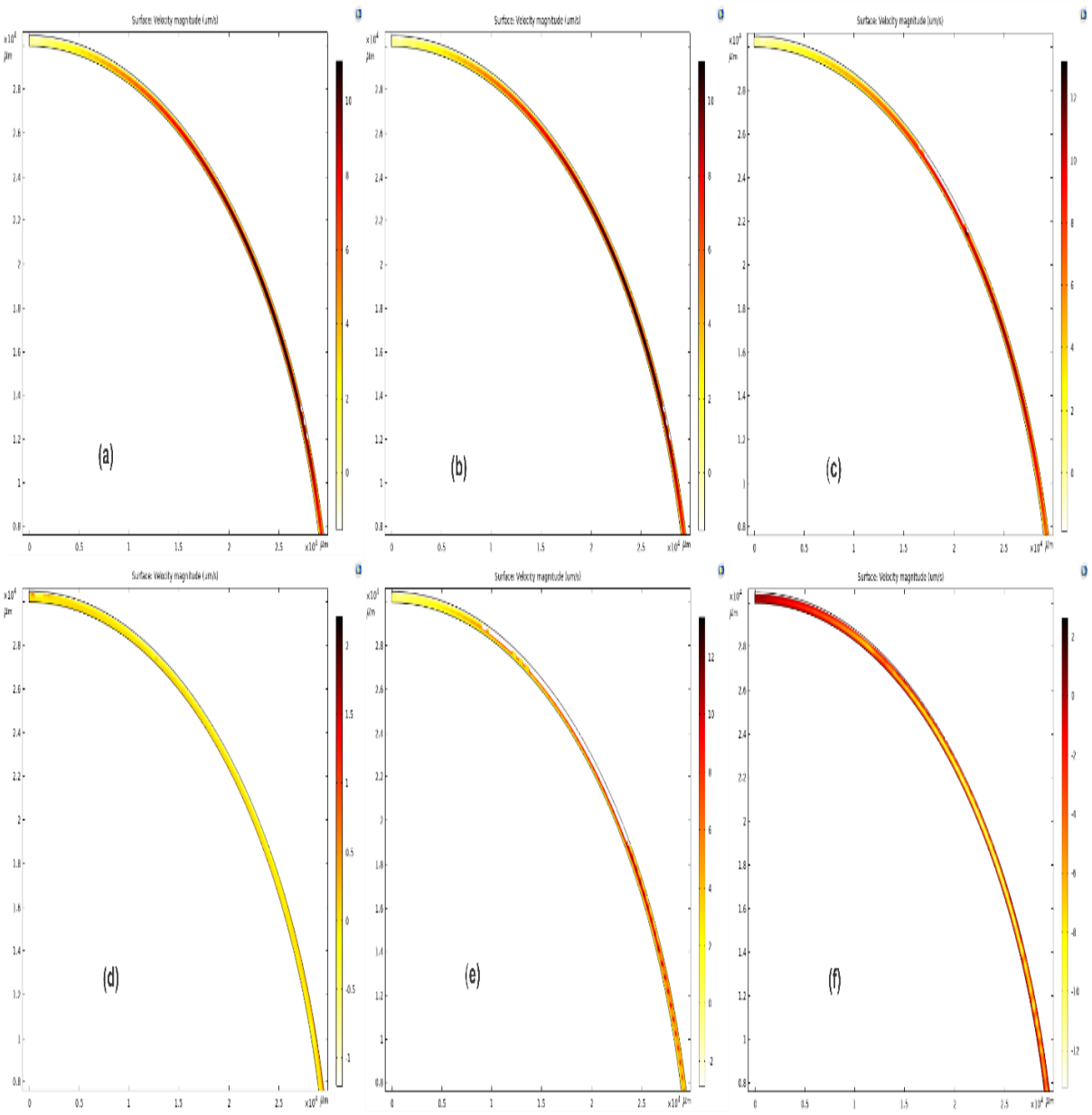

Fig.5.7.2 Mesh refinement study of 2D axisymmetric laminar flow, two phases, moving mesh surface contour of mesh concerning swept mesh data set (a)Swept mesh, and coarse mesh (b) Swept and normal mesh (c) Swept and finer mesh (d) Swept and extremely fine (e) Swept and adaptive mesh (f) Adaptive and extremely fine mesh* (*Table 5.5.1).

In Fig.5.7.2, the Mesh refinement study was conducted on 2D axisymmetric laminar flow, two phases, moving mesh surface contour of swept mesh compared with coarse, normal, finer, extremely fine and adaptive mesh data set. Each plot is compared with the data set of swept mesh using join operator.

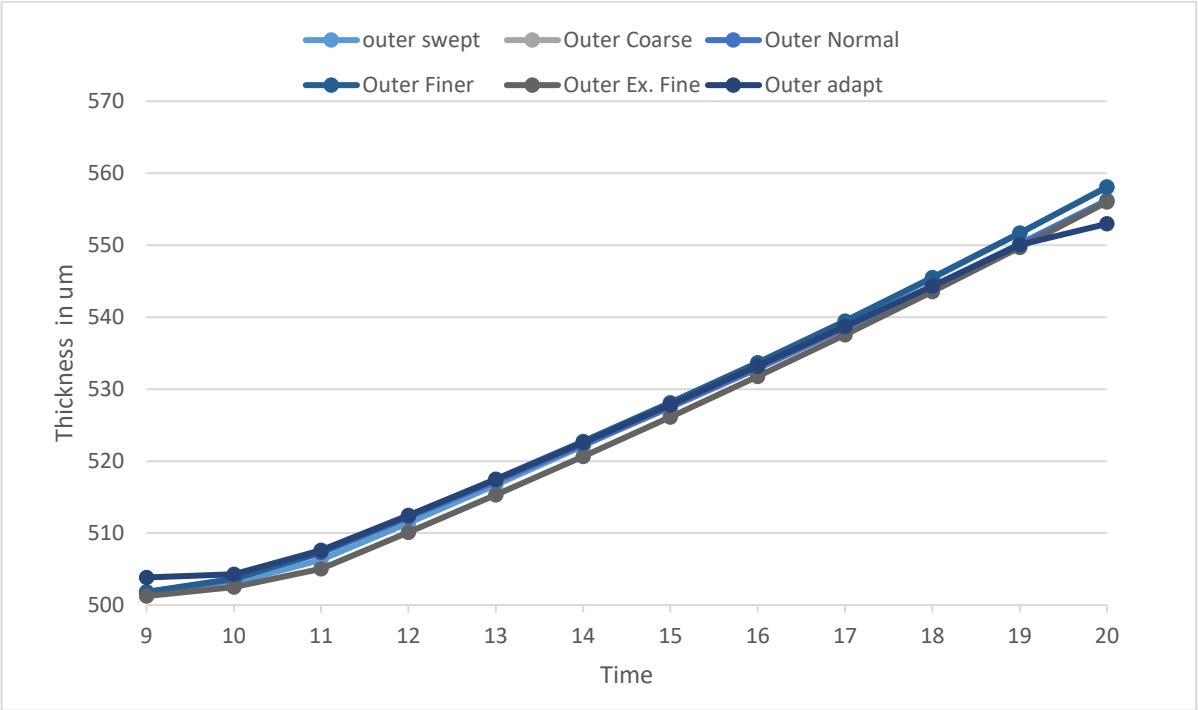

Fig.5.7.3 Mesh refinement study: on film thickness at the equator of a sphere having initial fluid thickness hf 500µm at a speed of 100rad/s

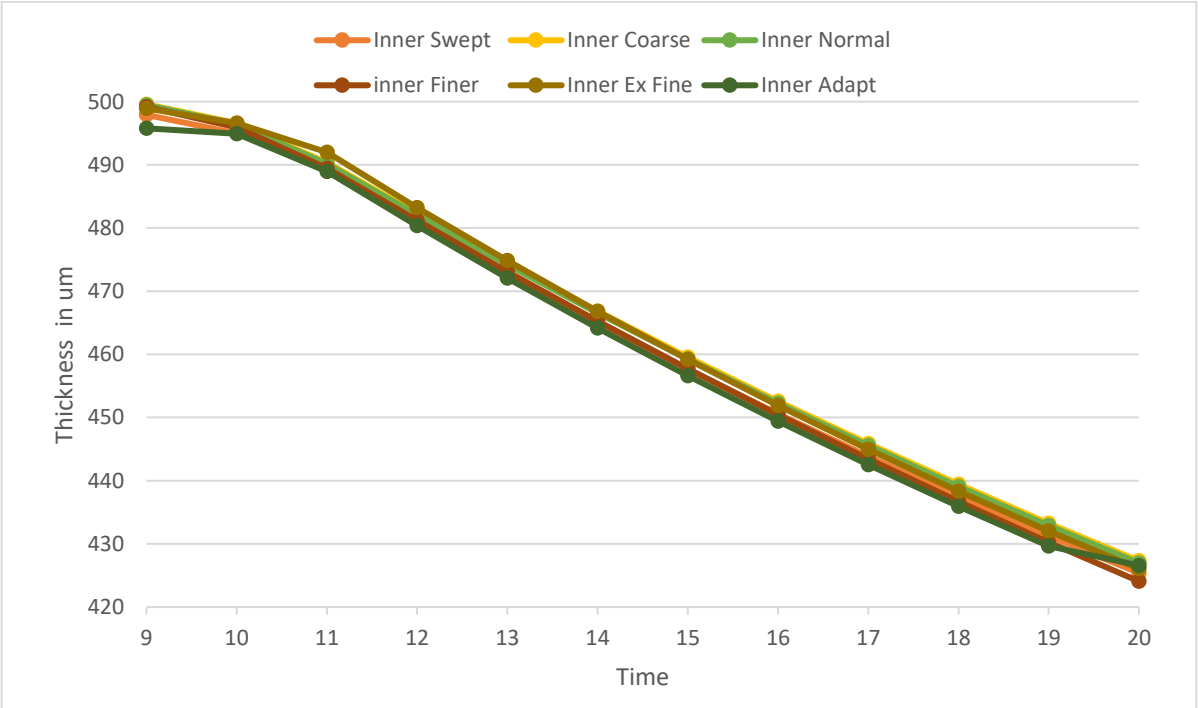

Fig.5.7.4 Mesh refinement study: on film thickness at the north pole of a sphere having initial fluid thickness hf 500µm at a speed of 100rad/s

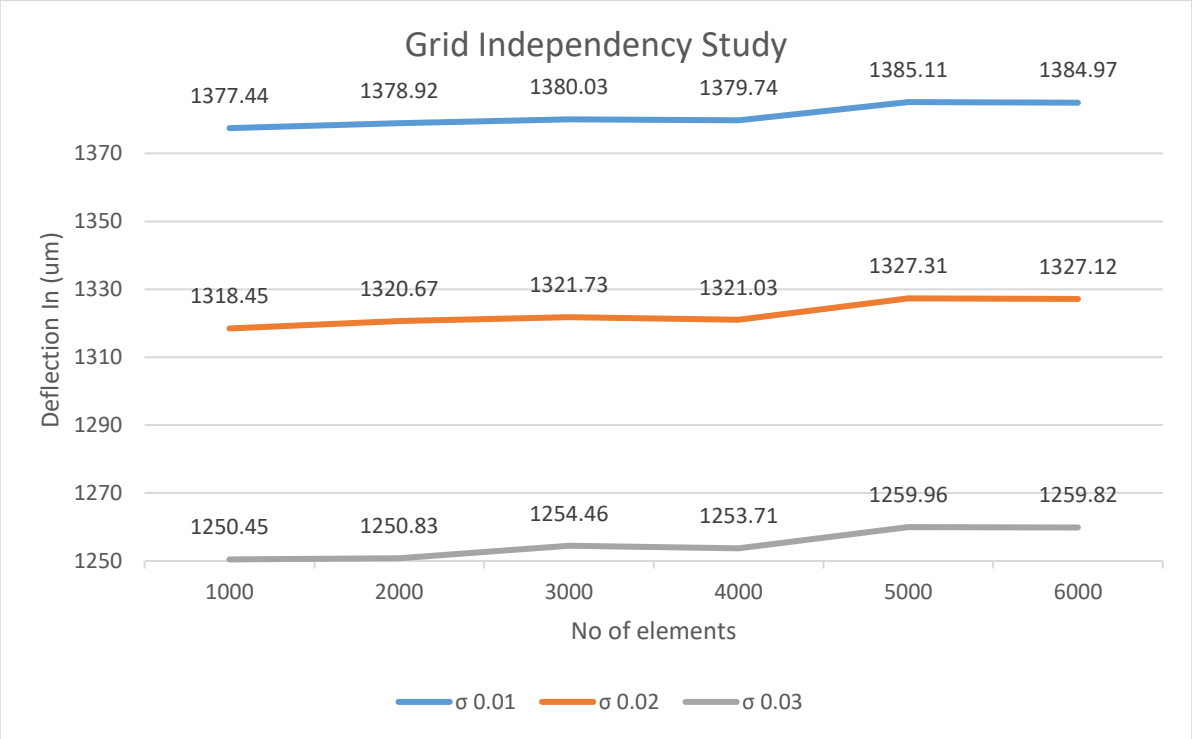

Fig.5.7.5 Grid Independent study of 2D axi-symmetric COMSOL time-dependent model of initial thickness hf of 500µm, angular velocity 100rad/s, time 100s of various surface tension.

Description	**Swept Mesh**	**Coarse Mesh**	**Normal Mesh**	**Finer Mesh**	**Ex Fine Mesh**	**Adaptive Mesh**
Minimum element quality	**0.9958**	0.5922	0.5137	0.5475	0.5924	0.4805
Average element quality	**0.9969**	0.7502	0.7244	0.7259	0.7425	0.6565
Quad/Triangular	**12000**	13582	13551	13518	13486	22388
Edge element	**1240**	13580	13549	13516	13484	15578
Area ratio	**0.9969**	0.8415	0.4507	0.486	0.3712	0.223

Table 5.7.2 Mesh statistics of different mesh configuration used for mesh refinement study (a) Swept mesh (b) Coarse mesh (c) Normal mesh (d) Finer mesh (e) Extremely fine mesh, and (f) Adaptive mesh

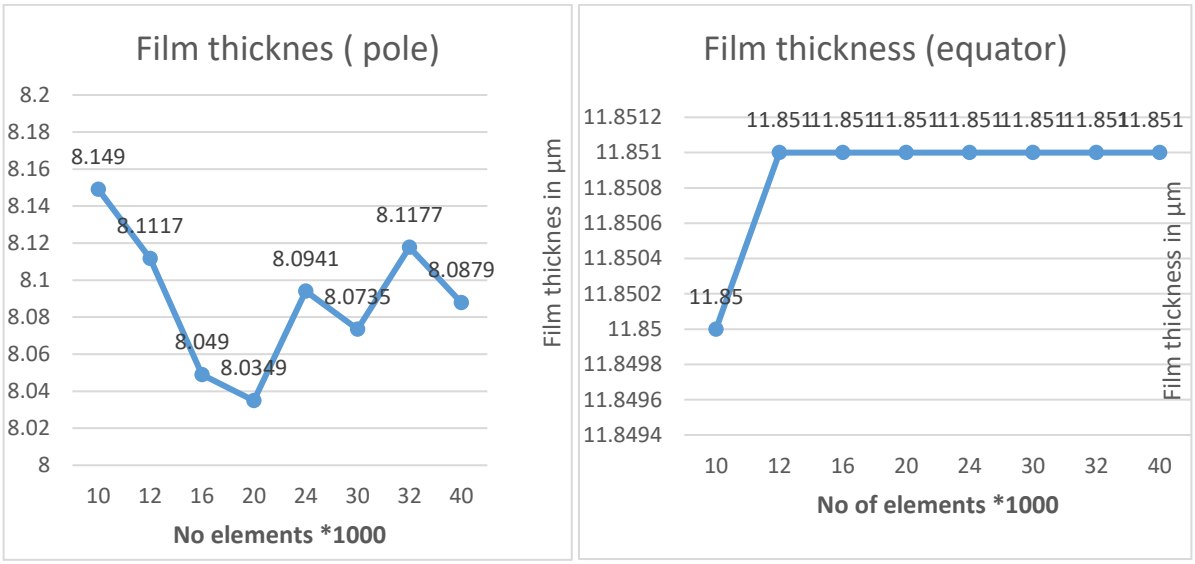

Fig.5.7.6 Gird independence time-dependent study of the 2D axi-symmetric model of initial thickness hf 10µm,3500 rpm, time 20s at varying dynamic viscosity of 34.2m Pa.s

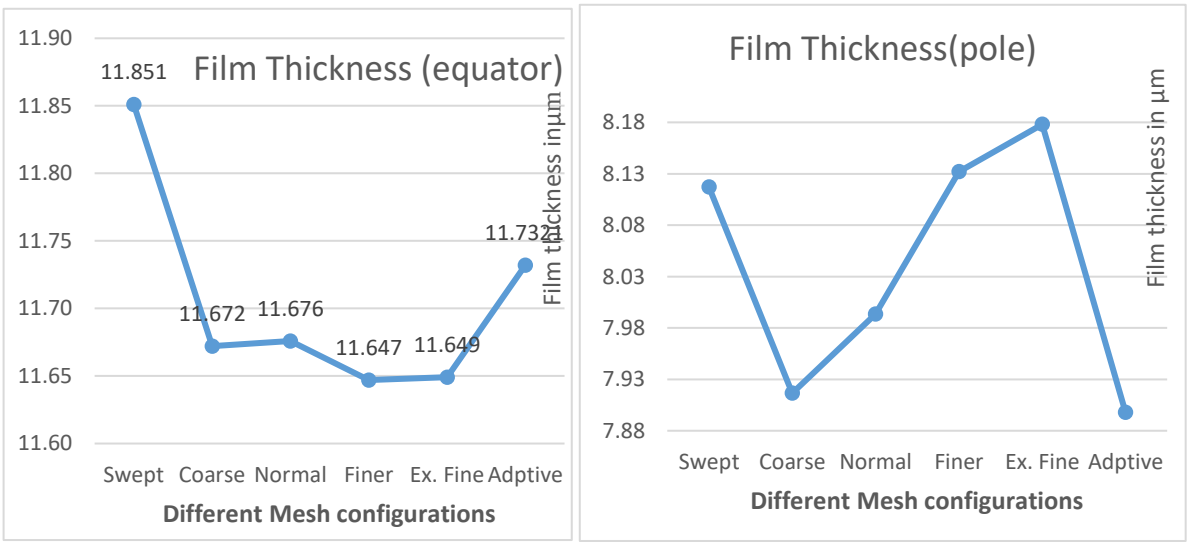

Fig.5.7.7 Mesh refinement study using different Mesh configurations of the 2D axi-symmetric model of initial thickness hf 10µm,3500 rpm, time 20s at varying dynamic viscosity of 34.2m Pa.s

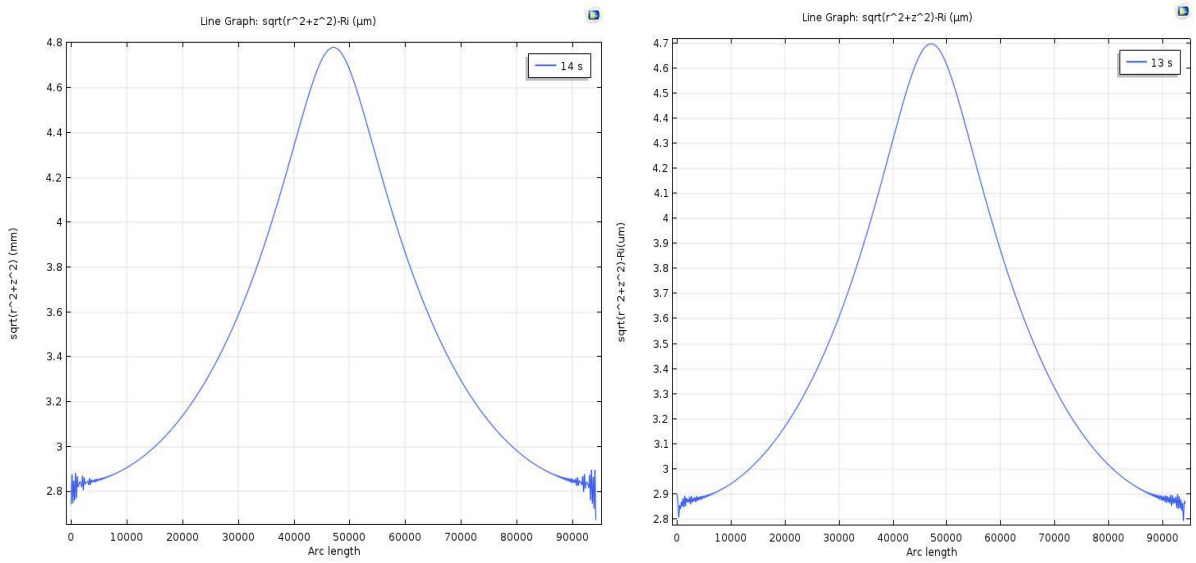

(a) (b)

Fig.5.7.8 Surface plot of thickness at an angular speed of 3500rpm, initial film thickness (hf) 4µm for varying viscosity for (a) at 14s (b) at 13s.

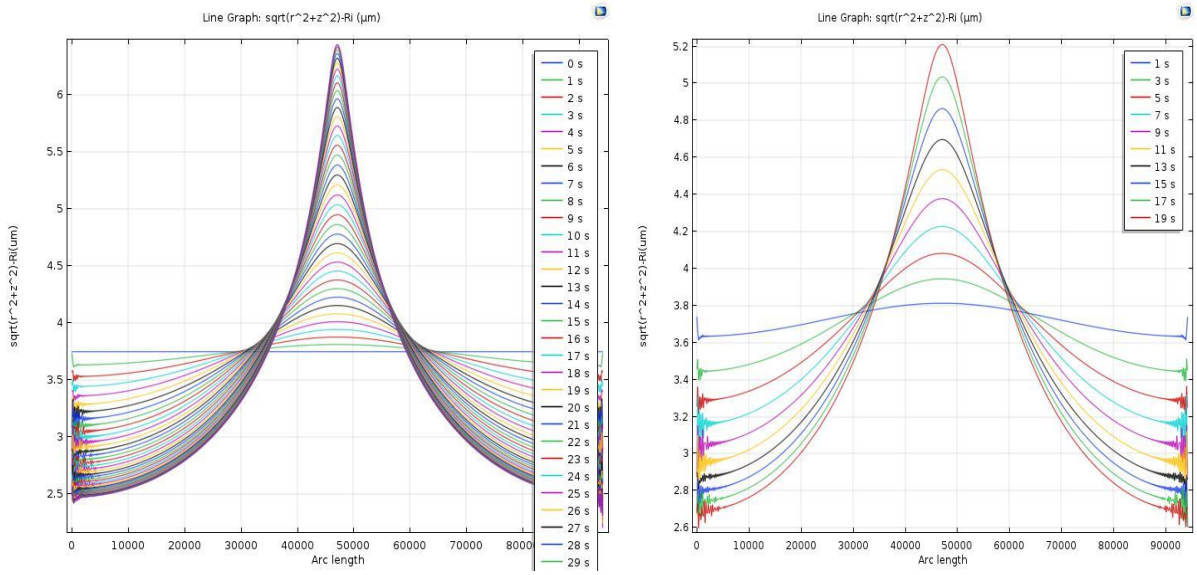

(a) (b)

Fig.5.7.9 Parametric sweep of time with surface plot of thickness at an angular speed of 3500rpm, an initial film thickness(hf) of 4µm for varying viscosity for (a) 40s (b) 20s.

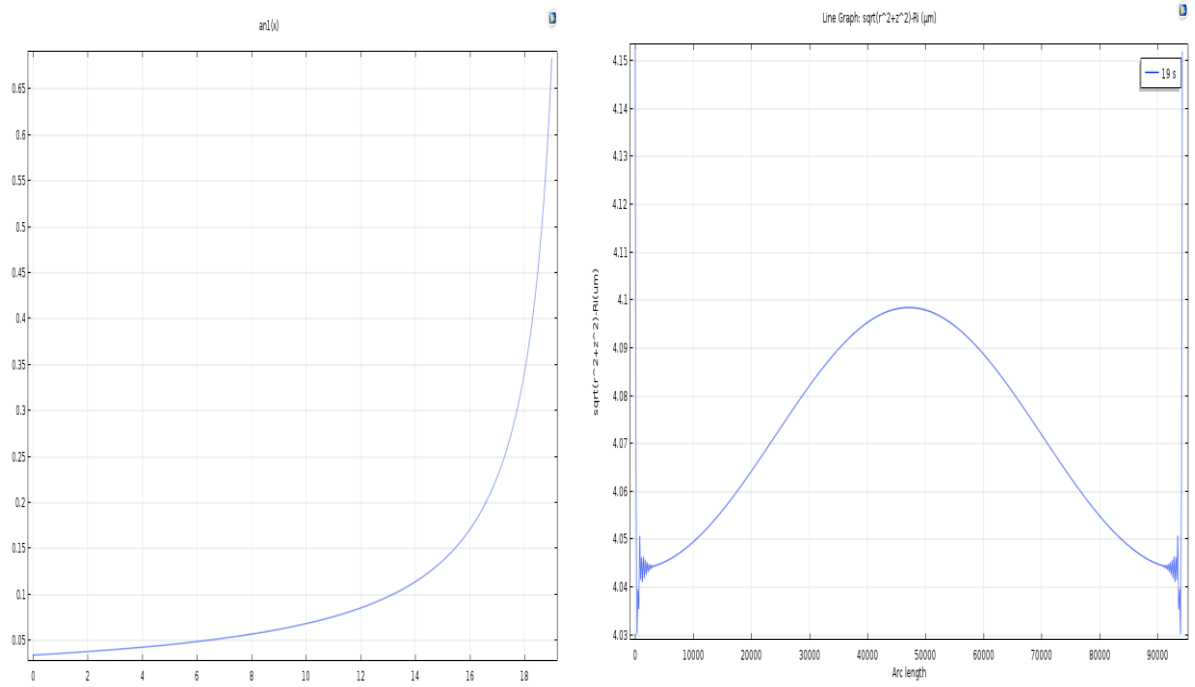

(a) ***(b)***

Fig.5.7.10 (a) Viscosity variation with time used for material property. (b) Time dependent analysis with a surface plot of thickness at an angular speed of 3500rpm, an initial film thickness(hf) of 4.08µm for varying viscosity for 19s.

A numerical study was conducted exploiting COMSOL Multiphysics 5.3a to explain the incompressible, two-dimensional axi-symmetric, made of laminar flow module, presuming incompressible flow, two-phase moving mesh. To mimic the experimental procedure, the thickness used for modeling was 4.08µm which is considered as the initial film thickness. The numerical analysis was done by structured swept mesh sequence of 12000 elements. An implicit time-stepping method for Backward Differentiation Formula (BDF) was used with variable order time stepping to regulate the step variables for convergence automatically. The time-dependent study was conducted for 19s. Two separate cases were examined: (a) model without viscosity variation function (inbuilt material property, ***Fig. 5.7.8***) and (b) model with viscosity variation with time used for a material property (***Fig.5.7.10***).

5.8 COMSOL 3D MODEL

A 3D COMSOL model has been designed around the z-axis of rotation. It was created by the Boolean operation of difference from two concentric spheres of constant thickness. The difference between these two layers of spheres represents the fluid thickness. The fluid material used in this model is engine oil since it has similar fluid properties to the polymer solution used for coating in the actual test. Laminar two-phase flow, coupled with moving meshes, was used for analysis, with no-slip condition acting on the inner surface wall of the fluid layer and, for the outer surface, zero radial displacement and free deformation. The meshing has been developed using tetrahedral elements (fine) to create a smooth mesh over the surface. To get different layers of mesh pattern, mapped and distribution meshes were used**.** The total number of elements is around two hundred thousand, and a time-dependent study was performed.

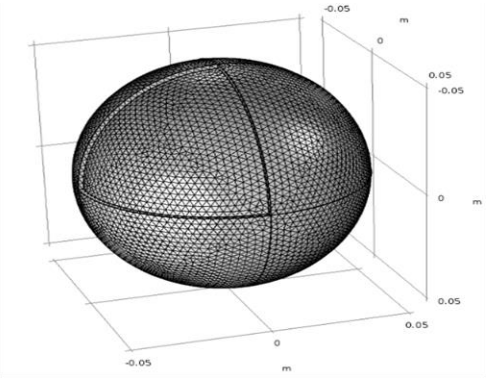

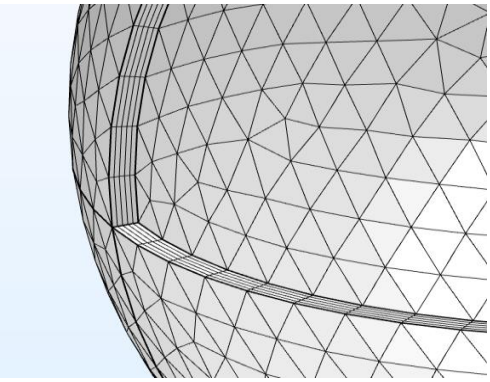

Fig.5.8.1 Meshed 3D model ***Fig. 5.8.2 Enlarged view of sweep and distribution mesh***

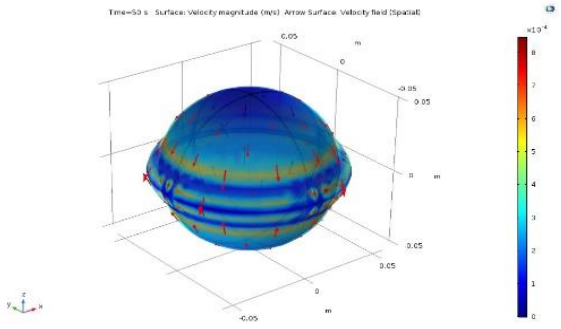

Fig.5.8.3 Surface velocity contour 3D COMSOL Model

Fig.5.8.3 shows the 3D COMSOL model velocity contour and how the film thickness gets thicker closer to the equator and thinner in the poles.

6 MULTI-AXIS SPIN COATING DEVICE

6.1 TWO-AXIS OF ROTATION SPIN COATER CONCEPTUAL DESIGN

The first multi-axis spin coater conceptual design includes two hollow squares, rotating in opposite directions, as shown in Figure 1. These hollow squares were meant to be made of a low-density metal aluminium which is held together by shafts.

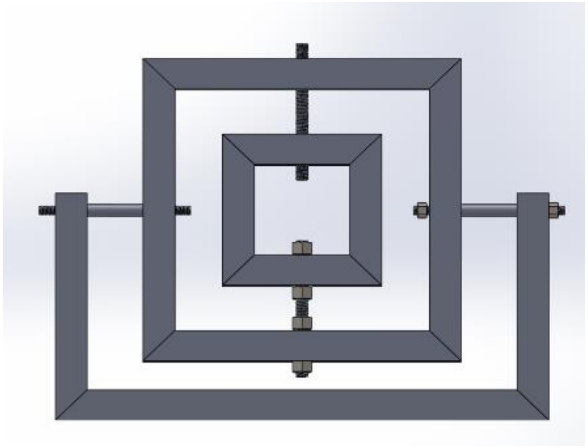

Fig.6.1.1 Two-axis spin coater conceptual design 1

It contains two brushless DC motors which drive both the hollow squares. The first motor rotates the outer square frame, and the inner square frame can be rotated by the electrical motor, which was installed inside the outer square shell. Each hollow shell can be connected to the electrical motor by shafts and bearings. The electrical connection can be made using a high-speed slip-ring for the rotating brushless motor inside the outer square frame.

6.2 THREE-AXIS OF ROTATION SPIN COATER CONCEPTUAL DESIGN-1

A conceptual model for multi-axis spin coating device was created using SOLIDWORKS software. Three independent axes of rotation are possible (x, y, and z-axis). The material selected for the middle and the inner part is aluminium alloy whereas for the outer, fixture parts and the bearings are stainless steel shown in the figure ***(Fig. 6.2.2).***

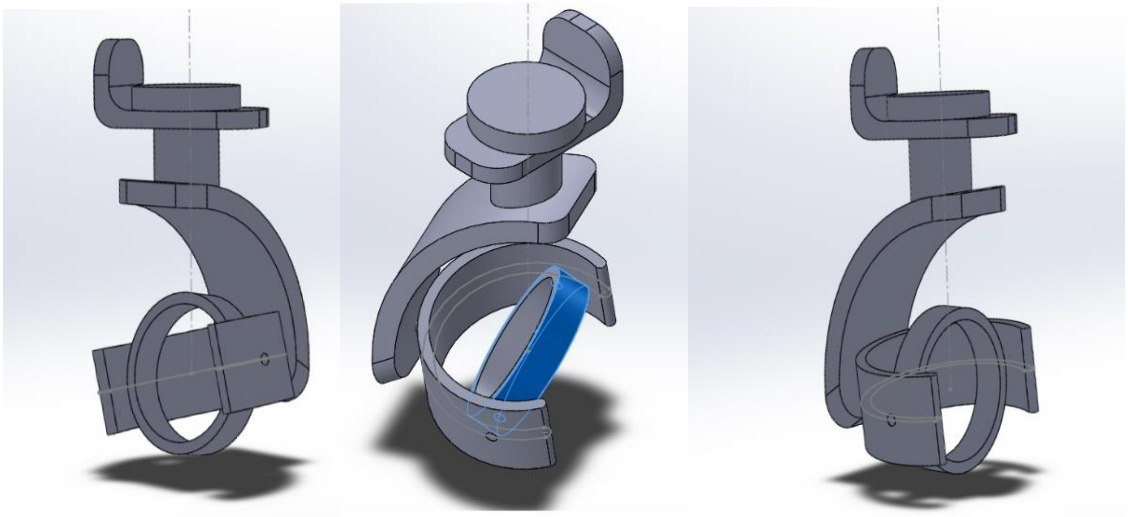

6.2.1 Three-Axis of Rotation Spin Coater Conceptual Design-2

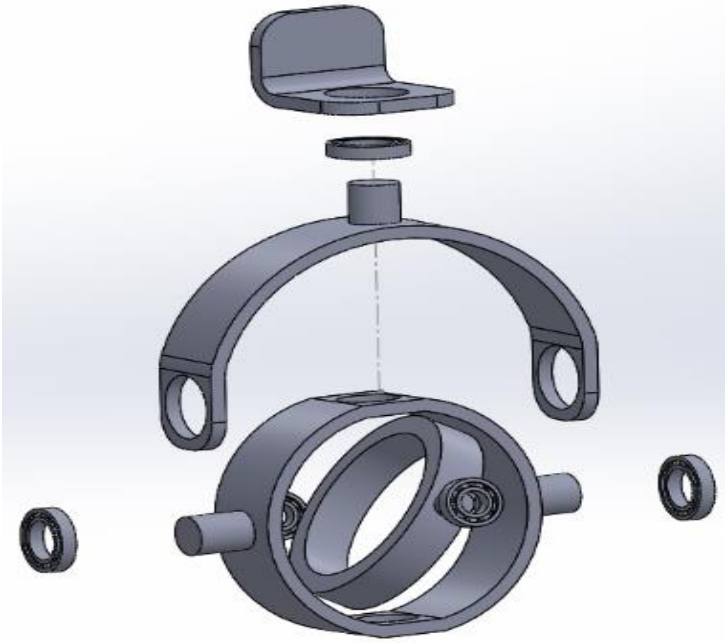

Fig.6.2.2 Three-Axis Rotation final design Spin Coater Model

CONCLUSION

We have extended our study towards spin coating on the curved surface using glass and hemispherical metal substrates. A comparison study was conducted on a spin-coated flat substrate silicon wafer and a hemispherical glass substrate when the material was spun at a constant angular speed of 3500rpm and coated with a photo resistive polymer solution AZ1518 (MicroChemical, Germany). The thickness of the film measured was 2.55µm and 2.85 µm, respectively using an optical profilometer. The objective of conducting the study was to analyze the behaviour of spin coating on a curved surface and how it differs from a flat surface.

In this study, we examined the film thickness at the pole of a glass hemispherical substrate of diameter 60mm using an Atomic Force Microscope (AFM) and optical profilometer, Profilm3D. The substrate was spun at a uniform angular speed of 3500rpm and coated with a photo resistive polymer solution AZ1518. The thickness of the film measured using AFM was 2.63µm and 2.85µm using an optical profilometer. It was seen that the variation of film thickness measured using these devices was marginal at 7.71%.

The radial distribution of the spin-coated hemispherical glass substrate was examined using the optical profilometer, and the result was compared with different published works of literature. The radial distribution of thickness obtained from the hemispherical glass substrate was in good agreement with published data. When $\frac{r}{R} < 0.6$, the radial distribution was almost uniform. A similar pattern of radial distribution was compared (***Fig. 3.3.1*** and ***Fig. 3.3.2***) to the published literature. When the radial position was above $\frac{r}{R} > 0.6$, there was an increase in the thickness of the distribution. It was not possible to attain the same data for validation since each paper used different photoresist polymer solution and angular speed. We validated the spin-coated hemispherical glass substrate at 3500 rpm with Feng & Sun mathematical model. It was seen that both the distributions showed a similar trend.

A numerical investigation was carried using COMSOL Multiphysics 5.3a to solve the incompressible, two-dimensional Navier-Stokes equations, using the laminar flow microfluidic module, assuming 2-D axi-symmetric, two-phase, moving mesh, and time-dependent model. An implicit time-stepping method for Backward Differentiation Formula (BDF) was used, with variable order time-stepping to adjust the step parameters for convergence achievement automatically.

7 FUTURE WORK

7.1 CHARACTERISTIC STUDY OF HEMISPHERICAL SPIN COATING

A study can be carried on the radial and the circumferential distribution of thickness on hemispherical glass substrates. An articulating base (SL20) and adjustable angle plate (AP 180) can be used for future study.

Fig. 7.1.1 Articulating base and adjustable angle plate

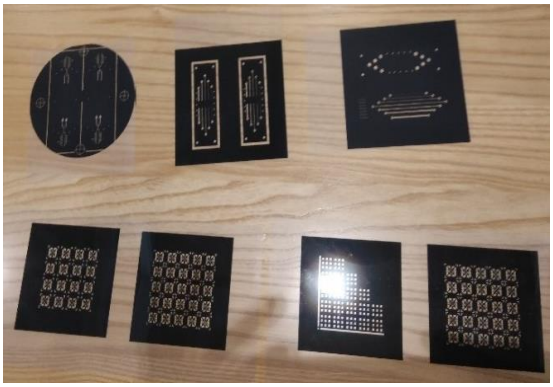

Fig.7.1.2 Masking tapes

Thor labs' SL20 Articulating Base ***(Fig.7.1.1)*** is a high-precision ball and socket mounting platform that delivers smooth spherical rotation over an entire hemisphere.

Thor labs' Adjustable Angle Plate AP 180 provides a full semicircular movement at 15° increments with ±18 Arcmin precision. The mounting platform can be placed at 13 discrete stages by adjusting the linchpin. The engravings on the mount help the angular locations and the associated pin locations for each inclination. By changing the hex locking screw, the plate can be positioned at any angle other than the 13 discrete stages. The maximum permissible load allowed while using the linchpin is 15.8 kg at 60° inclination.

The masking tape ***(Fig.7.1.2)*** can be used on the coated glass substrate to get precise edges for thickness measurement for optical profilometer as well as the AFM.

7.2 PARAMETRIC STUDY OF SINGLE-AXIS SPIN COATER

(a) Different diameters of glass substrates (30-80mm)

A study can be carried on the radial and circumferential distribution of thickness on hemispherical glass substrates of various diameters (30-80mm)

(b) Different dimensions of the metal substrate (30-80mm)

A study can be accompanied on the radial and circumferential distribution of thickness on hemispherical metal substrates of various diameters (30-80mm)

Fig.7.2.1 Glass substrates

Fig.7.2.2 Metal substrates

(c) A parametric study using different photo resistive polymer.

A study can be carried on the radial and circumferential distribution of thickness on hemispherical glass substrates using different photo resistive polymer (various viscosity)

(d) Analyse the vertical centrifugal force.

A study on the characteristic behaviour of the radial and circumferential distribution of film thickness on a hemispherical substrate by tilting the existing experimental set up (single-axis spin coater).

7.3 NUMERICAL MODEL USING COMSOL.

(a) A parametric study of a 2D axi-symmetric model (various speed and liquid) and validate with the experimental result.

(b) A parametric study of the 3D model (various speed and liquid) and validate with the

experimental result.

7.4. MULTI-AXIS SPIN COATER (3-AXIS ROTATION).

(a) To build a conceptual model for multi-axis spin coating device ***(Fig.6.2.2).***

(b) To experiment on spherical substrates using a developed multi-axis spin coater using the following steps:

(i) A parametric study of 3 axis spin coater on glass and spherical metal substrate.

(ii) Different dimensions of the glass substrates 30-80mm diameter.

(iii) Different sizes of the metal substrates 30-80mm diameter.

(iv) A parametric study of film thickness using different photo resistive polymer.

REFERENCES

Acrivos, A., Shah, M., & Petersen, E. (1960). On the flow of a non-Newtonian liquid on a rotating disk. *Journal of Applied Physics, 31*(6), 963-968.

Birnie, D. P., Zelinski, B. J., Marvel, S. P., Melpolder, S. M., & Roncone, R. L. (1992). Film/substrate/vacuum-chuck interactions during spin-coating. *Optical Engineering, 31*(9), 2012-2021.

Bornside, D., Macosko, C., & Scriven, L. (1989). Spin coating: One-dimensional model. *Journal of Applied Physics, 66*(11), 5185-5193.

cells, a. s. s. (2020). Thin Film Solar Module-A-Si Panel, Used for DC and AC Home Solar PV System | Global Sources.

chematscientific. (2020). Spin Coating Technology.

Chen, L.-j., Liang, Y.-y., Luo, J.-b., Zhang, C.-h., & Yang, G.-g. (2009). Mathematical modeling and experimental study on photoresist whirl-coating in convex-surface laser lithography. *Journal of Optics A: Pure and Applied Optics, 11*(10), 105408.

Cochran, W. (1934). *The flow due to a rotating disc.* Paper presented at the Mathematical Proceedings of the Cambridge Philosophical Society.

Comprehensive Introduction to Physics, PDEs, and Numerical Modeling. (2020).

COMSOL. (2020a). COMSOL Documentation.

COMSOL. (2020b). COMSOL: Multiphysics Software for Optimizing Designs.

COMSOL. (2020c). COMSOL_ReferenceManual.pdf.

COMSOL Multiphysics | Manualzz. (2020).

Dandapat, B., & Ray, P. (1994). The effect of thermocapillarity on the flow of a thin liquid film on a rotating disc. *Journal of Physics D: Applied Physics, 27*(10), 2041.

Efficiently Mesh Your Model Geometry with Meshing Sequences. (2020).

Emslie, A. G., Bonner, F. T., & Peck, L. G. (1958). Flow of a viscous liquid on a rotating disk. *Journal of Applied Physics, 29*(5), 858-862.

Evans, P., Schwartz, L., & Roy, R. (2004). Steady and unsteady solutions for coating flow on a rotating horizontal cylinder: Two-dimensional theoretical and numerical modeling. *Physics of Fluids, 16*(8), 2742-2756.

Feng, X.-g., & Sun, L.-c. (2005). Mathematical model of spin-coated photoresist on a spherical substrate. *Optics express, 13*(18), 7070-7075.

Flack, W. W., Soong, D. S., Bell, A. T., & Hess, D. W. (1984). A mathematical model for spin coating of polymer resists. *Journal of Applied Physics, 56*(4), 1199-1206.

Hall, D. B., Underhill, P., & Torkelson, J. M. (1998). Spin coating of thin and ultrathin polymer films. *Polymer Engineering & Science, 38*(12), 2039-2045.

Hansen, E. B., & Kelmanson, M. A. (1994). Steady, viscous, free-surface flow on a rotating cylinder. *Journal of Fluid Mechanics, 272*, 91-108.

Howell, P. (2003). Surface-tension-driven flow on a moving curved surface. *Journal of engineering mathematics, 45*(3-4), 283-308.

Jenekhe, S. A., & Schuldt, S. B. (1984). Coating flow of non-Newtonian fluids on a flat rotating disk. *Industrial & engineering chemistry fundamentals, 23*(4), 432-436.

JimE. (2019). Interference Colors: Polymer Coating Defect - ProfilmOnline - Surface Imaging, Analysis, and Measurement Software for 3D Profilometers and AFMs.

Jose, B. (2020). Images - ProfilmOnline - Surface Imaging, Analysis, and Measurement Software for 3D Profilometers and AFMs.

Kang, D., Nadim, A., & Chugunova, M. (2016). Dynamics and equilibria of thin viscous coating films on a rotating sphere. *Journal of Fluid Mechanics, 791*, 495-518.

Khodabocus, M. I., Sellier, M., & Nock, V. (2019). Dynamics of Thin Film Under a Volatile Solvent Source Driven by a Constant Pressure Gradient Flow. *Fluids, 4*(4), 198.

Lee, A., Brun, P.-T., Marthelot, J., Balestra, G., Gallaire, F., & Reis, P. M. (2016). Fabrication of slender elastic shells by the coating of curved surfaces. *Nature communications, 7*, 11155.

Lee, D.-H. (2013). 3-Dimensional profile distortion measured by stylus type surface profilometer. *Measurement, 46*(1), 803-814.

Liu, H., Fang, X., Meng, L., & Wang, S. (2017). Spin coating on spherical surface with large central angles. *Coatings, 7*(8), 124.

Mahmoodi, S., Guoqing, H., & Khajavi, M. N. (2016). Two-dimensional spin coating with a vertical centrifugal force and the effect of artificial gravity on surface leveling. *Journal of Coatings Technology and Research, 13*(6), 1123-1137.

Mahmoodi, S., Hassan, D. A., Hojjati-Najafabadi, A., Li, W., Liao, L., Moshayedi, A. J., . . . Khajavi, M. N. (2020). Quality enhancement of copper oxide thin film synthesized under elevated gravity acceleration by two-axis spin coating. *Ceramics International, 46*(6), 7421-7429.

Manske, L., Graves, D., & Oldham, W. (1990). Dynamic measurements of film thickness over local topography in spin coating. *Applied physics letters, 56*(23), 2348-2350.

Meshing, M. B. o. (2020). Mesh / Basics of Meshing.

Meyerhofer, D. (1978). Characteristics of resist films produced by spinning. *Journal of Applied Physics, 49*(7), 3993-3997.

microchemicals. (2020). Spin-coating of Photoresists - spin_coating_photoresist.pdf.

Microfluidics Software - For Simulating Microfluidics Devices. (2020).

Middleman, S. (1987). The effect of induced air-flow on the spin coating of viscous liquids. *Journal of Applied Physics, 62*(6), 2530-2532.

Mouhamad, Y., Mokarian-Tabari, P., Clarke, N., Jones, R., & Geoghegan, M. (2014). Dynamics of polymer film formation during spin coating. *Journal of Applied Physics, 116*(12), 123513.

NanoscienceInst. (2020). Optical Profilometry - Nanoscience Instruments.

Pang, H., Yin, S., Deng, Q., Qiu, Q., & Du, C. (2015). A novel method for the design of diffractive optical elements based on the Rayleigh–Sommerfeld integral. *Optics and Lasers in Engineering, 70*, 38-44.

R.G. Shepherd, M. S., E. Boujo. (2020, 6-10 December 2020). *Modelling and Simulation of Spin Coating on a Spherical Substrate.* Paper presented at the AFMC 2020, Australia.

Ramsay, J., Sellier, M., & Ho, W. H. (2020a). Eliminating Boundary Layer Separation on a Cylinder with Nonuniform Suction. *International Journal of Aerospace Engineering, 2020*.

Ramsay, J., Sellier, M., & Ho, W. H. (2020b). Non-uniform suction control of flow around a circular cylinder. *International Journal of Heat and Fluid Flow, 82*, 108559.

Ray, S. S. (2013). *Environmentally friendly polymer nanocomposites: types, processing and properties*: Elsevier.

Roy, R. V., Roberts, A., & Simpson, M. (2002). A lubrication model of coating flows over a curved substrate in space. *Journal of Fluid Mechanics, 454*, 235-261.

Sahu, N., Parija, B., & Panigrahi, S. (2009). Fundamental understanding and modeling of spin coating process: A review. *Indian Journal of Physics, 83*(4), 493-502.

Schwartz, L., & Weidner, D. (1995). Modeling of coating flows on curved surfaces. *Journal of engineering mathematics, 29*(1), 91-103.

Shimoji, S. (1989). Numerical analysis of the spin-coating process. *Journal of Applied Physics, 66*(6), 2712-2718.

Spin Coating ofPhotoresists. (2007). Retrieved from http://web.mit.edu/scholvin/www/nt245/Documents/resists.AN.spin_coating_photoresist.pdf

Szott, M., & Ruzic, D. (2020). 2-D moving mesh modeling of lithium dryout in open surface liquid metal flow applications. *Fusion Engineering and Design, 154*, 111512.

Tanner, L. (1979). The spreading of silicone oil drops on horizontal surfaces. *Journal of Physics D: Applied Physics, 12*(9), 1473.

Tyona, M. (2013). A theoritical study on spin coating technique. *Advances in materials Research, 2*(4), 195.

Washo, B. (1977). Rheology and modeling of the spin coating process. *IBM Journal of Research and Development, 21*(2), 190-198.

Weidner, D. E. (2018). Analysis of the flow of a thin liquid film on the surface of a rotating, curved, axisymmetric substrate. *Physics of Fluids, 30*(8), 082110.

Wu, L. (2006). Spin coating of thin liquid films on an axisymmetrically heated disk. *Physics of Fluids, 18*(6), 063602.

Yoon, J. S., Yoo, Y. E., & Choi, D. S. (2012). A study on the fabrication of rounded patterns by spin coating of photoresist on silicon substrate with microstructures. *Polymer Engineering & Science, 52*(3), 499-506.

APPENDIX

MATLAB Validation

A.1 Spin-coated on a spherical substrate (2000RPM)

```
c_0 = 0.00015;
R = 20e-3; %m
rho = 1050; %kg/m^3
omega = 2000; %rps
mu = .03826; %Pa.s
g = 0; %m/s^2
C =0.014;
F = (0.03*rho)/(mu.*sqrt(omega));
r = 2e-3:2e-3:16e-3;

A = 3*mu*R*F*sqrt(omega);

B = (1-c_0)*((2*rho*omega^2.*sqrt(R^2-r.^2)) -
(((rho*(omega^2).*(r.^2))./(sqrt(R^2-r.^2)))) - 2*g);

D = (A./B).^(1/3);

h_f = c_0.*D;

plot(r*10^3,h_f*10^9)
```

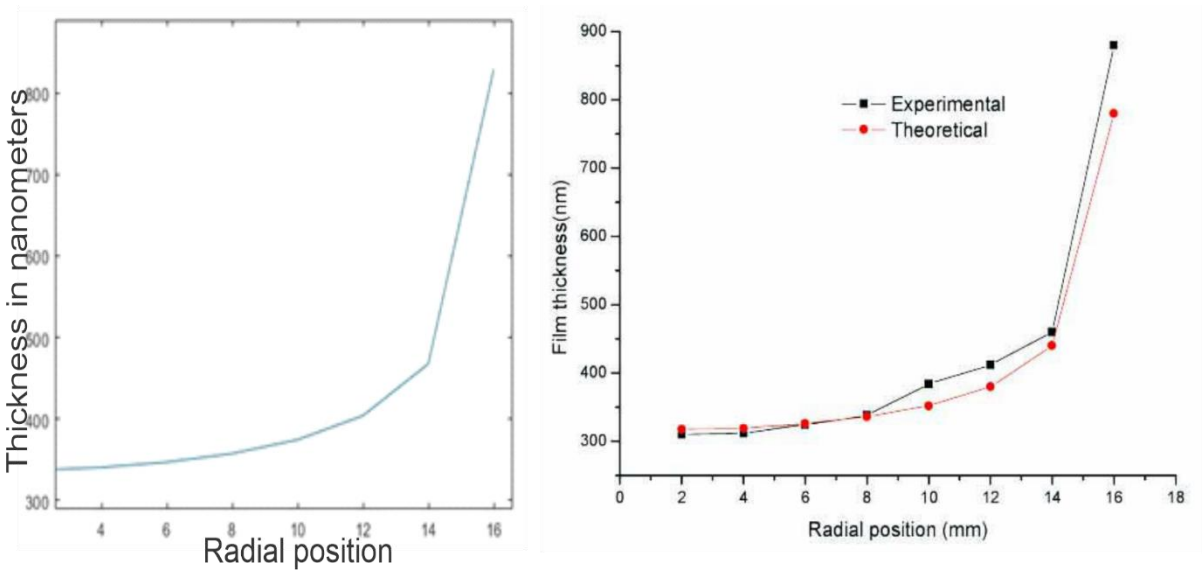

Fig. A.1 Radial distribution thickness (a) from MATLAB(b) from the published literature (Feng & Sun, 2005)

The final thickness of film on a spherical substrate from the mathematical model

$$h_f = S_f = c_0 h_{\frac{1}{3}} = c_0 \left[\frac{3\mu R.C\sqrt{\omega}}{(1-c_0)(2\rho\omega^2\sqrt{R^2-r^2} - \frac{\rho\omega^2 r^2}{\sqrt{R^2-r^2}} - 2g)} \right]^{\frac{1}{3}} \quad (1)$$

where, c_0 is the density of non-volatile polymer material in the photo resistive solution.

Here, r is the radial position, ω is the angular velocity, R is the sphere radius, ρ is the material density of the fluid, C is the laboratory and device coefficient, S_f is the final solute thickness, h_f is the ultimate film thickness, and g is the gravitation force. The mathematical expression with experimental results on a spherical concave substrate of radius 20mm, the angular speed of 2000rpm, c_0 =0.015, g= 0, $\mu/\rho \cdot C\sqrt{\omega}$ =0.03 $\frac{m^2}{s^2}$, moreover, tested and validated the film thickness by atomic force microscope (AFM).

A.2 Spin-coated on a spherical substrate (3500RPM)

```
c_0 = 0.0014;
R = 30e-3; %mm
rho = 1060; %kg/m^3
omega = 3500; %rpm
mu = .03826; %Pa.s
g = 9.81; %m/s^2
C =0.014;
F = (0.03*rho)/(mu.*sqrt(omega));
r = 0:1.1e-3:25e-3;

A = 3*mu*R*F*sqrt(omega);

B = (1-c_0)*((2*rho*omega^2.*sqrt(R^2-r.^2)) -
(((rho*(omega^2).*(r.^2))./(sqrt(R^2-r.^2)))) - 2*g);

D = (A./B).^(1/3);

h_f = c_0.*D;

plot(r/R,h_f*10^6)
```

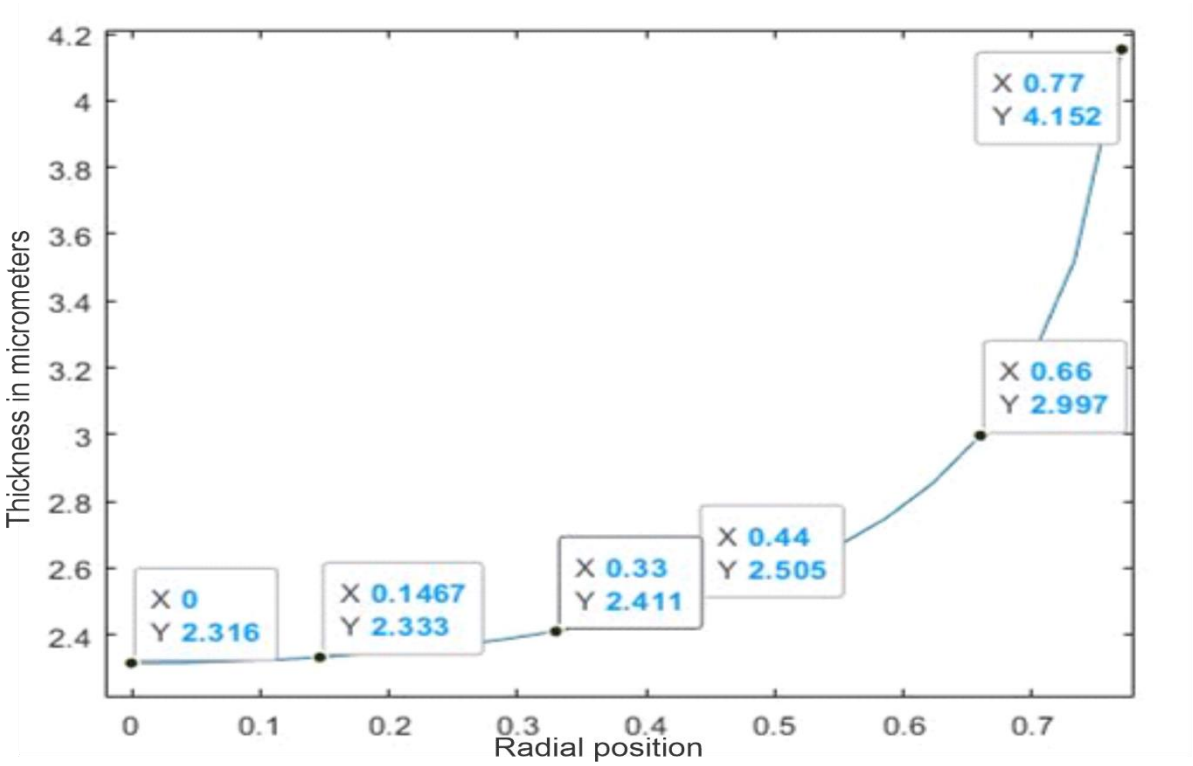

Fig.A.2 Matlab validation of experimental result

A.3 Spin-coated on a spherical substrate (2000,3000, 4000,5000,6000 RPM)

```
c_0 = 0.00121;
R = .03; %m
rho = 1060; %kg/m^3
omega = 2000; %rpm
mu = .03826; %Pa.s
g = 9.81; %m/s^2
C =0.014;
F = (0.03*rho)/(mu.*sqrt(omega));
r = 0:.0011:.024;

A = 3*mu*R*F*sqrt(omega);

B = (1-c_0)*((2*rho*omega^2.*sqrt(R^2-r.^2)) -
(((rho*(omega^2).*(r.^2))./(sqrt(R^2-r.^2)))) - 2*g);

D = (A./B).^(1/3);

h_f = c_0.*D;

plot(r,h_f*10^6)
```

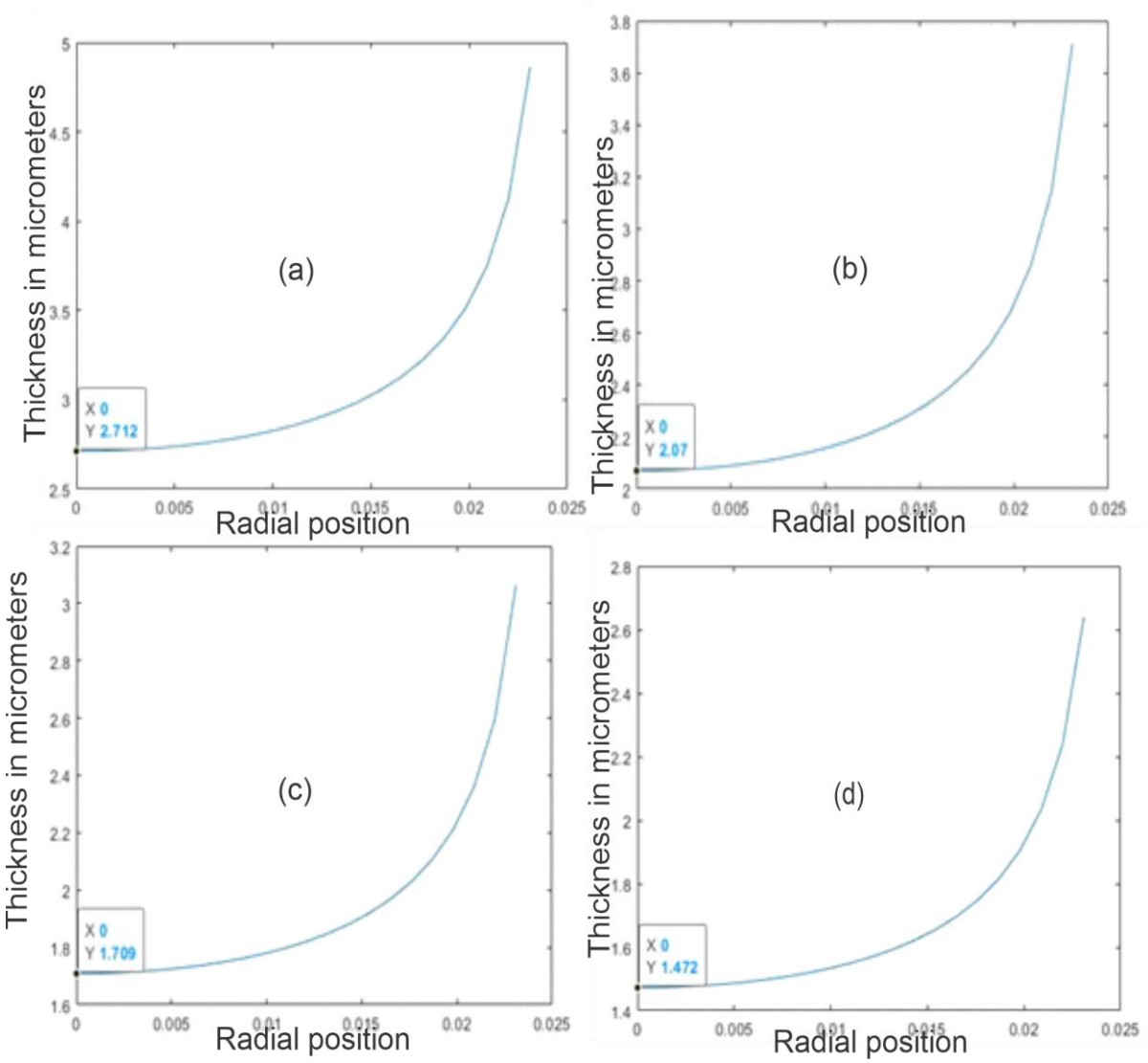

Fig.A.3 Matlab validation of AZ1518 datasheet

PHYSICAL and CHEMICAL PROPERTIES

AZ	1505		1518	1529	1514H	1512HS	1518HS
Solids content [%]	17.7		29.9	34.0	27.8	26.5	30.4
Viscosity [cSt at 25°C]	6.3		34.2	80.0	24.2	18.0	33.0
Absorptivity [l/g*cm] at 398nm	0.80		1.30	1.36	1.22	1.32	1.50
Solvent	methoxy-propyl acetate (PGMEA)						
Max. water content [%]	0.50						
Spectral sensitivity	310 - 440 nm						
Coating characteristic	striation free						
Filtration [µm absolute]	0.1			0.2	0.1		

FILM THICKNESS [µm] as FUNCTION of SPIN SPEED (characteristically)

spin speed [rpm]	2000	3000	**4000**	5000	6000
AZ 1505	0.71	0.58	**0.50**	0.45	0.41
AZ 1512HS	1.70	1.39	**1.20**	1.07	0.98
AZ 1514H	1.98	1.62	**1.40**	1.25	1.14
AZ 1518 and AZ 1518HS	2.55	2.08	**1.80**	1.61	1.47
AZ 1529	4.10	3.35	**2.90**	2.59	2.37

Fig. A.4 Photoresistive polymer AZ1518 Data sheet ("Spin Coating ofPhotoresists," 2007)